

UC Santa Barbara

UC Santa Barbara Electronic Theses and Dissertations

Title

Structure and Properties of Phase-Separating Dielectric Soft Media

Permalink

<https://escholarship.org/uc/item/8fj017sx>

Author

Martin, Jonathan

Publication Date

2020

Peer reviewed|Thesis/dissertation

University of California Santa Barbara

**Structure and Properties of Phase-Separating
Dielectric Soft Media**

A Dissertation submitted in partial satisfaction
of the requirements for the degree of
Doctor of Philosophy in
Chemical Engineering

by

Jonathan M. Martin

Committee Members:

Glenn H. Fredrickson, Chair

Carlos J. Garcia-Cervera

Rachel A. Segalman

M. Scott Shell

March 2020

The Dissertation of Jonathan M. Martin is approved.

Professor Carlos J. Garcia-Cervera

Professor Rachel A. Segalman

Professor M. Scott Shell

Professor Glenn H. Fredrickson, Committee Chair

December 2019

Acknowledgements

I would like to begin by thanking my advisor, Glenn Fredrickson, whose patience, guidance, flexibility, and thought-provoking ideas emboldened me to explore the science surrounding my field of study, and to embrace creativity when building models to try to answer interesting questions. I would also like thank my other Thesis committee members – Carlos Garcia-Cervera, Rachel Segalman, and M. Scott Shell – whose advice and direction helped me develop the indispensable skill of synthesizing otherwise nebulous scientific findings into a novel, coherent narrative.

My colleagues in the Fredrickson group have also provided many fruitful discussions and interactions during my time at UCSB. The mentorship I found in Kris Delaney and Wei Li instilled in me the importance of precision and a complete lack of ambiguity when presenting math or science, and I am grateful for the interactions I had with them. I also had many meaningful discussions with Doug Grzetic, Scott Danielsen, and Kevin Shen, whose research was near enough to mine that we could talk at length about the science we'd been thinking about.

I am incredibly grateful to my friends, and the many small interactions we shared over the past several years – everything from the joy of playing a game together, to linking each other funny pictures on Messenger; these passing moments of human interaction provided much-needed joy during the inevitable times that no joy was to be found in my research. I would also like to thank Carol Tsai, whose endless ability to support, encourage, and find reasons to laugh helped me through the most difficult years of my Graduate education.

Lastly, I am grateful to my parents, Michael and Diane Martin, who encouraged my curiosity – particularly when it came to math and science – throughout my childhood, and into my post-secondary years. Without their constant support and encouragement, this Thesis most certainly would not exist.

JONATHAN M. MARTIN

Curriculum Vitae

EDUCATION

University of California, Santa Barbara *September 2014 - December 2019*
Ph.D. Chemical Engineering GPA: 3.69

Arizona State University (ASU) *August 2010 - May 2014*
B.S.E. Chemical Engineering with honors GPA: 3.85
B.S. Computational Mathematical Sciences with honors
Summa Cum Laude

HONORS & AWARDS

Mitsubishi Chemical Fellowship 2016
Outstanding Honors Thesis ASU SEMTE Celebration of Excellence, 2014
Undergraduate Research Grant ASU FURI Program, 2012-2013
ASU Dean's List 2010-2014

EMPLOYMENT

University of California, Santa Barbara **Santa Barbara, CA**
Graduate Student 2014-2019
Teaching Assistant Fall 2015, Fall 2016, Winter 2018

Washington University in St. Louis **St. Louis, MO**
Undergraduate Researcher (REU) Summer 2013

Western Technologies **Flagstaff, AZ**
Engineering Technician May-July, 2012

Arizona State University **Tempe, AZ**
Undergraduate Researcher 2012-2014
Undergraduate Teaching Assistant Fall 2011

WORKS

J.M. Martin, K.T. Delaney, and G.H. Fredrickson. Effect of an electric field on the stability of binary dielectric fluid mixtures. *Accepted to J Chem Phys* (2020).

J.M. Martin, W. Li, K.T. Delaney, and G.H. Fredrickson. SCFT study of diblock copolymer melts in electric fields: Selective stabilization of orthorhombic Fddd network phase. *Macromolecules* (2018).

J.M. Martin, W. Li, K.T. Delaney, and G.H. Fredrickson. Statistical field theory description of inhomogeneous polarizable soft matter. *J Chem Phys* (2016).

M. Lengyel, K. Shen, D.M. Lanigan, J.M. Martin, X. Zhang, and R.L. Axelbaum. Trace level doping of lithium-rich cathode materials. *J Mater. Chem. A.* (2016).

Honors Thesis: J.M. Martin, V.D. Kodibagkar, and K. Rege. Modeling and characterization of mass transfer kinetics in tumor tissue using dynamic contrast enhanced magnetic resonance imaging (2014).

PRESENTATIONS

- event: APS March Meeting
- title: Electric field-induced critical point shift in a binary dielectric fluid
- date: March 2019

- event: APS March Meeting
- title: Understanding electric field effects in phase-separating soft matter
- date: March 2018

- event: ICB TAB Review (Poster Session)
- title: Modulating structure and properties of soft materials using an electric field:
A field-theoretic study
- date: August 2017

- event: APS March Meeting
- title: Phase stability of a binary simple fluid in an applied electric field
- date: March 2017

- event: APS March Meeting
- title: Selective stabilization of the Fddd diblock copolymer microphase in an applied electric field
- date: March 2016

- event: BMES Annual Meeting (Poster Session)
- title: Simulating delivery, binding, and clearance of a novel hypoxia-binding contrast agent
- date: September 2013

Abstract

Structure and Properties of Phase-Separating Dielectric Soft Media

by

Jonathan M. Martin

The use of field-theoretic representations has emerged as an increasingly attractive and flexible method for describing the statistical behavior of soft materials, granting direct access to thermodynamically-derived structures and properties of interest, while avoiding the computational expense of a traditional explicit particle model. Leveraging the recently-developed complex Langevin (CL) method for full field-theoretic simulation of exact fluctuating field theories, along with the ever-advancing capabilities of academic and industrial computing infrastructures, field-theoretic descriptions of charge-containing soft matter systems – such as polyelectrolyte solutions and polymerized ionic liquids – permit the direct simulation of inhomogeneous, strongly-fluctuating dense fluids of charged species, illuminating the collective thermal motion, and associated electrostatic correlations, of coarse-grained charge-containing molecules. Beyond the already vast materials design space available to this class of field theories, one detail that has thus far been omitted is the explicit polarizability carried by all molecular species contained in a real, charge-containing soft matter system.

This thesis describes the construction and implementation of a molecularly-informed field theory for a fluid of polarizable media, assigning “bead” molecules with a polarizability *via* a simple Drude oscillator model. Beads can optionally carry a net free charge or be connected in chains to produce electrolyte and polymer models, respectively. By constructing a simple fluid model of oppositely charged, polarizable electrolyte beads, which is then solved analytically using a simple Gaussian fluctuation approximation, the model is shown to self-consistently include: short-range van der Waals (VdW) attractions between polarizable beads, short-range ion-dipole attractions between the net free charge and net dipole moment of neighboring beads, dielectric screening of electrostatic correlations due to intervening polarizable beads, and a long-range Debye-Hückel net ion-ion interaction, subject to the charge-screening and dielectric-

screening effects of the bulk fluid.

Subsequently adopting a fluid model of polarizable, charge-neutral beads, the role of an applied electric field in shifting the phase stability of a binary dielectric fluid is explored. An electric field, \mathbf{E}_0 , is introduced, which interacts with polarizable beads, inducing a directional response in the average fluctuation behavior of the fluid, which is identified as its dielectric displacement, \mathbf{D} . Linearizing \mathbf{D} with respect to \mathbf{E}_0 leads to an explicit molecularly-based expression for the average dielectric constant of the fluid mixture, ϵ , through the relation $\mathbf{D} = \epsilon\mathbf{E}_0$. In the linear response regime, the composition dependence of ϵ completely specifies the applied field-dependent contribution to the miscibility of the fluid, which is cast in the form of a contribution χ_E to a Flory interaction parameter. Using a Gaussian approximation to the field theory, an analytical expression for χ_E is obtained, which illuminates the role of structural and electrostatic contrast between dissimilar molecules on their demixing behavior in the presence of an applied field. Specifically, contrast between wavevector-dependent, single-molecule correlation functions, $\hat{\Lambda}_{A/B}(k)$, emerges as a necessary ingredient for electric field-induced mixing, corresponding to $\chi_E < 0$; the form of each correlation function is determined by the structure of its corresponding molecular species. The character of χ_E is considered in three classes of binary systems: a binary simple fluid, a homopolymer blend, and a homopolymer solution. For each class of system, the predicted sign of χ_E is determined by examining the asymptotic behavior of each $\hat{\Lambda}_{A/B}$.

Due to their large size relative to the length-scale associated with individual monomers, microphase-forming block copolymers (BCPs) are often simulated at the mean-field level using self-consistent field theory (SCFT). To determine the dielectric behavior of a BCP melt, it is similarly appropriate to adopt a mean-field description of electrostatic behavior. With this in mind, a modified SCFT formalism is constructed, which simulates the behavior of a BCP of dielectric monomer species, interacting with an applied electric field; the model is subsequently used to determine the phase behavior of such a system. When different dielectric constants are assigned to each monomer type, the electric field penalizes the interfaces between species domains that are not parallel to the field. To minimize this penalty, each BCP microphase can be expected to adopt an associated preferred orientation relative to the electric field vector. The phase diagram is therefore constructed by comparing the free energy of each competing phase at its thermodynamically-preferred orientation. The stability regions of the sphere and network phases are found to shrink with increasing field strength, in favor of the disordered, cylindrical,

and lamellar phases. Additionally, the double gyroid network phase is more strongly disfavored than the orthorhombic Fddd network phase, such that the predicted region of stability for the Fddd phase is shifted to larger segregation strength (lower temperature).

Contents

1	Introduction and Motivation	1
1.1	Recent Progress in Field-Theoretic Simulation of Charged Soft Materials	1
1.2	Embedding Dielectric Behavior	3
1.3	Electric Field Effects	6
2	Field Theory for Polarizable Soft Media	13
2.1	Background	13
2.2	Polarizable Bead Model	16
2.2.1	Drude Oscillator Polarizability Model	16
2.2.2	Single-Bead Partition Function and Operators	20
2.2.3	Field-Theoretic Forces and Inhomogeneous Electrostatic Operators	22
2.2.4	Extension to Dielectric Polymer Melts and Solutions	23
2.3	Solution Methods	25
2.3.1	Mean-Field Theory	26
2.3.2	Gaussian Fluctuation Approximation	27
2.3.3	Field-Theoretic Simulations	29
2.3.4	Gibbs Ensemble Method for Incompressible Phase Coexistence	32
2.4	Systems of Interest	36
2.4.1	Binary Electrolyte Bead Fluid	36
2.4.2	Binary Dielectric Polymer Blend	46
3	Electric Field-Induced Critical Point Shift in Binary Dielectric Fluids	50
3.1	Background	50
3.2	Field Theory for a Binary Dielectric Fluid in an Applied Electric Field	54
3.2.1	Mean-Field Dielectric Behavior	57
3.2.2	Extended Gaussian Analysis: Coupled Fluctuation Modes	58
3.3	Dielectric Response	64
3.3.1	Dielectric Displacement	65
3.3.2	Linear Dielectric Behavior and the Dielectric Constant	67

3.3.3	Dielectric Fluid in a Fixed Displacement Field	74
3.3.4	Field-Dependent Miscibility Contributions	81
3.4	Results	84
3.4.1	Binary Dielectric Simple Fluid	84
3.4.2	Dielectric Homopolymer Blend	87
3.4.3	Dielectric Homopolymer Solution	90
3.5	Discussion	95
3.5.1	Concluding Remarks	100
3.5.2	Water Molecule and General Atomistic Single-Molecule Constructions	102
4	Field Effects in Phase-Separating Block Copolymer Systems	107
4.1	Background	107
4.2	Theory and Model	110
4.2.1	Dielectric Block Copolymer: Field-Theoretic Representation	110
4.2.2	Single-Chain Operators	112
4.2.3	SCFT Procedure	114
4.3	Results and Discussion	116
4.3.1	Orientation-Dependent Dielectric Response	116
4.3.2	Diblock Phase Stability in an Applied Electric Field	120
4.4	Conclusion	125
5	Concluding Remarks	129

Chapter 1

Introduction and Motivation

1.1 Recent Progress in Field-Theoretic Simulation of Charged Soft Materials

Over the past couple of decades, the use of statistical field theories has emerged as an attractive and flexible method for investigating the equilibrium behavior of fluctuating soft matter systems. Although field theories have found a particularly welcoming home in the simulation of polymer melts and solutions,^{1,2} one can derive a corresponding field theory for virtually any statistical model of interacting particles.

Using an exact mathematical transformation, a traditional model of explicitly interacting particles is recast as a model of interacting auxiliary fields, which decouple particle-particle pair interactions into equivalent particle-field interactions. When the species within the model contain multiple particles per molecule – presumably linked by some specified topology of bonded interactions – their associated *intramolecule* interactions are unaffected by the field transformation, retaining the structure of particle-particle pair potentials.

Freely-translating molecules, consisting of one or more particles, each subsequently enter the field theory through an independent configurational integral over their internal particle degrees of freedom, referred to as a *single-molecule partition function*. In addition to its associated bonded interactions, a molecule's partition function is also weighted by the interactions of its particles with the auxiliary fields, which act as an effective chemical potential environment due

to non-bonded particle pair interactions.

At the cost of relinquishing access to dynamical properties of a system, which would be readily apparent from the trajectory of an equivalent particle simulation, this field-theoretic representation circumvents several disadvantages typically associated with a particle model, including: large computational cost of enumerating all particle pair interactions, which becomes increasingly prohibitive for dense systems; packing frustration, which resists reconfiguration of particles in dense systems, slowing exploration of phase space, and further limiting the maximum particle count permitted in a simulation; and difficulty evaluating macroscopic properties that require explicit knowledge of the free energy (*e.g.* the chemical potential of a particle species requires free energy evaluations before and after an *insertion* move). Additionally, the existence of the single-molecule partition function prescribes a well-defined segregation between the internal molecular details of any species included in the system, and the character of the fluctuating field theory that exactly accounts for all non-bonded pair interactions between particles, irrespective of their assigned intramolecule attachments; this property has been heavily leveraged in the development of polymer field theories,³ and it paves a straightforward path for introducing molecules of arbitrary complexity into the field theory.

More recently, the study of charged soft material systems – and in particular, charged polymeric systems – has drawn significant interest, due in part to the potential industrial applications of such materials in devices utilized in the energy sector, including batteries,^{4,5} supercapacitors,⁶ and fuel-cell membranes.⁷ Charge-containing polymer systems are capable of exhibiting complex, fluctuation-induced phenomena, including phase separation into macroscopic, polymer-rich “coacervate phases”^{7,8} or segregation into spatially-repeating “micelle” complexes of oppositely-charged chain segments.^{9,10}

With applications such as these in mind, significant progress has been made in development of field theories for charged polymeric systems, using the “Model F”³ field-theoretic framework, which corresponds to a system of particles that interact *via* a non-specific repulsive contact potential, in addition to a long-range Coulomb interaction between any specified charges, which is screened by the dielectric constant of the background. Any charged particles that are introduced interact with a corresponding auxiliary field that acts as an effective electric potential. Due to the limitless extensibility of the single-molecule partition function,

this conceptually simple formalism has birthed several novel results in the characterization of fluctuating charged soft matter systems, including a pair of early papers^{11,12} that computed inhomogeneous density profiles for binary mixtures of oppositely charged polyelectrolyte pairs, illuminating architecture-dependent phase-separation behavior: in the limiting case of a binary homopolymer blend of oppositely charged monomer species, the chains aggregated into a macroscopic coacervate phase; alternatively, when each chain was covalently bonded to a homopolymer of charge-neutral monomers, the resulting blend of block copolymers instead phase-separated into periodically-repeating micelles, consisting of a dense core of charged monomers, surrounded by a corona of the charge-neutral end blocks. More recently, the phase behavior of coacervate-forming polymer solutions has been considered in detail, contrasting the behavior of a polyampholyte to that of a pair of oppositely charged polyelectrolytes,¹³ as well as considering in detail the role of charge sequence, valence, and other asymmetry effects in block polyampholyte systems.¹⁴

1.2 Embedding Dielectric Behavior

Although the Model F formalism has seen great previous success, illuminating self-consistently emergent charge physics, such as architecture-dependent Debye-like screening of charge correlations,^{12,15} one missing ingredient is the presence of explicitly polarizable species, which if included would alter the screening environment experienced by the fluctuating charged species, influencing emergent material properties. The polarizability of molecular species in a fluid is simultaneously responsible for: net attractive dipole-dipole interactions between individual molecules, dielectric screening of electrostatic correlations, and bulk dielectric behavior, among other electrostatic properties of fluids. Although it is common practice, and often sufficient, to phenomenologically include each of these behaviors when constructing a molecular model (*e.g.* imposing the r^{-6} attractive potential of a Lennard-Jones model, which accounts for the average London interaction between polarizable molecules¹⁶), doing so significantly limits the breadth of electrostatic phenomena that can emerge from the fluctuating behavior of the model.

For example, one can account for the average dielectric behavior of a charge-containing system by defining a screened Coulomb interaction between charges, which is reduced relative

to the vacuum Coulomb interaction by a factor of the average dielectric constant. Although this procedure will correctly specify the average Coulomb potential between charges, it will not account for any other behaviors that arise due to the polarizability of fluctuating molecular species within the fluid, including ion-dipole interactions that act on charged molecules, and local variations in the dielectric constant due to density fluctuations. If one instead constructed their model with explicitly polarizable molecular species that interacted electrostatically, all of these behaviors would emerge self-consistently.

Although one could in principle construct and simulate such a particle model of explicitly polarizable molecules, the requirement that all fluctuating dielectric species be represented as explicit particles essentially forbids the use of an implicit solvent model; this would render virtually all liquid-state models dense. Consequently, a field theory representation, wherein computational cost doesn't increase with particle density, is particularly well-suited for simulation of this proposed class of fluid models.

In the present thesis, I discuss development of a field theory model of explicitly polarizable molecular species, generated by introducing polarizable and/or dipolar "beads" into the Model F field-theoretic structure, which carry a pair of equal and opposite partial charges, and consequently possess a net dipole moment. By further leveraging the character of the single-molecule partition function, these dipole partial charges enter as bound particles of each molecular species, and the resulting field theory retains the Model F structure, with a single electrostatic field that interacts with all charges within the system, irrespective of designation. Having only prescribed an unscreened Coulomb pair interaction between charges, I show that this fluctuating model of polarizable, and optionally charged, molecular species self-consistently gives rise to dipole-dipole and ion-dipole net attractions, dielectric screening of electrostatic correlations, and macroscopic dielectric response to an applied electric field. The thesis is structured as follows:

In Chapter 2, I introduce the polarizable molecular model and its associated field theory.¹⁷ The molecular species are assigned a net polarization *via* partial charges affixed to each bead's center of mass, in addition to an optional unpaired charge, which if included gives the bead the character of an electrolyte. The partial charges are tethered to the center of mass by a harmonic spring, corresponding to induced-dipole behavior. Since the Coulomb interaction

is infinite at contact, with corresponding singularities in the free energy and thermodynamic properties of a fluid of charged particles, it is necessary to smear all charges with a Gaussian, Γ , which has width a . This procedure has been found to render properties obtained from a field theory convergent in the continuum limit,^{18,19} and we will find here that short-range average interactions due to electrostatic fluctuations will yield properties that are proportional to a^{-n} , where n is a positive integer.

I define the structure of the single-bead partition function associated with such a molecule, which enumerates the interaction of each of the bead’s charges with the Model F electrostatic field. In the present induced-dipole case, the statistical behavior of the bead’s partial charges can be collectively approximated by a single parameter – which I identify as the bead’s *polarizability* – that determines the linear correspondence between the bead’s average polarization response, and the local electric field at the bead’s center of mass. I further demonstrate that these polarizable beads can be linked into dielectric polymer chains using traditional polymer linker models, and that the specified connectivity properties enter the field theory *via* the structure of an associated *single-chain partition function*.

I proceed in the later sections of the chapter by implementing a procedure described by Wang,²⁰ wherein a Gaussian fluctuation analysis was applied to a Model F field-theoretic framework that described a fluid of small-molecule electrolytes, revealing qualitative electrostatic phenomena that arose due to fluctuations in the local electric potential, such as a Born self-energy of ions that depends on the local dielectric environment. Applying this approach to the corresponding field theory for a homogenous binary fluid of polarizable electrolyte beads, I show that electrostatic fluctuations self-consistently give rise to: wavevector-dependent dielectric screening of electrostatic correlations, short-range *van der Waals* attractions between fluctuating polarizable beads, and long-range *Debye-Hückel* interactions between the free charges on beads, among other electrostatic phenomena. Applying the same procedure to a field theory for a binary blend of dielectric polymer chains, I demonstrate that to Gaussian order, the dielectric screening behavior of a fluid is insensitive to molecular architecture properties, depending purely on the dielectric properties prescribed at the single-bead level.

1.3 Electric Field Effects

Externally-applied electric fields have the attractive property of directly interacting with local charges that exist throughout the chemical structure of any molecular species, which renders them – in principle – a universally-applicable means by which to alter the equilibrium and/or dynamical properties of a fluid. Non-electrolyte molecular species (*i.e.* possessing no net charge) polarize in the presence of an electric field, and the average linear response of a fluid of such molecules is quantified by its *dielectric constant*, which is a well-accepted property of materials.²¹

Although dielectric response is evidently a universal behavior exhibited by any non-electrolyte species in the presence of an applied electric field, the dielectric constant is an average, macroscopic material property, which does not provide any information about the local, microscopic responses at the scale of individual molecules. Consequently, direct prescription of a molecule’s dielectric constant when constructing a model constitutes an *implicit coarse-graining* of all length-scales of electrostatic phenomena, and it is therefore only appropriate for predicting electric field-induced changes in properties of the fluid that are apparent at the mean-field level. Beyond the mean-field level of description, it is necessary to impose dielectric properties at the scale of individual molecules – where the level of coarse-graining is determined by the sophistication of the imposed molecule-electric field interaction, but in all cases is restricted to single-molecule details – elucidating the field-induced fluctuation behavior that gives rise to the average dielectric response of the fluid, in addition to any other field-induced shifts in average material properties.

For example, it has been shown that the dielectric constant of a binary mixture of two molecular species is in general a nonlinear function of its composition, $\epsilon(\phi)$.^{22–26} Although some universal approximate behaviors can give rise to such a nonlinearity – such as imposing the Clausius-Mosotti relation,²⁷ which identifies a nonlinear relation between the dielectric constant of a dilute fluid and the average molecular polarizability of its constituent species, or by enforcing the correspondence between a material’s dielectric constant and its optical properties²⁸ – the dielectric constants of the two pure species contained in a mixture provide no information about the composition-dependence of its dielectric behavior. This composition

dependence ultimately derives from the field-dependent response of fluctuating, interacting dielectric molecular species.

The composition dependence of the dielectric constant of a binary fluid mixture is also known in theory to determine the magnitude and direction of an electric field-induced shift of the mixture’s critical point, where ($\epsilon''(\phi) < 0$) corresponds to a field-dependent response that favors *mixing*.²³ Although some existing experimental literature^{22,23} has directly compared the field-induced critical point shifts of binary fluid mixtures to the composition dependence of their observed dielectric constants, the validity of this assumed correspondence remains relatively unscrutinized; there is evidently a need for a molecularly-informed model of binary dielectric mixtures, which would permit the calculation of mixtures’ dielectric constants from prescribed molecular properties.

In Chapter 3, I extend the field theory detailed in the preceding chapter by including a uniform applied electric field, \mathbf{E}_0 , that acts on the beads of the fluid. Apart from a reference term due to the vacuum free energy contribution of \mathbf{E}_0 , the Model F structure of the field theory is preserved, and the applied field enters as a simple shift in the local electric field experienced by the beads, evident in the structure of the resulting single-molecule partition function. By imposing a simple isotropic polarizability response of beads to the local field, the corresponding model I derive specifies only the most general average properties of a polarizable molecule, consistent with an overarching desire to ascertain universal, chemistry-independent dielectric phenomena. It should be noted, however, that finer molecular details – such as anisotropy and/or higher-order multipole response due to the relative placement of partially charged moieties – can be readily introduced *via* appropriate additions to the structure of the single-molecule partition function. I also define species-dependent smearing functions, $\Gamma_{A/B}$, with corresponding widths $a_{A/B}$, which act on the center of mass and charges of each respective bead type, and which impart dissimilar beads with contrasting correlation behavior when $a_A \neq a_B$.

Within this statistical model, the applied field vector \mathbf{E}_0 is included as a fixed state variable, and I identify the dielectric displacement, \mathbf{D} , as its thermodynamically-conjugate observable property, obtained by taking an \mathbf{E}_0 derivative of the corresponding free energy; further linearizing \mathbf{D} with respect to \mathbf{E}_0 yields the form $\mathbf{D} = \epsilon\mathbf{E}_0$, where ϵ is the observed dielectric constant

of the fluid. The dielectric constant is thus identified as an average thermodynamic property deduced from the field-dependent behavior of the fluctuating fluid, in the limit of vanishing applied field strength.

I also show that one can construct an analogous field theory for a dielectric fluid between two infinite plates of fixed surface charge density, which generate a uniform displacement field \mathbf{D}_0 that acts on the medium. Within this *fixed-displacement ensemble*, the average electric field can be obtained from a \mathbf{D}_0 derivative of the relevant free energy, and an observed dielectric constant can subsequently be inferred from the linear relation, $\mathbf{E} = \epsilon^{-1}\mathbf{D}_0$. I show that the earlier-specified *fixed-electric field ensemble* is correctly obtained from the present fixed- \mathbf{D}_0 ensemble by an appropriate Legendre transform, which physically corresponds to connecting the charged plates to a battery, fixing the electric potential drop – and consequently the average electric field – between them.

When the linearized expression for \mathbf{D} is rendered accurate by a choice of fixed \mathbf{E}_0 with sufficiently small magnitude, ϵ becomes the only non-fixed quantity that enters the electric field free energy contribution; consequently, one can deduce the electric field-dependence of any average property of the fluid by taking derivatives of the dielectric constant with respect to the appropriate state variable of the system’s free energy (*e.g.* the electric field-dependence of the fluid’s heat capacity will be proportional to $T(\partial^2\epsilon/\partial T^2)$, for temperature T).

Similarly, taking two composition derivatives of ϵ for a binary mixture identifies the sign and magnitude of an electric field-induced shift in the stability limit (spinodal). I subsequently define an expression, χ_E , which quantifies the field-dependent contribution to an effective Flory interaction parameter between the two molecular species of the mixture; its form specifies the correspondence between underlying molecular properties and an observed field-induced shift in phase stability. From the expression for χ_E obtained by a Gaussian approximation, which integrates over the contribution due to each fluctuation “mode”, with associated wavevector \mathbf{k} , one can determine that χ_E will be strictly positive – yielding electric field-induced demixing – in the absence of any contrast in each species’ molecular structure. The molecular structure of each species determines fluctuation behavior in the fluid according to wavevector-dependent correlation functions, $\hat{\Lambda}_{A/B}(k)$; electric field-induced mixing, corresponding to $\chi_E < 0$, is only observed for certain ranges of species properties, and in all cases requires structural contrast

($\hat{\Lambda}_A \neq \hat{\Lambda}_B$).

I subsequently consider the character of χ_E – which is proportional to $\epsilon''(\phi)$ and has the same sign – in three classes of binary mixtures, whose field-dependent miscibility responses have been considered experimentally in the literature: a binary simple fluid,^{22,23} a homopolymer blend,^{29–32} and a homopolymer solution.³³ In each system, sufficient contrast in the associated lengths, $a_{A/B}$, of each species’ smearing functions can give rise to field-induced mixing. In addition to smearing, the conformational entropy of a polymer chain also contributes to its correlation behavior – selectively enhancing or suppressing correlations that have wavelength $\ell = 2\pi k^{-1}$ significantly larger or smaller than its Kuhn length, respectively. Consequently, polymer blend systems of sufficient conformational asymmetry can exhibit field-induced mixing, even in the absence of any contrast due to species-dependent smearing functions. In a polymer solution, solute molecules will admit relatively larger correlations for ℓ less than the polymer’s Kuhn length, b , but will be small relative to the polymer chain’s contribution when $\ell \gtrsim b$; when both species have the same smearing length, a , the relative weight of these two regimes of structural asymmetry is determined by a comparison of a and b .

Finally, I directly compare these qualitative observations to corresponding results from experimental literature. Interestingly, the majority of experimental results found to contradict my qualitative predictions (*i.e.* systems that exhibited field-induced mixing, whereas my model predicts field-induced demixing for any sensibly-parametrized representation of each system) proved to be chemistry pairs that are known in the literature to exhibit hydrogen bonding behavior. Further noting that $\epsilon(\phi)$ has been measured in the literature for several hydrogen-bonding chemistry pairs^{24–26} – revealing broad, easily-identified ranges of compositions that satisfy $\epsilon''(\phi) < 0$ – I hypothesize that the predictive scope of my isotropic model of molecular polarizability is unsurprisingly limited to mixtures whose dielectric behavior is at most weakly-dependent on anisotropic correlations; the highly-anisotropic, highly-localized dipole-dipole coupling behavior associated with hydrogen-bonding interactions³⁴ evidently violates that restriction. Inspired by the success of a simple dipole-coupling model that predicted $\epsilon(\phi)$ for the hydrogen-bonding mixture H₂O-DMSO, to good agreement with experiment,²⁶ I conclude the chapter by discussing proposed modifications to the structure of the single-molecule partition function, which anisotropically couple a molecule’s net dipole moment to the nearby

behavior of the electric field, giving rise to desirable dipole correlations.

Throughout Chapter 3, I discuss the origin and structure of a thermally averaged dielectric constant, requiring dielectric properties to be assigned at the scale of single beads, so that their emergent fluctuation behavior can be observed. However, when one is only interested in properties that emerge in the absence of fluctuations, it is sufficient to impose dielectric behavior at the continuum scale, with the understanding that the literature value of any chemistry’s dielectric constant was obtained from an experimental measurement of the average dielectric behavior of a fluctuating material.

Although such a mean-field approach yields a trivial homogeneous response when applied to Model F field theories, a mean-field description of dielectric fluids can nevertheless yield novel, non-trivial responses to an applied field when coupled to a field theory that imposes species-dependent repulsive interactions, generating spatially inhomogeneous mean-field fluid configurations. These configurations are determined using the well-known self-consistent field theory (SCFT) simulation procedure, which has proven especially useful for simulating high molecular weight block copolymer (BCP) melts.^{3,35} BCP melts consist of a single chain type, with multiple “blocks” of dissimilar monomer types covalently bonded sequentially. Due to the immiscibility of differing monomers, BCPs are known to demix into *microphases* that consist of repeating patterns of domains with contrasting composition; by explicitly prescribing contact pair repulsions between dissimilar monomer pairs, one can generate models for BCP systems that predict microphase separation, even at the mean-field level of simulation.

In the absence of an underlying molecular model for the dielectric behavior of fluid species, SCFT simulations of dielectric fluids in an electric field require a phenomenologically-prescribed *closure* that couples the spatially-inhomogeneous electric field – related to a corresponding electric potential $\psi(\mathbf{r})$ by the expression $-\nabla\psi(\mathbf{r})$ – to a fluid’s instantaneous configuration; each molecular species then interacts locally with this electric field, according to its average dielectric response, conveniently quantified by its literature dielectric constant. The well-accepted closure for field theories of this class³⁶ is performed by constructing an inhomogeneous profile for the local dielectric constant, $\epsilon(\mathbf{r})$, from a linear mixing of the species’ pure-phase dielectric constants, weighted by their local volume fraction. The inhomogeneous electric field is then required to obey Gauss’ Law, $\nabla \cdot [\epsilon(\mathbf{r})\nabla\psi(\mathbf{r})] = 0$; further requiring that the average value of

$-\nabla\psi(\mathbf{r})$ be \mathbf{E}_0 serves to insert the prescribed applied field vector, and also uniquely specifies $-\nabla\psi(\mathbf{r})$ as a solution of the PDE.

Interestingly, this phenomenologically-imposed electrostatic model is equivalently obtained by taking the mean-field limit of the molecularly-informed field theory detailed in Chapter 3, provided no Gaussian smearing is imposed. The mean-field condition for the corresponding electrostatic field reveals the same Gauss’ law structure, where the local dielectric constant is obtained from a linear mixing of each bead species’ polarizability, weighted by its local density profile.

In Chapter 4, I report a study of the phase behavior of a diblock copolymer melt in the presence of an applied electric field. Systems of this class have been found in literature^{37,38} to undergo alignment of their microstructure along the electric field vector, and previous theoretical work^{39–42} has successfully simulated this behavior at the mean-field level using the above electrostatic model, in tandem with a “Model E”³ field theory for an incompressible block copolymer melt, with a contact repulsion of strength χ between dissimilar monomer types.

Using this same formalism, I specify contrasting dielectric constants for each of the two monomer species (A and B), as well as an applied field vector, \mathbf{E}_0 . For a block copolymer melt with these properties, in the presence of the applied field, I generate a phase diagram, which graphically depicts the regions of stability associated with each of the canonical block copolymer microphases,^{1,2,35,43–47} in the 2-dimensional space $(f, \chi N)$, where f is the volume fraction of A -type monomers in the melt, χ is the imposed contact repulsion between A and B monomers, and N is the degree of polymerization of the chain. Comparing my phase diagram to its unperturbed ($\mathbf{E}_0 \rightarrow \mathbf{0}$) analog, which reproduces the well-known phase diagram originally obtained by Matsen,³⁵ I observe that an applied electric field shifts phase boundaries in favor of microphases that are more strongly anisotropic; in addition to favoring the trivially anisotropic cylinder and lamellar phases, an applied field also favors the orthorhombic Fddd network phase relative to the cubic double gyroid phase. The latter result is found to occur because the Fddd phase admits a stronger dependence of its electrostatic free energy on the orientation of \mathbf{E}_0 ; this property permits Fddd to adopt a minimizing orientation that renders its electric field free energy contribution smaller than that of double gyroid, which stabilizes the Fddd phase when the unperturbed relative stability of the otherwise-preferred double gyroid phase is sufficiently

small.

Chapter 2

Field Theory for Polarizable Soft Media

2.1 Background

Inhomogeneous, charge-containing soft fluids constitute a wide range of physical systems, including ionomer melts,⁴⁸ block copolymer architectures containing an arbitrary combination of charge-neutral blocks and blocks carrying a net charge of either sign,⁹ and polymerized ionic liquids.⁴⁹ Due to the presence of strong fluctuations at the length-scale of individual charged molecular species, the use of classical statistical thermodynamic models has proven to be the standard approach for predicting the equilibrium behavior of these materials. Indeed, many of the complex electrostatic phenomena known to appear in these systems have been successfully predicted using either explicit particle models of charged species¹⁵ or an equivalent Model F field-theoretic representation.^{11,13,14} The latter technique employs an exact transformation that decouples the pairwise interactions of individual particles, along with their associated fluctuating configurational degrees of freedom, into interactions between fluctuating fields.³ There has been great success in applying this method to soft media systems possessing novel electrostatic properties, including fluctuating simulations of two-component polyelectrolyte solutions,^{11–13} and solutions containing a net-charged block polyampholyte chain in the presence of explicitly-accounted simple counterion molecules.¹⁴

Although these fluctuating field-theoretic simulations (FTS) successfully illuminate many novel behaviors, such as the experimentally-observed coacervation and micellization phase separation phenomena, one limitation of the Model F field theory employed in these studies is the assumption of uniform bulk dielectric behavior; due to this approximation, the coexisting phases identified by the field theory necessarily possess the same permittivity, and consequently the same Coulomb interaction between charges. In a real system, the polarization of polymer species and any solvent molecules generates the local dielectric environment, so that coexisting phases will in general have contrasting average permittivities, with corresponding shifts in the local charge physics. For example, in an aqueous solution of a coacervate-forming charged polymer species, exclusion of strongly dipolar water molecules from the polymer-rich coacervate phase will reduce its permittivity relative to the dilute, water-rich phase.

It is also known in the literature⁵⁰ that the Born solvation energy of an ion is inversely proportional to the local permittivity of its environment, so that the contrast in permittivity between two coexisting phases of an inhomogeneous fluid will induce a preferred partitioning of any charged species into the higher dielectric domains. Without knowledge of the permittivity contrast between the two phases, this effect cannot be included in the behavior of the system.

In the ongoing work of Wang *et. al.*,^{20,51,52} significant progress has been made in illuminating this behavior using a Model F field theory. In one such study,²⁰ Wang employs a *smearred* representation of electrolyte monopole charges, which suppresses electrostatic interactions below some specified small length-scale, effectively imparting these charged molecules with a finite size. Using this model, Wang derives a self-energy for an electrolyte molecule that is of the Born Solvation⁵⁰ form, which is rendered finite by the smearing procedure, and which is sensitive to the position of the molecule within an inhomogeneous dielectric medium $\epsilon(\mathbf{r})$. It should be noted, however, that this dielectric profile is externally imposed in Ref. 20, presupposing knowledge of $\epsilon(\mathbf{r})$, so that $\epsilon(\mathbf{r})$ must be assumed non-fluctuating, or must be coupled to the behavior of the fluid by some phenomenological closure.

In a subsequent study,⁵¹ Wang proposes an alternative field theory, for which the configuration of a fluid of explicit water molecules is constructed from particles possessing both permanent and induced dipoles. By breaking the symmetry of the fluid with the introduction of a single unpaired point charge at the origin, the corresponding configuration of the water

molecules will have an inhomogeneous equilibrium configuration that can be computed with SCFT; an associated spherically-symmetric dielectric profile, $\epsilon(r)$, is then computed, giving the local dielectric constant at a distance r from the ion center. Integrating over this inhomogeneous dielectric environment, Wang computes the Born solvation energy of several simple electrolytes in water, to good agreement with experimental values, demonstrating the predictive power of the Model F field theory representation for dielectric behavior.

We note that Wang’s procedure considers an isolated, non-fluctuating system consisting of a single point charge, neglecting the influence of charge-charge interactions, as well as fluctuation-induced dipole-dipole interactions between water molecules. To simulate systems outside the reach of this regime, where pair interactions between all species give rise to the observed properties of the system, we combine Wang’s single-molecule structure for a dielectric molecule with the highly general structure of the Model F electrostatic field theory, introducing a molecular “bead” unit, which is assigned a polarizability using a similar Drude oscillator model for its fluctuating paired partial charges; we also adopt the charge smearing procedure identified in Ref. 20. Generating the resulting field theory from a simple particle model that prescribes an unscreened Coulomb pair interaction between both *paired* and *unpaired* molecular charges, each instantaneous system configuration has a corresponding inhomogeneous dielectric profile, which self-consistently determines the character of electrostatic fluctuations within the fluid. We further show that these polarizable and/or charged beads can be joined into dielectric polymer/polyelectrolyte chains of arbitrary architecture, using any traditional polymer linker model and associated bonded interaction.

Representing a simple binary mixture of polarizable electrolyte molecules within this general electrostatic model, we show that the behavior of the electrostatic auxiliary field admits a close analogy to continuum dielectric theory, with fluctuating *field-theoretic operators* that include a non-local permittivity function, $\tilde{\epsilon}(\mathbf{r}, \mathbf{r}')$, which specifies the dielectric screening of correlations between positions \mathbf{r} and \mathbf{r}' , due to intervening polarizable beads. Attacking the field theory with a simple Gaussian approximation, we show that electrostatic fluctuations give rise to a long-ranged average interaction between electrolyte charges that has the structure of a Yukawa potential,⁵³ embedding screening effects due to the bulk dielectric screening behavior of the fluid, in addition to screening *via* the Debye-Hückel coordination behavior of electrolytes;

the interaction contributes to the osmotic pressure of the fluid with the expected scaling in ionic strength.⁵⁴ One can also identify the presence of two short-range, partially-screened average pair interactions between beads, due to ion-dipole and dipole-dipole interactions between the respective electrostatic properties of two beads; for a dilute fluid, each interaction gives a leading-order osmotic pressure contribution that has the form of a second Virial coefficient. The dipole-dipole interaction can be further shown to induce phase-separation of the fluid when the two bead types have contrasting polarizabilities, parametrized as a Flory-Huggins net repulsion of magnitude χ , consistent with existing electrostatic immiscibility models.⁵⁵ Further considering a binary blend of dielectric homopolymer chains, with no electrolyte properties specified, we show that at Gaussian order, the character of density fluctuations is dependent on the connectivity properties of each chain – correctly recovering the behavior derived by Edwards⁵⁶ in the concentrated regime – but that electrostatic fluctuations are insensitive to molecular architecture, emanating from interactions that occur at the scale of individual polarizable beads.

2.2 Polarizable Bead Model

2.2.1 Drude Oscillator Polarizability Model

We begin by introducing a molecular “bead” unit, which carries 3 charges in total, one is a free charge on its center of mass, and the others are paired partial charges of equal, opposite valence. The latter charges are affixed to the bead by a spring of strength K .

The fluid consists of n beads, such that its electrostatic potential energy can be obtained from summing the bare Coulomb interactions of all charge pairs,

$$\beta U_e(\mathbf{r}^{3n}) = \frac{\ell_B}{2} \sum_i^{\text{charges}} \sum_j^{\text{charges}} \frac{q_i q_j}{|\mathbf{r}_i - \mathbf{r}_j|}, \quad (2.1)$$

where ℓ_B is the vacuum Bjerrum length, and we employ CGS electrostatic units ($4\pi\epsilon_0 = 1$).

The internal spring potential of each bead enters the potential of the system according to,

$$\beta U_k(\mathbf{r}^{3n}) = \sum_{i=1}^n \frac{K}{2} |\mathbf{s}_i|^2, \quad (2.2)$$

where \mathbf{s}_i gives the separation vector between the partial charges of bead i .

To regularize the field theory, we replace the point-like behavior of each charge of the molecule with a Gaussian smearing function, such that we can define a smeared microscopic charge density as

$$\bar{\rho}_e(\mathbf{r}) = \sum_i^{\text{charges}} q_i \Gamma(\mathbf{r} - \mathbf{r}_i) \quad (2.3)$$

where $\Gamma(\mathbf{r}) \equiv (2\pi a^2)^{-3/2} e^{-r^2/(2a^2)}$ is a Gaussian with characteristic length a , which serves to impose a finite length-scale for the bead size. In the limit $a \rightarrow 0$, the Dirac delta function is recovered and $\bar{\rho}_e(\mathbf{r})$ becomes a microscopic density representation of the point charges of the beads.

The electrostatic potential energy due to the smeared charges of the fluid can be written as

$$\beta U_e(\mathbf{r}^{3n}) = \frac{\ell_B}{2} \int d\mathbf{r} \int d\mathbf{r}' \frac{\bar{\rho}_e(\mathbf{r}) \bar{\rho}_e(\mathbf{r}')}{|\mathbf{r} - \mathbf{r}'|}. \quad (2.4)$$

Here, $\ell_B = \beta e^2$ is the vacuum Bjerrum length, e the elementary charge, and $\beta = (k_B T)^{-1}$ the reciprocal thermal energy scale.

The use of a smeared representation for charges regularizes the theory, such that electrostatic interactions are finite at contact. We will later show that this is a necessary step in rendering short-ranged contributions to the osmotic pressure and single-molecule self energy finite.

We also introduce a smeared microscopic bead density, defined as

$$\bar{\rho}(\mathbf{r}) = \sum_{i=1}^n \Gamma(\mathbf{r} - \mathbf{r}_i), \quad (2.5)$$

so that the bead center of mass carries the same smearing as its charges, and any spherically symmetric potential of mean force $u(r)$ will act on the smeared beads according to

$$\beta U_r = \frac{\beta}{2} \int d\mathbf{r} \int d\mathbf{r}' \bar{\rho}(\mathbf{r}) u(|\mathbf{r} - \mathbf{r}'|) \bar{\rho}(\mathbf{r}') \quad (2.6)$$

For the present theoretic description, we choose the simple case of a contact excluded volume potential, scaled by a parameter u , to resist the attractive electrostatic interactions that will

emerge in fluctuating systems. It is given by

$$u(r) = k_B T u[\delta(r)]^3 \quad (2.7)$$

where the 1-dimensional Dirac delta function is cubed to match the dimensionality of the volume integrals in Eq. 2.6. Inserting this form for $u(r)$ into Eq. 2.6 recovers

$$\beta U_r = \frac{u}{2} \int d\mathbf{r} [\bar{\rho}(\mathbf{r})]^2 \quad (2.8)$$

Representing the bead fluid in the Canonical ensemble, the partition function is given by

$$\mathcal{Z}(n, V, T) = \mathcal{Z}_0 \int d\mathbf{r}^{3n} e^{-\beta(U_e + U_k + U_r)} \quad (2.9)$$

with

$$\mathcal{Z}_0 = \frac{V^n}{n!} \quad (2.10)$$

a translational entropy (ideal gas) contribution for indistinguishable beads.

The particle theory can be reexpressed as a corresponding field theory, applying a Hubbard-Stratonovich (HS) transform for each type of pair interaction,³ which introduces two auxiliary fields $\varphi(\mathbf{r})$ and $w(\mathbf{r})$ that decouple electrostatic and excluded volume interactions, respectively. The transformation reveals a form of the partition function that is given by a functional integral over all configurations of each field:

$$\mathcal{Z}(n, V, T) = \frac{\mathcal{Z}_0}{\mathcal{Z}_\varphi \mathcal{Z}_w} \int \mathcal{D}\varphi \int \mathcal{D}w \exp(-H[\varphi, w]) \quad (2.11)$$

where $H[\varphi, w]$ is an effective Hamiltonian given by

$$H[\varphi, w] = \frac{1}{2} \int d\mathbf{r} \left[\frac{1}{4\pi\ell_B} |\nabla\varphi(\mathbf{r})|^2 + \frac{1}{u} [w(\mathbf{r})]^2 \right] - n \ln Q[i\bar{\varphi}, i\bar{w}] \quad (2.12)$$

and $\mathcal{Z}_\varphi, \mathcal{Z}_w$ are normalization factors that arise from the HS transforms, and are given by

$$\mathcal{Z}_\varphi = \int \mathcal{D}\varphi \exp\left(-\frac{1}{8\pi\ell_B} \int d\mathbf{r} |\nabla\varphi(\mathbf{r})|^2\right) \quad \mathcal{Z}_w = \int \mathcal{D}w \exp\left(-\frac{1}{2u} \int d\mathbf{r} [w(\mathbf{r})]^2\right), \quad (2.13)$$

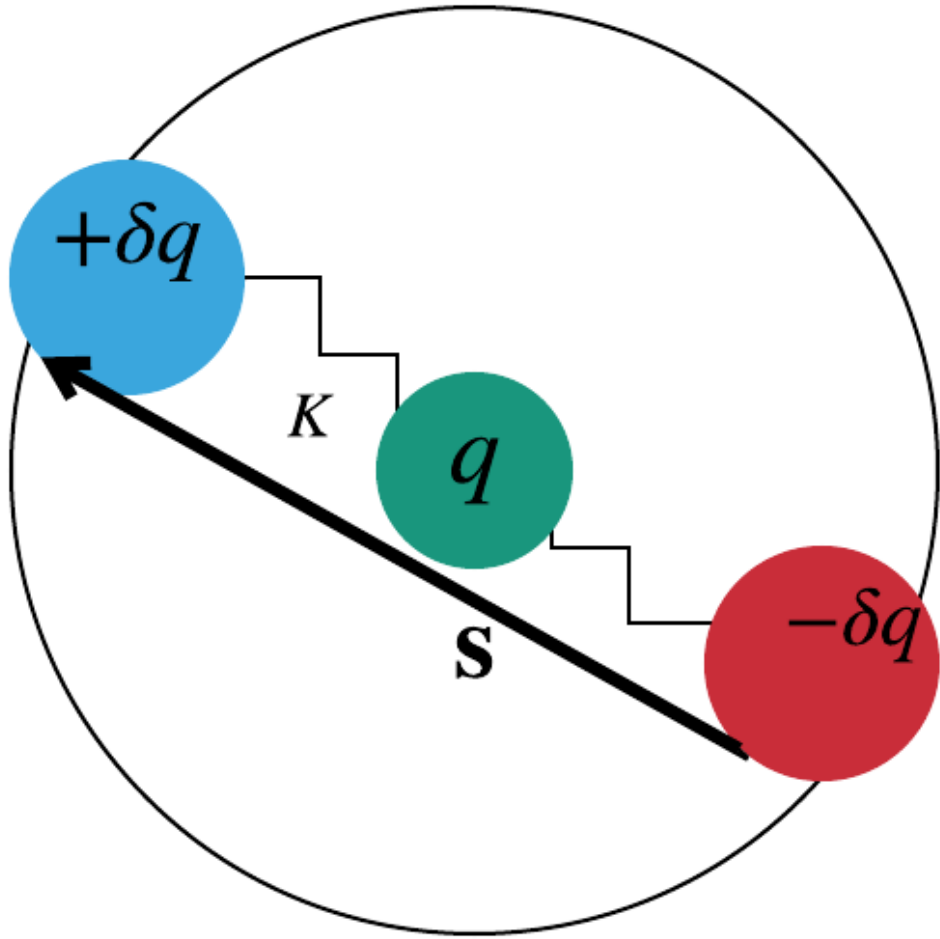


Figure 2.1: Diagram of the Drude oscillator bead. A free charge of valence q sits at the bead center of mass. The partial charges have valence $\pm\delta q$, have a separation vector \mathbf{s} , and are tethered to the bead center of mass by a spring of strength K .

which enforce the normalization, $\mathcal{Z}(0, V, T) = 1$.

The object $Q[i\bar{\varphi}, i\bar{w}]$ is the single-molecule partition function, obtained by considering a single representative bead molecule interacting with effective fields $i\bar{\varphi}, i\bar{w}$. It has previously been shown that smearing the charge and bead densities (Eqs. 2.3,2.5) in the preceding particle-based theory is equivalent to subjecting an unsmeared bead to the complex-valued, smeared fields $i\bar{\varphi} = i \int d\mathbf{r}' \Gamma(\mathbf{r} - \mathbf{r}') \varphi(\mathbf{r}')$ and $i\bar{w} = i \int d\mathbf{r}' \Gamma(\mathbf{r} - \mathbf{r}') w(\mathbf{r}')$.¹⁸ Discussion of the form of $Q[i\bar{\varphi}, i\bar{w}]$ is deferred to the following section.

The Helmholtz free energy is then directly obtained from the expected thermodynamic connection formula,

$$\beta \mathcal{A}(n, V, T) = -\ln \mathcal{Z} \quad (2.14)$$

We conclude the present section by emphasizing the modularity of the field theory that is evident in the structure of Q : one can introduce any internal constraints to the molecules that make up the fluid (e.g. connecting beads into coarse-grained polymer chains) and the field theory will retain the same Model F structure, provided no additional non-bonded interactions are added.

2.2.2 Single-Bead Partition Function and Operators

If we assume that the partial charges of each bead fluctuate symmetrically about its center of mass, we need only integrate over two degrees of freedom to obtain the bead's partition function: the center of mass position of the bead, \mathbf{r} , and the separation vector between the paired partial charges, \mathbf{s} . Choosing the valence of the free charge at the bead center of mass to be q and the partial charges to have valence $\pm\delta q$, the partition function for the bead is given by

$$Q[i\bar{\varphi}, i\bar{w}] = \frac{K^{3/2}}{(2\pi)^{3/2} V} \int d\mathbf{r} \int d\mathbf{s} e^{-(K/2)|\mathbf{s}|^2 - i\bar{w}(\mathbf{r}) - iq\bar{\varphi}(\mathbf{r}) - i\delta q[\bar{\varphi}(\mathbf{r}+\mathbf{s}/2) - \bar{\varphi}(\mathbf{r}-\mathbf{s}/2)]} \quad (2.15)$$

where the pre-factor normalizes the integral so that $Q[0, 0] = 1$. The first term in this Boltzmann factor is the internal energy of the Drude oscillator spring, and the second term originates from the interaction of the bead center of mass with the smeared chemical potential field $i\bar{w}(\mathbf{r})$.

The remaining terms give the interaction of each of the charges of the bead with the smeared electrostatic field $i\bar{\varphi}(\mathbf{r})$.

If we approximate $i\bar{\varphi}(\mathbf{r})$ as slowly-varying, so that its spatial derivatives are small relative to $K^{1/2}$, the latter two (dipole) terms in Eq. 2.15 can be expanded about \mathbf{r} to $O(|\mathbf{s}|^2)$, the integral over \mathbf{s} can be performed analytically, and a simplified form for $Q[i\bar{\varphi}, i\bar{w}]$ obtained:

$$Q[i\bar{\varphi}, i\bar{w}] \approx \frac{1}{V} \int d\mathbf{r} e^{-i\bar{w} - iq\bar{\varphi} - (\alpha/2)|\nabla\bar{\varphi}|^2} \quad (2.16)$$

where $\alpha \equiv (\delta q)^2/K$ is the *polarizability* of the molecule. Although the present field theory is valid for either representation of $Q[i\bar{\varphi}, i\bar{w}]$, the simpler form specified in Eq. 2.16 proves to be more convenient.

An important and ubiquitous concept within statistical field theories is the existence of spatially inhomogeneous single-molecule operators, which are obtained by taking a functional derivative of $\ln Q$ with respect to one of the fluctuating fields. The resulting operator will have the character of a spatially varying density that is thermodynamically conjugate to that field.

In the present polarizable field theory, two such densities exist: Taking a $w(\mathbf{r})$ derivative of $\ln Q$ yields an operator for the local number density of beads, given by,

$$\tilde{\rho}(\mathbf{r}; [\phi, w]) = -n \frac{\delta \ln Q[i\bar{\phi}, i\bar{w}]}{\delta i\bar{w}(\mathbf{r})} = \frac{n}{QV} e^{-i\bar{w} - iq\bar{\phi} - (\alpha/2)|\nabla\bar{\phi}|^2}, \quad (2.17)$$

illuminating the instantaneous density profile of beads, given field configurations φ and w .

Similarly, one can define a charge density operator that is conjugate to the fluctuating electrostatic field $\varphi(\mathbf{r})$, given by

$$\begin{aligned} \tilde{\rho}_e(\mathbf{r}; [\phi, w]) &= -n \frac{\delta \ln Q[i\bar{\phi}, i\bar{w}]}{\delta i\bar{\phi}(\mathbf{r})} = \tilde{\rho}_f(\mathbf{r}; [\phi, w]) - \beta e \nabla \cdot \tilde{\mathbf{P}}(\mathbf{r}; [\phi, w]) \\ &= q\tilde{\rho}(\mathbf{r}; [\phi, w]) - \nabla \cdot [\alpha\tilde{\rho}(\mathbf{r}; [\phi, w])[-i\nabla\bar{\varphi}(\mathbf{r})]] \end{aligned} \quad (2.18)$$

where $\tilde{\rho}_f(\mathbf{r}; [\phi, w]) = q\tilde{\rho}(\mathbf{r}; [\phi, w])$ is a free charge density operator that arises from the free/monopole charge located at each bead's center of mass, and $\tilde{\mathbf{P}}$ is a polarization density operator that is conjugate to the local electric field, $-i\nabla\bar{\varphi}$, arising from the induced-dipole partial charges of each bead.

2.2.3 Field-Theoretic Forces and Inhomogeneous Electrostatic Operators

In addition to illuminating the behavior of beads at instantaneous field configurations, these bead density operators enter the so-called “field forces”, which are obtained by taking a field functional derivative of H , and dictate the fluctuation behavior of each field. Although these spatially inhomogeneous operators are complex-valued and act on field degrees of freedom, one can identify a clear analogy to the real-valued Hamiltonian mechanics of a fluctuating particle model, wherein the force on a given particle can be obtained by differentiating the system’s Hamiltonian with respect to the particle’s position. In both the particle and field-theoretic representations, these forces act on the system’s fluctuating degrees of freedom, tethering them to their equilibrium values.

The forces on the two fields of the present field theory, are given by,

$$\frac{\delta H[\varphi, w]}{\delta \varphi(\mathbf{r})} = -\frac{1}{4\pi\ell_B} \nabla^2 \varphi(\mathbf{r}) + i\Gamma * \tilde{\rho}_e(\mathbf{r}; [\varphi, w]) \quad (2.19)$$

and

$$\frac{\delta H[\varphi, w]}{\delta w(\mathbf{r})} = \frac{1}{u} w(\mathbf{r}) + i\Gamma * \tilde{\rho}(\mathbf{r}; [\varphi, w]), \quad (2.20)$$

where the symbol $*$ denotes a convolution.

As discussed in Ref. 17, the force acting on the electrostatic field, φ , admits several interesting physical interpretations: applying the convolution $4\pi\ell_B(\beta e)^{-1}i\Gamma*$ (where e is the elementary charge) to both sides of Eq. 2.19 yields,

$$4\pi\ell_B i\Gamma * \frac{\delta H[\varphi, w]}{\delta \varphi(\mathbf{r})} = \nabla \cdot \tilde{\mathbf{D}}(\mathbf{r}; [\varphi, w]) - 4\pi\ell_B \Gamma * \Gamma * \tilde{\rho}_f(\mathbf{r}; [\varphi, w]), \quad (2.21)$$

where we have inferred an inhomogeneous dielectric displacement operator, given by,

$$\tilde{\mathbf{D}}(\mathbf{r}; [\varphi, w]) = -i(\beta e)^{-1} \nabla \bar{\varphi}(\mathbf{r}) + 4\pi\Gamma * \Gamma * \tilde{\mathbf{P}}(\mathbf{r}; [\varphi, w]). \quad (2.22)$$

One can further express $\tilde{\mathbf{D}}$ as a nonlocal function of the inhomogeneous electric field,

$-(\beta e)^{-1}i\nabla\bar{\varphi}$, according to:

$$\tilde{\mathbf{D}}(\mathbf{r}; [\varphi, w]) = (\beta e)^{-1} \int d\mathbf{r}' \tilde{\epsilon}(\mathbf{r}, \mathbf{r}'; [\varphi, w])[-i\nabla\bar{\varphi}(\mathbf{r}')], \quad (2.23)$$

which identifies the two-point function,

$$\tilde{\epsilon}(\mathbf{r}, \mathbf{r}'; [\varphi, w]) = \delta(\mathbf{r} - \mathbf{r}') + 4\pi\ell_B\Gamma * \tilde{\rho}(\mathbf{r}; [\varphi, w])\Gamma(\mathbf{r} - \mathbf{r}'), \quad (2.24)$$

as a non-local dielectric permittivity.

Although $\tilde{\mathbf{D}}$ vanishes when averaged, the relation specified by Eq. 2.22 has a close analogy to the equation, $\mathbf{D} = \mathbf{E} + 4\pi\mathbf{P}$, from continuum dielectric theory.²¹

In Chapter 3, we will show that a polarizable bead fluid subjected to an applied field \mathbf{E}_0 will have volume-averaged macroscopic \mathbf{D} and \mathbf{P} that exactly satisfy this condition. Similarly, the behavior identified in Eq. 2.23 has a macroscopic analog, $\mathbf{D} = \epsilon\mathbf{E}_0$, describing the linear dielectric response of a fluid to an applied field, \mathbf{E}_0 .

2.2.4 Extension to Dielectric Polymer Melts and Solutions

Beyond the simplest fluid model of unconnected polarizable beads, one can construct polarizable and/or charged polymer chains. As an example, we consider an electroneutral blend of oppositely charged, equal-length polyelectrolyte chains. The beads that make up each chain type carry a net monopole charge of $\pm q$, and also have a polarizability α_{\pm} . We can thus define the effective chemical potential fields,

$$w_{\pm}(\mathbf{r}) = i\bar{w}(\mathbf{r}) \pm qi\bar{\varphi}(\mathbf{r}) + \frac{\alpha_{\pm}}{2}|\nabla\bar{\varphi}(\mathbf{r})|^2, \quad (2.25)$$

which enumerate all the non-bonded interactions experienced by a + or - charged bead.

Since the bonded interactions that link beads into polymer chains are internal degrees of freedom of their corresponding molecules, they remain agnostic to the underlying pair interactions that generate w_{\pm} . Consequently, one can construct polymers of any of the classical chain models, and subsequent insertion of the effective chemical potential field $w_{\pm}(\mathbf{r})$ will automatically impart the chain segments with a net charge and polarizability.

For the case that each polyelectrolyte is a discrete chain of $N + 1$ beads, their corresponding internal degrees of freedom can be integrated according to,

$$Q_{\pm}[i\bar{\varphi}, i\bar{w}] = \frac{1}{V} \int d\mathbf{r} q_{\pm}(\mathbf{r}, N; [i\bar{\varphi}, i\bar{w}]), \quad (2.26)$$

so that Q_{\pm} gives a *single-chain partition function* for each polymer type.

The function q_{\pm} gives a chain propagator object, which can be interpreted as the position-dependent probability density function for a chain that is $j + 1$ beads in length, and which terminates at the position \mathbf{r} . Recognizing the coupled integrals over each bead's position as steps of a Markov process,³ one obtains the recursive definition,

$$\begin{aligned} q_{\pm}(\mathbf{r}, j + 1; [i\bar{\varphi}, i\bar{w}]) &= e^{-w_{\pm}(\mathbf{r})} \int d\mathbf{r}' q(\mathbf{r}', j; [i\bar{\varphi}, i\bar{w}]) \Phi(\mathbf{r} - \mathbf{r}'; \mathbf{r}') \\ q_{\pm}(\mathbf{r}, 0; [i\bar{\varphi}, i\bar{w}]) &= e^{-w_{\pm}(\mathbf{r})}, \end{aligned} \quad (2.27)$$

where $\Phi(\Delta\mathbf{r}; \mathbf{r})$ gives a normalized bond transition probability function, which gives the probability density of the successful formation of a link with vector $\Delta\mathbf{r}$, originating from position \mathbf{r} ; its form depends on the linker model specified for the chain. When Φ is independent of the starting position, it can be said to be translationally invariant, rendering the integral in Eq. 2.27 a convolution.

One such model is the “freely-jointed chain”, for which a bond of fixed length b connects consecutive beads; in the limit of large N , a freely-jointed chain with segment length b will have an unperturbed radius of gyration, $R_g = b(N/6)^{1/2}$, and we can therefore identify b as the chain's *Kuhn Length*. The bond-transition probability function is given by:

$$\Phi(\Delta\mathbf{r}) = \delta(|\Delta\mathbf{r}| - b). \quad (2.28)$$

The use of a Dirac delta-function here has the effect of discarding any jumps for which the length of the resulting bond is not exactly b . For this case, the volume integral of Eq. 2.27 can be replaced by an integral over the unit sphere, giving:

$$q_{\pm}(\mathbf{r}, j + 1; [i\bar{\varphi}, i\bar{w}]) = e^{-w_{\pm}(\mathbf{r})} \int d\mathbf{u} q_{\pm}(\mathbf{r} - b\mathbf{u}, j; [i\bar{\varphi}, i\bar{w}]). \quad (2.29)$$

Another simple model for bead connectivity assumes a harmonic potential between adjacent beads, referred to as the “discrete Gaussian chain.” The statistical weight of such a bond is Gaussian in its length. The bond transition probability for this chain model is given by:

$$\Phi(\Delta\mathbf{r}) = \left(\frac{3}{2\pi b^2}\right)^{\frac{3}{2}} \exp\left(-\frac{3|\Delta\mathbf{r}|^2}{2b^2}\right). \quad (2.30)$$

The discrete Gaussian chain model can be interpreted of as a smeared form of the freely-jointed chain, which permits bond lengths to fluctuate, but recovers the same b -dependent statistical behavior in the limit of large N .

A “continuous Gaussian chain” (CGC) model can be obtained by defining a discrete chain of N_s beads, requiring $R_g = b(N/6)^{1/2}$, and taking the limit $N_s \rightarrow \infty$.³ The result replaces Eq. 2.27 with a diffusion-like partial differential equation given by:

$$\frac{\partial}{\partial s} q_{\pm}(\mathbf{r}, s; [i\bar{\varphi}, i\bar{w}]) = \left[\frac{b^2}{6}\nabla^2 - w_{\pm}(\mathbf{r})\right] q_{\pm}(\mathbf{r}, s; [i\bar{\varphi}, i\bar{w}]) \quad q_{\pm}(\mathbf{r}, 0; [i\bar{\varphi}, i\bar{w}]) = 1 \quad (2.31)$$

Here $s \in [0, N]$ is a continuous segment index that replaces the discrete bead index j of the previous model. Eq. 2.31 has the character of a linear PDE, and it has been shown to be amenable to highly efficient, pseudospectral operator-splitting methods.³ The CGC model is also amenable to perturbation expansions in powers of w_m , a property that was exploited by a now historic paper illuminating the phase stability of a diblock copolymer melt.⁵⁷ Indeed, unless a physical property of the simulated polymer chemistry renders the CGC model inappropriate, it is the most common naïve choice for representing the statistical behavior of a polymer within a field theory.

2.3 Solution Methods

The field theory introduced here replaces the configuration integrals of a traditional partition function for a particle model with highly-dimensional functional integrals over the configurations of the fluctuating fields, φ and w . In order to evaluate these complicated objects and reap the rewards associated with a field theory representation, a number of numerical and analytical methods have developed.

However, regardless of the method used to evaluate the partition function, \mathcal{Z} , one will inevitably obtain thermodynamic observables by directly differentiating the Helmholtz free energy \mathcal{A} . If a closed form for \mathcal{A} has been computed using an analytical approximation, the desired observable is immediately obtained by differentiating this expression. On the other hand, differentiating the unapproximated form for \mathcal{A} yields corresponding *field-theoretic operators*, which are functionals of the fields φ and w , and must be thermally averaged; specific examples of these objects are discussed in more detail in the following sections.

2.3.1 Mean-Field Theory

In the simplest mean-field solution method, one may pursue the saddle-point configurations, φ^* and w^* , of the two fields, which extremize H according to:

$$\left. \frac{\delta H[\varphi, w]}{\delta \varphi(\mathbf{r})} \right|_{\varphi^*, w^*} = \left. \frac{\delta H[\varphi, w]}{\delta w(\mathbf{r})} \right|_{\varphi^*, w^*} = 0, \quad (2.32)$$

so that the forces given in Eqs. 2.19 & 2.20 vanish, and one can draw close analogy to the correspondence of equilibrium with 0 net force in a particle system. The mean-field approximation then assumes that this configuration dominates the functional integrals that enter \mathcal{Z} , and the free energy is obtained from $\beta\mathcal{A}(n, V, T) = -\ln \mathcal{Z}_0 + H[\varphi^*, w^*]$.

For any prescribed molecular architecture, the condition given in Eq. 2.32 for the present field theory yields homogeneous imaginary saddle-point configurations for both fields, given by:

$$i\varphi^* = \varphi_0 \quad iw^* = u\rho_0, \quad (2.33)$$

where φ_0 is an arbitrary real constant, which we choose to be 0 for convenience, and we have returned to the single-component bead fluid system introduced in Section 2.2.1, so that $\rho_0 = n/V$ is the average total bead density. Inserting these field configurations into the Hamiltonian immediately yields the free energy:

$$\beta\mathcal{A}(n, V, T) = -\ln \mathcal{Z}_0 + \frac{V}{2}u\rho_0^2, \quad (2.34)$$

admitting no contribution from electrostatics. Evidently, a solution to the field theory that

includes fluctuations is necessary to infer physical properties of the fluid that arise from electrostatic interactions.

Although the mean-field approximation yields a trivial saddle-point solution for the present polarizable field theory, one can obtain novel behaviors at the mean-field level by considering a field theory that includes species-dependent contact interactions. When the saddle-point configurations for the corresponding fields are spatially inhomogeneous, they cannot be deduced analytically, and must be calculated using an iterative numerical scheme known as self-consistent field theory (SCFT).²

2.3.2 Gaussian Fluctuation Approximation

Dielectric Homopolymer Solution

Beyond the simplest mean-field approximation, one can include the lowest-order fluctuation contributions to \mathcal{Z} , obtained by expanding H to second order in fluctuations of the fields about their saddle points. To illuminate molecular architecture effects that enter a Gaussian-order analysis, we presently assume a single-component solution of n Homopolymer chains with degree of polymerization N and Kuhn length b , where each segment has polarizability α and no monopole charge; we adopt the CGC model described in Section 2.2.4, so that the effective field experienced by each segment is, $w^{eff}(\mathbf{r}) = i\bar{w}(\mathbf{r}) + (\alpha/2)|\nabla\bar{\varphi}(\mathbf{r})|^2$.

Defining $\omega(\mathbf{r}) \equiv w(\mathbf{r}) - w^*$ to give the w -field fluctuations, the Hamiltonian can be written as the sum, $H[\varphi, w] = H[\varphi^*, w^*] + H_S[\varphi, \omega]$, so that H_S collects fluctuation contributions to H :

$$H_S[\varphi, \omega] = \frac{1}{2} \int d\mathbf{r} \left[\frac{1}{4\pi\ell_B} |\nabla\varphi(\mathbf{r})|^2 + \frac{1}{u} (\omega(\mathbf{r})^2 + 2w^*\omega(\mathbf{r})) \right] - n \ln Q[i\bar{\varphi}, i\bar{\omega}]. \quad (2.35)$$

The lowest-order fluctuation contributions to \mathcal{Z} correspond to terms that are quadratic in the field fluctuations, φ and ω . Since the explicitly field-dependent terms of H_S are already second order or lower, only the single-chain partition function, Q , requires the evaluation of a truncated series in fields.

As discussed in Ref. 17, the electrostatic term in $\omega^{eff} \equiv w^{eff} - iw^*$ is already quadratic in the electrostatic field φ . Consequently, second-order φ fluctuations enter the first-order expansion of Q in ω^{eff} ; on the other hand, second-order ω fluctuations require a second order

expansion in ω^{eff} .

The resulting expansion for Q is more conveniently represented in Fourier space, with wavevector (k)-dependent prefactors that may be obtained from the weak inhomogeneity expansion for a CGC in the presence of the field ω^{eff} :³

$$Q[\varphi, \omega] = e^{-iN\hat{\omega}(0)} \left[1 - \frac{N}{2} \sum_{\mathbf{k} \neq 0} \hat{\Gamma}^2(k) [\alpha k^2 \hat{\varphi}(\mathbf{k}) \hat{\varphi}(-\mathbf{k}) + N \hat{g}_D(Nb^2 k^2/6) \hat{\omega}(\mathbf{k}) \hat{\omega}(-\mathbf{k})] + \dots \right], \quad (2.36)$$

where the Fourier transform is defined as, $\hat{f}(\mathbf{k}) = V^{-1} \int d\mathbf{r} f(\mathbf{r}) e^{-i\mathbf{k}\cdot\mathbf{r}}$, $\hat{\Gamma}(k) = e^{-(ak)^2/2}$ is the Fourier transform of the smearing function, and $\hat{g}_D(x) = (2/x^2)(e^{-x} + x - 1)$ is the Debye function.

We note that the φ -dependent terms in Eq. 2.36 admit no dependence on the Debye function, \hat{g}_D ; we can therefore say that the second-order dielectric behavior of the chains is agnostic to their molecular architecture, arising purely from properties prescribed at the scale of individual beads.

A Fourier representation can also be determined for the Hamiltonian H_S ; combining the resulting expression with the truncated form of Q gives:

$$H_S[\varphi, \omega] \approx \frac{V}{2} \sum_{\mathbf{k} \neq 0} \left[\hat{G}_{\varphi\varphi}^{-1}(k) \hat{\varphi}(\mathbf{k}) \hat{\varphi}(-\mathbf{k}) + \hat{G}_{ww}^{-1}(k) \hat{\omega}(\mathbf{k}) \hat{\omega}(-\mathbf{k}) \right]. \quad (2.37)$$

The second order kernels that enter the truncated form for H_S are Green's functions that enumerate the second order field correlations, defined by,

$$\begin{aligned} \hat{G}_{\varphi\varphi}(k) &= \langle \hat{\varphi}(\mathbf{r}) \hat{\varphi}(-\mathbf{k}) \rangle = \frac{4\pi\ell_B}{(1 + 4\pi\ell_B\alpha\rho_0\hat{\Gamma}^2(k))k^2} \\ \hat{G}_{ww}(k) &= \langle \hat{\omega}(\mathbf{r}) \hat{\omega}(-\mathbf{k}) \rangle = \frac{u}{1 + u\rho_0N\hat{\Gamma}^2\hat{g}_D(Nb^2k^2/6)}, \end{aligned} \quad (2.38)$$

which describe the wavevector-dependent screening behavior of the polymer solution. We defer further discussion of Green's functions to the following sections, wherein more complex molecular systems are considered, offering richer discussion of screening effects.

Noting that the functional integrals over the configurations of the real-space fields, φ and w , can be equivalently represented as the product of integrals, $\prod_{\mathbf{k}} \int d\hat{\varphi}(\mathbf{k}) \int d\hat{\omega}(\mathbf{k})$, where

each factor corresponds to an integral over the amplitude of the Fourier mode \mathbf{k} of each field fluctuation. Adopting the truncated form for H_S renders each of these factors an independent Gaussian over the field fluctuations, $\hat{\varphi}(\mathbf{k})$ and $\hat{w}(\mathbf{k})$, corresponding to each \mathbf{k} , which can be computed analytically. Noting that the Gaussian normalization factors \mathcal{Z}_φ and \mathcal{Z}_w behave similarly, one obtains:

$$\mathcal{Z} = \frac{\mathcal{Z}_0 e^{-H[\varphi^*, w^*]}}{\mathcal{Z}_\varphi \mathcal{Z}_w} \prod_{\mathbf{k}} \int d\hat{\varphi}(\mathbf{k}) \int d\hat{w}(\mathbf{k}) e^{-H_S[\varphi, w]} \approx \mathcal{Z}_0 e^{-H[\varphi^*, w^*]} \prod_{\mathbf{k}} \left[\frac{k^2 G_{\varphi\varphi}(k)}{4\pi\ell_B} \frac{G_{ww}(k)}{u} \right]^{1/2}. \quad (2.39)$$

The Gaussian approximation to the Helmholtz free energy is then obtained from the thermodynamic connection formula, $\beta\mathcal{A}(n, V, T) = -\ln \mathcal{Z}$; noting that the Fourier spectrum has the behavior $\sum_{\mathbf{k}} \rightarrow (2\pi)^{-3} V \int d\mathbf{k}$ in the thermodynamic limit ($V \rightarrow \infty$), the following expression for the free energy is obtained:

$$\beta\mathcal{A}(n, V, T) = -\ln \mathcal{Z}_0 + \frac{V}{2} u \rho_0^2 + \frac{V}{2(2\pi)^3} \int d\mathbf{k} \ln \left[\frac{4\pi\ell_B}{k^2 \hat{G}_{\varphi\varphi}(k)} \frac{u}{\hat{G}_{ww}(k)} \right], \quad (2.40)$$

where $\rho_0 = nN/V$ is presently identified as the average segment density.

We note that in the present system, no coupling exists between φ and w at Gaussian order, and the free energy can be expressed in terms of the two diagonal Green's functions. Evidently, Eq. 2.40 defines a general form for the Gaussian order free energy of a system with no φw couplings, where molecular details of a given system enter through the two diagonal Green's functions.

2.3.3 Field-Theoretic Simulations

Beyond the Gaussian approximation, which only includes the lowest order fluctuation contributions to the behavior of the fluid, we may instead perform a full numerical attack of the polarizable field theory, including all fluctuation contributions. Previous studies^{11–13,58} have made profitable use of the complex Langevin (CL) stochastic sampling scheme for studying field theories of the Model F³ class, elucidating the behavior of a variety of charged soft matter systems. As the present field theory also has this form, albeit with induced dipoles rather than monopole charges, we will employ the same approach.

Within the full field theory, observables of interest may be obtained by direct differentiation of \mathcal{A} , defined in Eq. 2.14:

$$O = \frac{\partial \mathcal{A}}{\partial x} = k_B T \left\langle \frac{\partial H[\varphi, w]}{\partial x} \right\rangle \equiv \langle \tilde{O}[\varphi, w] \rangle, \quad (2.41)$$

such that $\tilde{O}[\varphi, w]$ is a *field-theoretic operator* that is a functional of the two fields, φ and w , corresponding to the observable O . The parameter x can be any state variable of \mathcal{A} , and is subsequently identified as the property of the system that is *thermodynamically conjugate* to O . The notation $\langle \dots \rangle$ indicates the ensemble average,

$$\langle \tilde{O}[\varphi, w] \rangle = \frac{\int \mathcal{D}\varphi \int \mathcal{D}w \tilde{O}[\varphi, w] e^{-H[\varphi, w]}}{\int \mathcal{D}\varphi \int \mathcal{D}w e^{-H[\varphi, w]}}, \quad (2.42)$$

where \tilde{O} is averaged over the field configurations, with a weight specified by the Boltzmann-like factor, e^{-H} .

For the present case of a single-component fluid in the canonical ensemble, the appropriate state variables x are the number of bead molecules n , the system volume V , and the temperature T , with the expected conjugate observables from classical thermodynamics. In the present field theory, each of these properties will have a corresponding field-theoretic operator obtained from Eq. 2.41. This procedure is also applicable to other thermodynamic ensembles, where the appropriate free energy replaces \mathcal{A} ; x is then permitted to be any appropriate state variable of the new free energy. Any additional fixed properties of the system that are introduced – such as the presence of multiple bead types j , with total count n_j – will result in an additional state variables and corresponding conjugate observables.

Operators for second order derivatives of \mathcal{A} can similarly be inferred:

$$\frac{\partial^2 \mathcal{A}}{\partial x \partial y} = \frac{\partial O}{\partial y} = k_B T \left\langle \frac{\partial^2 H[\varphi, w]}{\partial x \partial y} - \text{cov} \left(\beta \tilde{O}[\varphi, w], \beta \tilde{R}[\varphi, w] \right) \right\rangle, \quad (2.43)$$

where y is an additional state variable of \mathcal{A} , $R = \partial \mathcal{A}_E / \partial y$ is its conjugate observable, and $\tilde{R} = k_B T (\partial H / \partial y)$ is the corresponding operator. The function, $\text{cov}(\tilde{a}, \tilde{b}) \equiv (\tilde{a} - a)(\tilde{b} - b)$ returns an operator for the covariance of the operators, \tilde{a} and \tilde{b} . Typical thermodynamic properties that have the character of a second order free energy derivative include the isothermal

compressibility, β_T , defined by,

$$\beta_T^{-1} = -V \left. \frac{\partial \Pi}{\partial V} \right|_{n,T} = V \left. \frac{\partial^2 \mathcal{A}}{\partial V^2} \right|_{n,T}, \quad (2.44)$$

and the constant-volume heat capacity of the system,

$$C_V = T \left. \frac{\partial S}{\partial T} \right|_{n,V} = T \left. \frac{\partial^2 \mathcal{A}}{\partial T^2} \right|_{n,V}, \quad (2.45)$$

both of which will have a corresponding field-theoretic operator of the form specified in Eq. 2.43.

To sample the functional integrals in Eq. 2.42, we introduce a fictitious time variable, t , and prescribe stochastic “complex Langevin” equations for the trajectories of the field configurations,^{3,19}

$$\begin{aligned} \partial_t[\varphi(\mathbf{r}, t)] &= -\lambda_\varphi \frac{\delta H[\varphi, w]}{\delta \varphi(\mathbf{r}, t)} + \eta_\varphi(\mathbf{r}, t) \\ \partial_t[w(\mathbf{r}, t)] &= -\lambda_w \frac{\delta H[\varphi, w]}{\delta w(\mathbf{r}, t)} + \eta_w(\mathbf{r}, t), \end{aligned} \quad (2.46)$$

where λ_φ and λ_w are mobility parameters, which specify the relative rate that each field proceeds along its trajectory, and η_φ and η_w are Gaussian-distributed random processes, which obey the properties defined in Ref. 3, consistent with the fluctuation-dissipation theorem. The objects, $\delta H/\delta \varphi$ and $\delta H/\delta w$, are “field forces” that resist deviations from the saddle-point (mean field) configurations of the fields, such that the equations of motion in Eq. 2.46 specify trajectories of the field configurations that are consistent with the weighting, e^{-H} .

Provided the system is ergodic, we may compute ensemble averages of operators by time-averaging:

$$\langle \tilde{O}[\varphi, w] \rangle \approx \frac{1}{n_t} \sum_{j=1}^{n_t} \tilde{O}[\varphi(t_j), w(t_j)], \quad (2.47)$$

where n_t is the number of timesteps in the trajectory. In the limit of large n_t , the average in Eq. 2.47 is exactly equivalent to the ensemble average defined in Eq. 2.42, rendering the CL procedure an exact numerical solution to the field theory.

2.3.4 Gibbs Ensemble Method for Incompressible Phase Coexistence

We have presented here 3 methods for computing properties of a dielectric and/or charged fluid, represented in the Canonical ensemble using a statistical field theory model. Since the field theory described in this chapter admits a purely homogeneous saddle-point condition, no phase coexistence can be deduced from the behavior of a single system, using either the mean-field or Gaussian approximation. In a CL simulation of the full field theory, phase separation manifests as inhomogeneous average behavior in the configuration of the fields, with a corresponding local bead density profile characterized by distinct regions (phases) in space that differ in average bead density; when more than one bead type is present in the system, each phase can have a different bead type composition, and the phase separation can be classified as a demixing event.

Although CL provides a powerful tool for identifying phase separation within a single system, CL simulations consist of a cell of finite size, and the energetically unfavorable interfaces that exist between emergent phases cannot be removed. In a real phase-separating system, when no molecular architecture effects limit the size of each phase, the phases will grow in size to reduce the relative weight of the interfaces, and in the thermodynamic limit, the system will segregate into infinitely large *macrophases*, rendering the relative free energy contribution of interfaces infinitesimal. Any attempt to characterize macrophase separation within a single CL simulation is thus marred by the finite size of the simulation cell, which admits a finite free energy contribution due to the existence of interfaces.

We relay here a procedure for calculating the equilibrium compositions of two coexisting macro-phases (*i.e.* a binodal curve), arising from the phase separation of two immiscible bead species. By representing each phase as a separate system, both will recover homogeneous average behavior, rendering the mean-field and Gaussian approximations suitable for solving each associated field theory, and removing the interfaces that would otherwise disrupt a CL calculation. Although this procedure is not employed to generate results in the present Thesis, it is directly applicable to the phase-separating systems described herein.

We begin with the existing Gibbs Ensemble relaxation method introduced by Panagiotopoulos,⁵⁹ and later applied to polymer field theories by Riggleman and Fredrickson,⁶⁰ wherein two subsystems (phases) are specified, which partition a supersystem of fixed volume and particle

number. Although the two phases are permitted to exchange volume and molecules to achieve mechanical and chemical equilibrium, they are otherwise isolated, and share no interface.

By further requiring that each phase has the same total average bead density, ρ_0 , we impose an incompressibility constraint, and the number of degrees of freedom that must be relaxed is reduced by 1; the constraint consequently reduces the computational cost of the procedure, and is appropriate when the underlying particle model includes a strong repulsive interaction between beads that suppresses density fluctuations. In the case of a 2-component system with this constraint, chemical equilibrium is achieved by swapping molecules of contrasting species identity between the two subsystems, in ratios that preserve the total particle count of both phases. The binodal is consequently computed by relaxing with respect to the volume partitioning of the supersystem, and the composition of one of the phases.⁶¹ The composition of the other phase is specified by mass conservation, having prescribed the average composition of the supersystem.

The supersystem is represented in the Canonical ensemble, containing n_A^T molecules of type A and n_B^T molecules of type B , with volume V^T . The average volume fraction of A -type beads in the supersystem is given by,

$$\phi^* = \frac{n_A^T N_A}{n_A^T N_A + n_B^T N_B} = \nu \phi^I + (1 - \nu) \phi^{II}, \quad (2.48)$$

where $\nu = V^I/V^T$ is the fraction of the total system volume occupied by phase I , which has volume V^I ; Equation 2.48 thus gives a mass conservation condition, which couples the compositions of the two phases. N_j gives the number of beads per molecule – for small molecules, it is set to 1, and for homopolymer chains, it is the degree of polymerization.

The equilibrium partitioning of the two phases minimizes the total free energy of the supersystem, giving the condition,

$$\begin{aligned} \left. \frac{1}{V^T} \frac{d(\beta \mathcal{A}^I + \beta \mathcal{A}^{II})}{d\nu} \right|_{\phi^I, \rho_0} &\rightarrow 0 \\ \left. \frac{1}{\rho_0 V^T} \frac{d(\beta \mathcal{A}^I + \beta \mathcal{A}^{II})}{d\phi^I} \right|_{\nu, \rho_0} &\rightarrow 0, \end{aligned} \quad (2.49)$$

where \mathcal{A}^p is the free energy of phase p .

To compute the partitioning that satisfies Eq. 2.49, we use a gradient descent scheme, with an associated fictitious time variable t ; combining Eqs. 2.48 and 2.49, one obtains the following equations of motion,

$$\begin{aligned}\partial_t \nu &= \lambda_{\nu\beta} \left[\rho_0^{-1} \Pi_{\rho_0}^I - \rho_0^{-1} \Pi_{\rho_0}^{II} - \frac{\phi^* - \phi^I}{1 - \nu} \Delta\mu^{II} \right] \\ \partial_t \phi^I &= \lambda_{\phi\beta} [\Delta\mu^{II} - \Delta\mu^I],\end{aligned}\tag{2.50}$$

where the relevant osmotic pressure is taken at fixed composition and total molecule density:

$$\Pi_{\rho_0}^p = - \left. \frac{\partial \mathcal{A}^p}{\partial V} \right|_{\phi, \rho_0, T},\tag{2.51}$$

and chemical equilibrium is established by a weighted difference of chemical potentials, which corresponds to a single, constant total particle number chemical potential:

$$\Delta\mu^p = \frac{1}{N_A} \left. \frac{\partial \mathcal{A}^p}{\partial n_A} \right|_{\rho_0, V, T} = \frac{1}{N_A} \mu_A^p - \frac{1}{N_B} \mu_B^p.\tag{2.52}$$

The variables λ_{ν} and λ_{ψ} are mobility parameters that may be adjusted to improve the stability of the method without altering the physics of the system.

We can thus understand the first equation in Eq. 2.50 as an exchange of volume between the two phases that preserves the chemical composition of phase I – the latter term of this equation arises from the change in composition of phase II that is induced by this exchange. Similarly, the latter equation of Eq. 2.50 seeks chemical equilibrium by swapping molecules of differing species identity between phases, such that the incompressibility constraint is honored.

Upon prescribing the composition of the supersystem, discretizing the equations of motion given by Eq. 2.50 into an appropriate “update” step for ν and ϕ^I , and choosing initial values for ν and ϕ^I , the following steps are performed iteratively: determine ϕ^{II} from the mass conservation condition given in Eq. 2.48, compute Π_{ρ_0} and $\Delta\mu$ of each phase using the desired field theory solution method, and update ν and ϕ^I according to the discretized equations of motion. The iteration can be terminated when the update step changes each of ν and ϕ^I by a value smaller than some prespecified tolerance.

It is also worth noting that this method does not require knowledge of the free energy, only

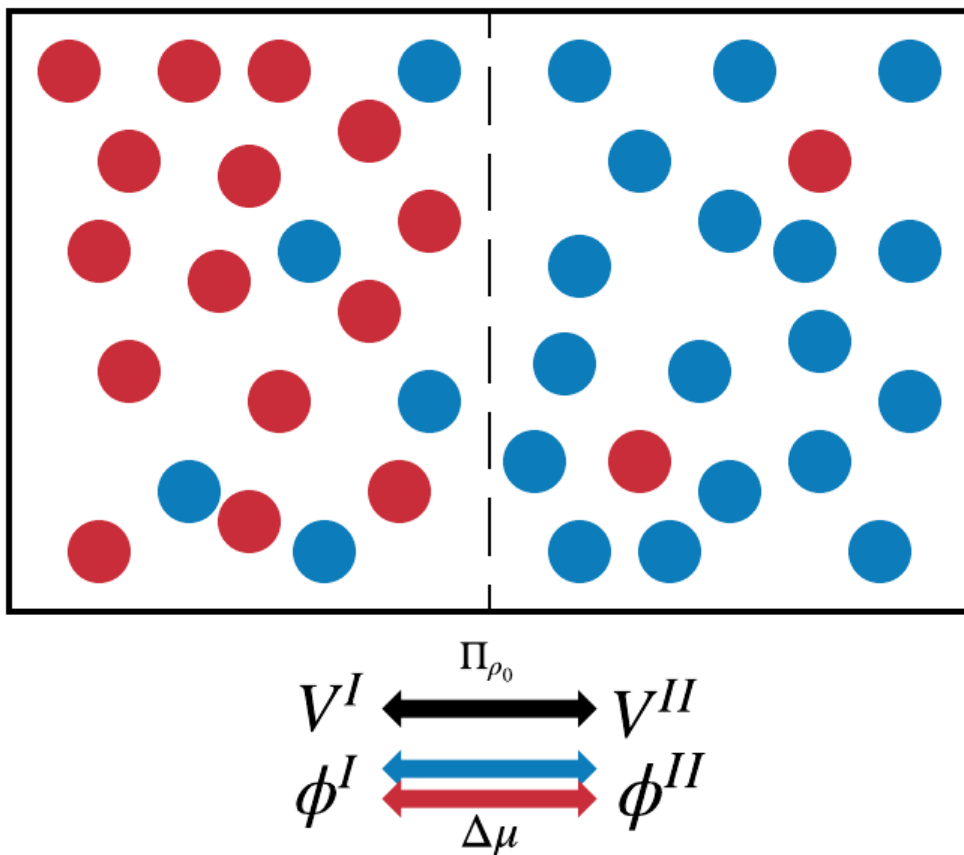


Figure 2.2: Schematic representation of the Gibbs relaxation procedure, for the case of a binary simple fluid mixture. Two boxes partition a larger, isolated box of fixed volume and particle number. The boxes are permitted to exchange volume. Prescribing a fixed number density of molecular units for both boxes, chemical equilibrium is achieved by swapping dissimilar molecules between boxes, which corresponds to fixed density composition changes.

its volume and particle-number derivatives; this makes the method particularly attractive when used in conjunction with a CL integrator for the desired theory, as the free energy is not readily available in a CL simulation,¹⁹ rendering a common tangent construction for computing the binodal curve inaccessible.

2.4 Systems of Interest

In the preceding sections, we introduced a field theory for charged and/or polarizable molecular species, described several analytical and numerical methods for computing thermodynamic observables from the field theory. In the present section, we consider two different soft matter systems, discussing the fluctuation behavior revealed using the Gaussian approximation.

In addition to computing associated Green's functions and discussing their asymptotic behavior, which informs the character of fluctuations within the fluid, we leverage the general form for the free energy given in Eq. 2.40, computing the osmotic pressure and chemical potential of each system directly from the corresponding Gaussian free energy of each system; physical interpretations of their analytical structure are subsequently discussed. We highlight the apparent screening behavior and thermally driven net attractions between beads, which self-consistently arise from the collective fluctuations of these simple polarizable unit molecules.

2.4.1 Binary Electrolyte Bead Fluid

We consider a 2-component bead fluid in the canonical ensemble, where two distinct components, A, B , are each described by the bead model introduced in Section 2.2. We respectively specify the polarizabilities of the components to be α_A, α_B and their free charge valences to be q_A, q_B . For a specified pair of free charges, the ratio of particle numbers of the two bead types is constrained by the electroneutrality condition, $q_A n_A + q_B n_B = 0$.

For each bead of type j , the single molecule partition function is obtained from,

$$Q_j[i\bar{\varphi}, i\bar{w}] \approx \frac{1}{V} \int d\mathbf{r} e^{-i\bar{w} - iq_j \bar{\varphi} - (\alpha_j/2) |\nabla \bar{\varphi}|^2}. \quad (2.53)$$

Expanding Q_j to second order in field fluctuations yields,

$$Q_j[i\bar{\varphi}, i\bar{\omega}] = e^{-i\hat{\omega}(\mathbf{0})} \left[1 - \frac{1}{2} \sum_{\mathbf{k} \neq \mathbf{0}} \hat{\Gamma}^2(k) [k^2 \hat{\varphi}(\mathbf{k}) \hat{\varphi}(-\mathbf{k}) + \hat{\omega}_j(\mathbf{k}) \hat{\omega}_j(-\mathbf{k})] + \dots \right], \quad (2.54)$$

where $\omega_j(\mathbf{r}) \equiv \omega(\mathbf{r}) + q_j \varphi(\mathbf{r})$ is the effective potential field due to contact repulsion and the bead's monopole charge.

Inserting this truncated Q_j for each species into the Hamiltonian H_S derived in Section 2.3.2, the coupling terms that depend on the product $\varphi\omega$ are found to be proportional to the quantity $q_A n_A + q_B n_B$, and thus vanish according to the electroneutrality condition; the present system consequently retains purely decoupled fluctuation behavior. The associated w Green's function is subsequently found to be,

$$\hat{G}_{ww}(\mathbf{k}) = \frac{u}{1 + u\rho_0 \hat{\Gamma}^2(\mathbf{k})}, \quad (2.55)$$

with the average total bead density given here by $\rho_0 = (n_A + n_B)/V$.

The electrostatic Green's function has the form,

$$\hat{G}_{\varphi\varphi}(\mathbf{k}) = \frac{4\pi\ell_B}{\hat{\epsilon}_0(k)[k^2 + \hat{\kappa}^2(\mathbf{k})]}, \quad (2.56)$$

which can be identified as the Debye-Hückel Green's function,⁵⁴ whose k dependence captures the effect of electrostatic screening due to a ‘‘Debye cloud’’ of correlated ions.

The function $\hat{\kappa}(\mathbf{k})$ is a wavevector-dependent inverse Debye screening length defined by:

$$\hat{\kappa}^2(\mathbf{k}) = \frac{4\pi\ell_B}{\hat{\epsilon}_0(k)} (q_A^2 \rho_A + q_B^2 \rho_B) \hat{\Gamma}^2(\mathbf{k}), \quad (2.57)$$

where each $\rho_j = n_j/V$ gives the average density of j type beads, and $\hat{\epsilon}_0(\mathbf{k})$ is a wavevector-dependent dielectric permittivity given by

$$\hat{\epsilon}_0(\mathbf{k}) = 1 + 4\pi\ell_B (\alpha_A \rho_A + \alpha_B \rho_B) \hat{\Gamma}^2(\mathbf{k}) \quad (2.58)$$

The electrostatic Green's function Eq. 2.56 has a complicated wavevector dependence, depending on multiple factors of the smearing function, in addition to the emergent Debye length,

κ^{-1} . For large wavevectors, $k \gtrsim 1/a$, all density-dependent terms are exponentially suppressed, such that $\hat{\kappa}^2(k) \sim 0$, $\hat{\epsilon}_0(k) \sim 1$, and $\hat{G}_{\varphi\varphi}(k) \sim 1/k^2$. In real space, the bare Coulomb kernel $G_{\varphi\varphi}(r) \sim 1/r$ is recovered, evidently indicating a length-scale sufficiently small that correlations do not reach nearby charges and dipoles, and their corresponding screening effects are not felt.

For small wavevectors $k \lesssim 1/a$, the smearing function tends to 1, such that the dielectric permittivity $\hat{\epsilon}_0(k)$ and the inverse Debye length $\hat{\kappa}(k)$ tend to their bulk values, $\epsilon_{mf} \equiv 1 + 4\pi(\alpha_A\rho_A + \alpha_B\rho_B)$ and $\kappa \equiv [4\pi(q_A^2\rho_A + q_B^2\rho_B)/\epsilon]^{1/2}$. The resulting real space Debye-Hückel kernel has the form of a Yukawa potential, $G_{\varphi\varphi}(r) \sim e^{-\kappa r}/(\epsilon_{mf}r)$, evidently experiencing screening from the bulk dielectric behavior of the fluid, in addition to exponential damping due to the correlated response of ions in the fluid.

Inserting the k -dependent Green's functions into Eq. 2.40, the Helmholtz free energy for the electrolyte fluid is immediately obtained:

$$\begin{aligned} \beta\mathcal{A}(n_A, n_B, V, T) &= -\ln \mathcal{Z}_0 + \frac{Vu}{2}\rho_0^2 \\ &+ \frac{V}{2(2\pi)^3} \int d\mathbf{k} \ln \left[\left(1 + u\rho_0\hat{\Gamma}^2(\mathbf{k}) \right) \left(\frac{\hat{\epsilon}_0(\mathbf{k})[k^2 + \hat{\kappa}^2(\mathbf{k})]}{k^2} \right) \right]. \end{aligned} \quad (2.59)$$

Osmotic Pressure

To ascertain the net fluctuation-induced interactions between beads within the homogeneous electrolyte fluid, it is instructive to evaluate the osmotic pressure, identifying repulsive or attractive terms by a positive or negative sign, respectively, in their contribution to the pressure. The latter compete with translational entropy and the prescribed repulsive excluded volume interaction, and will favor phase *condensation* of the fluid into two coexisting phases of contrasting total density. Additionally, the composition dependence of these attractive terms will influence the relative partitioning of the two bead types between the phases. If the two phases have contrasting bead-type compositions, the phase separation can be classified as a *demixing* behavior.

The pressure can be directly obtained from the free energy according to,

$$\Pi = -\frac{\partial\mathcal{A}}{\partial V} \Big|_{n_A, n_B, T}, \quad (2.60)$$

which gives the sum of terms,

$$\beta\Pi = \rho_0 + \frac{u}{2}\rho_0^2 + \beta\Pi_u + \beta\Pi_e \quad (2.61)$$

where Π_u and Π_e are fluctuation contributions to the pressure, defined by

$$\beta\Pi_u = -\frac{1}{4\pi^2} \int_0^\infty dk k^2 \left\{ \ln[1 + u\rho_0\hat{\Gamma}^2(k)] - \frac{u\rho_0\hat{\Gamma}^2(k)}{1 + u\rho_0\hat{\Gamma}^2(k)} \right\} \quad (2.62)$$

and

$$\beta\Pi_e = -\frac{1}{4\pi^2} \int_0^\infty dk k^2 \left\{ \ln \left[\hat{\epsilon}_0(k) + \frac{\hat{\epsilon}_0(k)\hat{\kappa}^2(k)}{k^2} \right] - \frac{[\hat{\epsilon}_0(k) - 1]k^2 + \hat{\epsilon}_0(k)\hat{\kappa}^2(k)}{\hat{\epsilon}_0(k)k^2 + \hat{\epsilon}_0(k)\hat{\kappa}^2(k)} \right\} \quad (2.63)$$

To evaluate Π_u , we assume the fluid is a dilute solution of the polarizable bead ions, so that it is appropriate to perform an expansion of the integrand in powers of small ρ_j . The leading second-order term gives,

$$\beta\Pi_u \sim -\frac{\sqrt{2}u^2}{128\pi^{3/2}a^3}\rho_0^2 + O(\rho_j^3), \quad (2.64)$$

which has the same leading order ρ_0^2 scaling as the mean-field excluded volume term; the combined prefactors can consequently be re-cast as a renormalized effective excluded volume, u_r .

We expand the latter electrostatic contribution as a sum of three integrals $\Pi_e = \Pi_{VDW} + \Pi_{DH} + \Pi_{ID}$, which are given by

$$\beta\Pi_{VDW} = -\frac{1}{4\pi^2} \int_0^\infty dk k^2 \left\{ \ln[\hat{\epsilon}_0(k)] - \frac{\hat{\epsilon}_0(k) - 1}{\hat{\epsilon}_0(k)} \right\} \quad (2.65)$$

,

$$\beta\Pi_{DH} = -\frac{1}{4\pi^2} \int_0^\infty dk k^2 \left\{ \ln \left[\frac{k^2 + \hat{\kappa}^2(k)}{k^2} \right] - \frac{\hat{\kappa}^2(k)}{k^2 + \hat{\kappa}^2(k)} \right\} \quad (2.66)$$

, and

$$\beta\Pi_{ID} = -\frac{1}{4\pi^2} \int_0^\infty dk k^2 \frac{\hat{\kappa}^2(k)[\hat{\epsilon}_0(k) - 1]}{\hat{\epsilon}_0(k)[k^2 + \hat{\kappa}^2(k)]} \quad (2.67)$$

The first term can be evaluated by again assuming dilute behavior, expanding the integrand

to second order in densities:

$$\beta\Pi_{VDW} \sim -\frac{\sqrt{2\pi}\ell_B^2}{8a^3} \sum_{j,k}^{A,B} \alpha_j \rho_j \alpha_k \rho_k + O(\rho_j^3). \quad (2.68)$$

Π_{VDW} can be interpreted as the signature of a *van der Waals* (VDW) interaction that arises from the net attraction between the fluctuating dipoles of nearby molecules. It admits no screening effects, due to the imposed dilute approximation, and has the scaling $1/a^3$ in the smearing length. This scaling in the prescribed properties of the fluid is consistent with the dipole-dipole contribution to the second Virial coefficient for polarizable ionic hard spheres with diameter a , which we show in the following section.

To illuminate the composition dependence of Π_{VDW} , it is instructive to define the linear combinations of densities, $\rho_0 = \rho_A + \rho_B$ and $\rho_- = \rho_A - \rho_B$, identifying terms that will favor condensation and demixing, respectively:

$$\beta\Pi_{VDW} = -\frac{\sqrt{2\pi}\ell_B^2(\alpha_A - \alpha_B)^2}{32a^3} [(\alpha_A + \alpha_B)^2 \rho_0^2 + 2(\alpha_A^2 - \alpha_B^2) \rho_0 \rho_- + (\alpha_A - \alpha_B)^2 \rho_-^2], \quad (2.69)$$

evidently revealing 3 terms. The first term is proportional to ρ_0^2 , favoring condensation of the fluid into two phases of contrasting total density, but not admitting any preference for demixing. The second term is proportional to the product $\rho_0 \rho_-$; although it contributes to phase behavior characterized by two coexisting phases of contrasting total bead density and composition, it becomes unimportant in the limit of pure condensation or pure demixing.

The last term is proportional to ρ_-^2 , and characterizes an effective immiscibility between the two bead types. It is proportional to the square of the polarizability contrast, consistent with existing immiscibility models,⁵⁵ arising from a net preference for the more strongly polarizable bead type to aggregate due to favorable VDW attractions. From this form, one can deduce an effective Flory-Huggins interaction parameter, χ_{VDW} ,

$$\chi_{VDW} = \frac{\sqrt{2\pi}\ell_B^2(\alpha_A - \alpha_B)^2}{16va^3}, \quad (2.70)$$

where v is a reference lattice site volume.

For dilute solutions, the second integral, Π_{DH} , is dominated by small wavevectors $k \sim \kappa$

much less than $1/a$. In this limit, $\hat{\kappa}(k)$ can be approximated by its bulk value, κ , and the integral performed analytically:

$$\beta\Pi_{DH} \approx -\frac{1}{24\pi}\kappa^3 \quad (2.71)$$

Equation 2.71 is the well-known *Debye-Hückel* result for a dilute electrolyte,⁵⁴ representing the contribution to the pressure from screened monopole-monopole interactions. We note that ϵ_{mf} is embedded in the definition of κ , so that that dielectric screening is implicit and emerges self-consistently in long-range electrostatic correlations.

The final pressure term arising from electrostatics, Π_{ID} , is defined by an integral whose dominant contribution is from large wavevectors with $k \sim 1/a$. As a consequence, the denominator of the integrand can be approximated by $\hat{\epsilon}(k)k^2$, and the integral performed analytically:

$$\beta\Pi_{ID} \approx -\frac{\sqrt{2\pi}\ell_B^2}{a}(q_A^2\rho_A + q_B^2\rho_B)(\alpha_A\rho_A + \alpha_B\rho_B) + O(\rho_j^3), \quad (2.72)$$

to second order in densities.

Π_{ID} is proportional to the product of the macroscopic ionic strength and the polarizability of the fluid. In the following section, we show that these scalings are consistent with the ion-dipole contributions to the second Virial coefficients for a binary gas of polarizable and charged hard spheres with diameter a .

Comparison to a Hard-Sphere Gas

Here we consider unsmeared polarizable electrolyte beads with a hard sphere diameter a , and we adopt the energy scale $k_B T = 1$. We calculate the second Virial coefficient by direct integration over the configurational degrees of freedom of a 2-body system. We will neglect ion-ion interactions between the free charges of molecules, as these terms are long-ranged, and consequently divergent for the unscreened 2-body case. Bare dipole-dipole (Van der Waals) and ion-dipole interactions, however, prove to be sufficiently short-ranged that their contribution may be approximated by a simple 2-body term for a dilute gas. We assign molecules of type i a polarizability α_i and a free charge of valence q_i . We again employ a Drude oscillator model, assigning the paired charges a valence of δq_i and their connecting spring constant $\delta q_i^2 \alpha_i^{-1}$, such

that the internal energy of a molecule of type i is given by:

$$u^i = \frac{\delta q_i^2}{2\alpha_i} |\mathbf{d}|^2 \quad (2.73)$$

where \mathbf{d} is the separation vector between the two opposing charges of the molecule.

The ion-dipole interaction between molecule 1, of type i , and molecule 2, of type j , can be determined by summing the Coulomb interactions of each molecule's free charge with the opposing molecule's paired charges:

$$\begin{aligned} U_{ID}^{ij} &= q_i \delta q_j \left(\frac{1}{|\mathbf{r}_1 - \mathbf{r}_2 - \mathbf{d}_2/2|} - \frac{1}{|\mathbf{r}_1 - \mathbf{r}_2 + \mathbf{d}_2/2|} \right) \\ &+ q_j \delta q_i \left(\frac{1}{|\mathbf{r}_1 + \mathbf{d}_1/2 - \mathbf{r}_2|} - \frac{1}{|\mathbf{r}_1 - \mathbf{d}_1/2 - \mathbf{r}_2|} \right) \end{aligned} \quad (2.74)$$

where \mathbf{r}_1 and \mathbf{r}_2 are the centers of mass of the two molecules, \mathbf{d}_1 and \mathbf{d}_2 are the separation vectors between the dipole charges of each molecule.

We can again use a multipole expansion, truncated at $O(\mathbf{d}\mathbf{d})$, to derive the instantaneous ion-dipole interaction:

$$U_{ID}^{ij} = (q_j \delta q_i \mathbf{d}_1 - q_i \delta q_j \mathbf{d}_2) \cdot \nabla_1 \frac{1}{|\mathbf{r}_1 - \mathbf{r}_2|} = -(q_j \delta q_i \mathbf{d}_1 - q_i \delta q_j \mathbf{d}_2) \cdot \frac{\mathbf{r}_1 - \mathbf{r}_2}{|\mathbf{r}_1 - \mathbf{r}_2|^3} \quad (2.75)$$

Integrating over all possible polarizations (vectors $\mathbf{d}_1, \mathbf{d}_2$) for the two molecules, and shifting molecule 1 to the origin obtains the potential of mean force for the ion-dipole interaction, to fourth order in charge:

$$w_{ID}^{ij}(r) = -(\alpha_i q_j^2 + \alpha_j q_i^2) \frac{1}{r^4} \quad (2.76)$$

Unsurprisingly, the average ion-dipole interaction is attractive when polarization is allowed to fluctuate, as configurations with the dipole moment of each molecule aligned along the electric field generated by the free charge of the other molecule will be preferred.

In similar fashion, we can derive the potential of mean force for the dipole-dipole interaction

by starting with the Coulomb interactions of all of the paired charges:

$$\begin{aligned}
U_{DD}^{ij} &= \frac{\delta q_i \delta q_j}{|\mathbf{r}_1 + \mathbf{d}_1/2 - \mathbf{r}_2 - \mathbf{d}_2/2|} - \frac{\delta q_i \delta q_j}{|\mathbf{r}_1 - \mathbf{d}_1/2 - \mathbf{r}_2 - \mathbf{d}_2/2|} \\
&- \frac{\delta q_i \delta q_j}{|\mathbf{r}_1 + \mathbf{d}_1/2 - \mathbf{r}_2 + \mathbf{d}_2/2|} + \frac{\delta q_i \delta q_j}{|\mathbf{r}_1 - \mathbf{d}_1/2 - \mathbf{r}_2 + \mathbf{d}_2/2|}
\end{aligned} \tag{2.77}$$

We employ a multipole expansion, this time about each molecule's center of mass for each term, recovering the instantaneous dipole-dipole interaction:

$$U_{DD}^{ij} = -\delta q_i \delta q_j \mathbf{d}_1 \mathbf{d}_2 : \nabla_1 \nabla_1 \frac{1}{|\mathbf{r}_1 - \mathbf{r}_2|} = -\delta q_i \delta q_j \mathbf{d}_1 \mathbf{d}_2 : \left[3 \frac{(\mathbf{r}_1 - \mathbf{r}_2)(\mathbf{r}_1 - \mathbf{r}_2)}{|\mathbf{r}_1 - \mathbf{r}_2|^5} - \frac{\mathbf{I}}{|\mathbf{r}_1 - \mathbf{r}_2|} \right]. \tag{2.78}$$

Integrating out polarization degrees of freedom and retaining terms that are fourth order in charge obtains the familiar $1/r^6$ Van der Waals potential of mean force:⁶²

$$w_{DD}^{ij}(r) = -2\alpha_i \alpha_j \frac{1}{r^6} \tag{2.79}$$

We can obtain the contribution of each interaction to the second Virial coefficient associated with the $\rho_i \rho_j$ term of the osmotic pressure by integrating the Mayer-f function ($e^{-w^{ij}} - 1 \approx -w^{ij}$) over all positions of the two molecules, with the cutoff $|\mathbf{r}_1 - \mathbf{r}_2| \geq a$ imposed by our assumption of hard spheres:

$$B_{ID}^{ij} = -4\pi(\alpha_i q_j^2 + \alpha_j q_i^2) \frac{1}{a} \tag{2.80}$$

$$B_{DD}^{ij} = -\frac{2\pi}{3} \alpha_i \alpha_j \frac{1}{a^3} \tag{2.81}$$

The contribution of each interaction to the osmotic pressure is quadratic in component densities, and given by $\Pi_e = \sum_i \sum_j B_e^{ij} \rho_i \rho_j$. For the case of a binary fluid of polarizable ionic molecules, performing this sum explicitly recovers terms that differ from their analogs in the Gaussian field theory of Chapter 2 by a simple pre-factor that arises from the difference in regularization procedure:

$$\Pi_{ID} = -\frac{8\pi}{a} (\alpha_A \rho_A + \alpha_B \rho_B) (q_A^2 \rho_A + q_B^2 \rho_B) \tag{2.82}$$

$$\Pi_{DD} = -\frac{4\pi}{3a^3} (\alpha_A \rho_A + \alpha_B \rho_B)^2 \tag{2.83}$$

Bead Self-Energy: Solvation and Partitioning

In the present chapter, we have restricted our analysis to homogeneous systems, and have inferred fluctuation-averaged net attractions between beads from pressure contributions that are negative in sign. These attractions, when sufficiently strong in magnitude, will give rise to phase separation behavior. To understand the partitioning and corresponding localization of polarizable electrolyte beads within an inhomogeneous, phase-separated complex fluid, one can examine the character of the self-energy of the bead, which we equivalently identify as an excess, fluctuation contribution to the bead's chemical potential.

In the present binary polarizable electrolyte bead fluid model, the chemical potential of bead type j can be obtained from the free energy according to,

$$\beta\mu_j = \left. \frac{\partial\beta\mathcal{A}}{\partial n_j} \right|_{n_{k \neq j}, V, T} = \ln \rho_j + u\rho_0 + \beta u_j + \beta v_j, \quad (2.84)$$

where the first two terms give a translational entropy and mean-field excluded volume contribution, respectively. u_j and v_j are self-energy terms due to electrostatic and excluded volume fluctuations, respectively. The former is given by:

$$\beta u_j = \frac{1}{4\pi^2} \int_0^\infty dk; k^2 \hat{\Gamma}^2(\mathbf{k})(\alpha_j k^2 + q_j^2) \hat{G}_{\varphi\varphi}(\mathbf{k}). \quad (2.85)$$

Examining the form for u_j , one can immediately identify a contribution to the bead's self-energy from its induced dipole and from its monopole charge. Assuming a dilute fluid, the leading order self-energy contribution due to the induced dipole will be dominated by large wavevectors, where the electrostatic Green's function recovers the character of a bare Coulomb kernel, $\hat{G}_{\varphi\varphi} \sim 4\pi\ell_B/k^2$. The resulting loop integral can be performed analytically, and gives:

$$\beta u_{j,D} \sim \frac{\ell_B \alpha_j}{4\sqrt{\pi} a^3} + O(\rho_j). \quad (2.86)$$

The monopole self-energy contribution has a complicated wavevector dependence, due to the behavior of the electrostatic Green's function. It can be further separated into two contributions,

which are found to be,

$$\beta u_{j,DH} = \frac{\ell_B q_j^2}{\pi} \int_0^\infty dk k^2 \frac{\hat{\Gamma}^2(k)}{\hat{\epsilon}_0(k)} \left[\frac{1}{k^2 + \hat{\kappa}^2(k)} - \frac{1}{k^2} \right] \quad (2.87)$$

,

$$\beta u_{j,B} = \frac{\ell_B q_j^2}{\pi} \int_0^\infty dk \frac{\hat{\Gamma}^2(k)}{\hat{\epsilon}_0(k)}. \quad (2.88)$$

The first term will be dominated by small wavevectors $k \sim \kappa$; replacing $\hat{\epsilon}_0$ and $\hat{\kappa}$ by their bulk values yields an integral that can be computed analytically, giving:

$$\beta u_{j,DH} \approx -\frac{\ell_B q_j^2}{2\epsilon_{mf}} \kappa \quad (2.89)$$

The latter term can be evaluated analytically by Taylor expanding the dielectric screening contribution, $\hat{\epsilon}_0^{-1}(k)$, which yields an infinite series of exact integrals:

$$\beta u_{j,B} = \frac{\ell_B q_j^2}{\pi} \sum_{r=0}^{\infty} [-4\pi\ell_B(\alpha_A\rho_A + \alpha_B\rho_B)]^r \int_0^\infty dk \hat{\Gamma}^{2r+2}(k) = \frac{\ell_B q_j^2}{2\sqrt{\pi}\epsilon_B a}. \quad (2.90)$$

In the latter expression, ϵ_B is an effective dielectric constant resulting from the expansion,

$$\epsilon_B = \left[\sum_{r=0}^{\infty} \frac{[-4\pi\ell_B(\alpha_A\rho_A + \alpha_B\rho_B)]^r}{\sqrt{r+1}} \right]^{-1} \approx 1 + 2^{3/2}\pi\ell_B(\alpha_A\rho_A + \alpha_B\rho_B), \quad (2.91)$$

and is reduced relative to the bulk ϵ_{mf} because of fluctuation contributions with wavelength close to the smearing length, which experience reduced dielectric screening effects.

These two terms together give a partially-screened Born solvation energy $u_{j,B}$ with a screened Debye-Hückel correction term $u_{j,DH}$.^{20,50} Because it accounts for long-ranged ion correlation behavior, the Debye-Hückel correction term is screened by the the bulk dielectric behavior of the fluid.

The excluded volume self-energy term, v_j , can be written as,

$$\beta v_j = \frac{1}{4\pi^2} \int_0^\infty dk k^2 \frac{u\hat{\Gamma}^2(k)}{1 + u\rho_0\hat{\Gamma}^2(k)} \sim \frac{u}{16\pi^{3/2}a^3} + O(\rho_0), \quad (2.92)$$

where the latter expression is obtained from a dilute approximation.

In a phase-separated, dense dielectric fluid, in which a small amount of these electrolyte beads are solvated, beads of type j will partition between each phase in a ratio that minimizes their average chemical potential, μ_j . When the density of electrolytes is dilute, the inverse Debye length becomes small, and the electrostatic self-energy is dominated by the sum of terms, $u_{j,D} + u_{j,B}$, which are minimized in the phase with the larger dielectric constant, ϵ_B . Consequently, the electrolyte will selectively partition into this phase. The mean-field excluded volume contribution to μ_j and its correction, v_j , do not affect partitioning of electrolyte beads because they only depend on the total density of the fluid, ρ_0 .

2.4.2 Binary Dielectric Polymer Blend

Here we consider a binary blend of n_A chains of type A and n_B chains of type B . We respectively assign them polarizabilities α_A, α_B and polymerization indices N_A, N_B . We assign no net monopole to the two segment types ($q_A = q_B = 0$). Adopting the CGC model, the second order expansion for each single-chain partition function, Q_j may be obtained from Eq. 2.36 by replacing α , N , and b with the species-dependent parameters α_j , N_j , b_j .

Since the φ -dependent term in the approximated Q_j is independent of the Debye function, the electrostatic Green's function is trivially obtained from Eq. 2.56 in the limit of no free charges, where each $\rho_j = n_j N_j / V$ is now an average density of type j segments, and the average total segment density is obtained from $\rho_0 = \rho_A + \rho_B$.

Evidently, the electrostatic behavior of a homogeneous binary fluid of polarizable chains is *insensitive to chain connectivity*. For large wavevectors, $\hat{G}_{\varphi\varphi}(\mathbf{k})$ tends to the bare Coulomb Green's function - corresponding to unscreened short-range electrostatic interactions $G_{\varphi\varphi}(r) \sim 1/r$. For small wavevectors, $\hat{G}_{\varphi\varphi}(\mathbf{k})$ tends to a Coulomb Green's function that depends on the bulk dielectric constant, indicating long-range interactions that are screened by the polarizable molecules of the solution; in real space: $G_{\varphi\varphi}(r) \sim 1/(\epsilon_m f r)$.

On the other hand, the w Green's function does include a contribution from the connectivity of the chains, with the form:

$$\hat{G}_{ww}(\mathbf{k}) = \frac{u}{1 + \hat{\gamma}_c(k)}, \quad (2.93)$$

and with the kernel,

$$\hat{\gamma}_c(k) = u\hat{\Gamma}^2(\mathbf{k}) [N_A\rho_A\hat{g}_D(R_{g,A}^2k^2) + N_B\rho_B\hat{g}_D(R_{g,B}^2k^2)]. \quad (2.94)$$

Comparing the form for $\hat{G}_{ww}(\mathbf{k})$ given by Eq. 2.93 to the bead case (Eq. 2.55), we can interpret the additional wavevector-dependence introduced by the Debye functions as a consequence of *chain connectivity* - bead-bead excluded volume contributions from wavevectors $k \gtrsim 1/R_g$ are suppressed by the screening effects of nearby fluctuating chains.

The Helmholtz Free energy is subsequently obtained from Eq. 2.40.

$$\beta\mathcal{A}(n_A, n_B, V, T) = -\ln \mathcal{Z}_0 + \frac{Vu}{2}\rho_0^2 + \frac{V}{2(2\pi)^3} \int d\mathbf{k} \ln [(1 + \hat{\gamma}_c(k)) \hat{\epsilon}_0(k)] \quad (2.95)$$

Osmotic Pressure

The osmotic pressure of the dielectric homopolymer blend is given by

$$\beta\Pi = \frac{n_A}{V} + \frac{n_B}{V} + \frac{u}{2}\rho_0^2 + \beta\Pi_u + \beta\Pi_{VDW} \quad (2.96)$$

We note that the ideal gas/translational entropy contribution to the pressure is given by the *chain density*, whereas interaction effects scale with *monomer density*, a signature of the effective reduction in the bead configuration space imposed by the chain connectivity constraints.

The fluctuating excluded-volume term is given by

$$\beta\Pi_u = -\frac{1}{4\pi^2} \int_0^\infty dk k^2 \left\{ \ln[1 + \hat{\gamma}_c(k)] - \frac{\hat{\gamma}_c(k)}{1 + \hat{\gamma}_c(k)} \right\} \quad (2.97)$$

In examining the asymptotics of the integrand of the fluctuation correction term, we find that the wavevector-dependence of $\hat{\gamma}_c$ indicates *competing length-scales*. Large wavevector fluctuations ($k \gtrsim 1/a$) are suppressed by the smearing function $\hat{\Gamma}$. However, if we assume a concentrated polymer solution, the dominant contribution will be from wavevectors $k \gtrsim 1/R_g$, as interactions on length-scales larger than R_g will be highly screened. Thus, for sufficiently long chains ($R_g \gg a$), the finite size of individual beads becomes inconsequential. In this limit, the

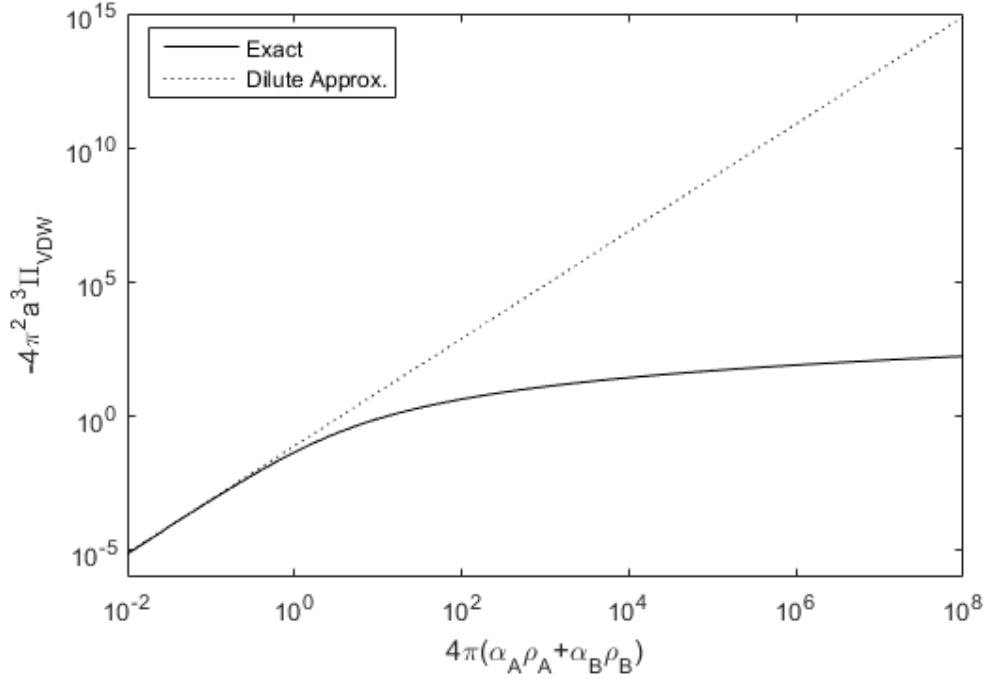


Figure 2.3: Plot of the numerical solution to Eq. 2.65 and its dilute leading-order approximation. Evidently Π_{VDW} is quadratic in density in the dilute regime, and tends to a sublinear scaling when dielectric screening becomes significant. Here, the thermal energy scale is set to $k_B T = 1$, so that the axes are scaled by dimensionless quantities.

integral can be evaluated analytically:

$$\beta \Pi_u \approx -\frac{1}{24\pi} \left[12u \left(\frac{\rho_A}{b_A^2} + \frac{\rho_B}{b_B^2} \right) \right]^{3/2} \quad (2.98)$$

This is the two-component analog of the well-known result derived by Edwards.^{56,63}

The electrostatic pressure contribution for the homopolymer blend, Π_{VDW} , has the same form as the analogous term for a small molecule mixture, given by Eq. 2.65. In Fig. 2.3, the second order dilute approximation for Π_{VDW} for a 2-component system is plotted, on log – log scale, as a function of the density-dependent dimensionless value that determines the dilute regime for electrostatics; the asymptotic approximation is compared to the full numerical solution to the loop integral for Π_{VDW} . Evidently, the second order density scaling is does not persist beyond the dilute regime, which occurs because of the density dependence of the dielectric screening function, $\hat{\epsilon}_0(k)$. Consequently, we can say that the crossover for the “electrostatic dilute regime” occurs when the contribution of the bead fluid to the bulk dielectric constant

ϵ_{mf} is $O(1)$.

Chapter 3

Electric Field-Induced Critical Point Shift in Binary Dielectric Fluids

3.1 Background

The use of an electric field to control the phase behavior and structure of dielectric fluid mixtures and soft materials has been a topic of interest for several decades. Two classes of systems that have been studied extensively are macrophase-separating binary systems – including small molecule mixtures and polymer solutions and blends – and microphase-separating systems, particularly block copolymer melts.

Paradoxically, the latter arguably more complicated system has proven less troublesome to describe. Experiment^{37,38} finds that placing a microphase-separating block copolymer melt in an electric field induces alignment of the morphology along the electric field vector. This behavior has been reproduced in simulation^{39,40,64,65} at the mean-field level by assuming a simple linear mixing rule in the composition-dependence of the local dielectric constant of the melt, and computing the resultant electrostatic contribution to the free energy of the system, which imparts a net penalty associated with interfaces that do not lie completely parallel to the electric field vector.

On the other hand, the role of an electric field in influencing the phase behavior of macrophase-separating systems has proven less straightforward to determine. Experiments with small

molecule,^{22,23} polymer solution,³³ and polymer blend³¹ systems, apart from two polymer blend results from one group,^{29,30} have all measured an electric field-induced shift in the critical point that *favors mixing*, evidently arising from a behavior that is relatively universal and not limited to a particular pair of chemistries. However, development of a consistent theory that predicts the sign and magnitude of this shift has been the source of some controversy.

In an early study,²² Debye and Kleboth considered the mixture of nitrobenzene and 2,2,4-trimethylpentane, measuring a shift of the critical point in favor of mixing when they applied an electric field. To describe this behavior, they proposed the following form for the free energy of the mixture in the presence of an applied field \mathbf{E}_0 ,

$$\mathcal{F} = \mathcal{F}_0 + V\epsilon \frac{|\mathbf{E}_0|^2}{8\pi}, \quad (3.1)$$

where \mathcal{F}_0 is the free energy in the absence of an electric field, V is the system volume, and ϵ is the dielectric constant of the mixture, which depends on its composition, ϕ . According to their ansatz, the sign of the quantity, $\partial^2\epsilon/\partial\phi^2$, determines the direction of any field-induced critical point (or spinodal boundary) shift, with a positive sign indicating enhanced mixing. When they measured ϵ as a function of ϕ for their binary system, they observed a depression relative to a linear mixing line that connects ϵ of the pure phase components, corresponding to $\partial^2\epsilon/\partial\phi^2 > 0$, in agreement with their critical point measurements.

Beaglehole later performed a similar investigation²³ using a mixture of aniline and cyclohexane, and also observed electric field-induced mixing, as well as $\partial^2\epsilon/\partial\phi^2 > 0$, when measuring the composition dependence of the dielectric constant of the fluid. He noted, however, that the sign of the electric field free energy contribution in Debye's paper is incorrect for a system experiencing a fixed applied electric field, and instead corresponds to a system experiencing a fixed displacement field. The former may be obtained from the latter by a Legendre transform,

$$\tilde{\mathcal{F}} = \mathcal{F} - V\epsilon \frac{|\mathbf{E}_0|^2}{4\pi} = \mathcal{F}_0 - V\epsilon \frac{|\mathbf{E}_0|^2}{8\pi}, \quad (3.2)$$

such that $\tilde{\mathcal{F}}$ is the correct free energy to describe the system, and it predicts field-induced mixing when $\partial^2\epsilon/\partial\phi^2 < 0$, in contradiction to Beaglehole's experiments. He hypothesized that

the second derivative of the ϵ vs. ϕ curve necessarily changes sign near the critical point, even if it was not apparent in experiments.

Onuki later published a letter,⁶⁶ in which he considered a binary dielectric fluid in a parallel plate capacitor setup. He assumed an arbitrary constitutive composition dependence for the local dielectric constant, $\epsilon(\phi(\mathbf{r}))$, and performed a perturbation expansion for composition fluctuations about the critical value, ϕ_c . For a fixed potential drop between the capacitor plates – corresponding to a fixed average electric field – Onuki determined that the field-induced critical point shift favored demixing when $\epsilon''(\phi_c) > 0$, consistent with Beaglehole’s claim, but nonetheless contradicting experiment.

Recently, Orzechowski and collaborators performed a similar analysis.⁶⁷ They assumed a purely local constitutive law for the dielectric constant, $\epsilon(\phi(\mathbf{r}))$, and derived a density functional for the electrostatic free energy of the system, given some inhomogeneous composition profile, $\phi(\mathbf{r})$, accurate to second order in fluctuations about the critical composition, ϕ_c . They remarked that within this free energy functional there are two terms dependent on the applied electric field: one proportional to $\epsilon''(\phi_c)$ and negative in sign, indicating a demixing contribution when $\epsilon''(\phi_c) > 0$, as well as one proportional to $\epsilon'(\phi_c)^2$ and positive in sign, unconditionally favoring mixing. They concluded that field-induced mixing therefore occurs when the latter term is larger in magnitude.

However, there is one subtlety of Orzechowski’s and Onuki’s analytical approaches that must be considered: their derivations assume a *purely local* constitutive model for the dependence of the dielectric constant on the fluid composition. On the other hand, the experiments performed by Debye and Kleboth, and later Beaglehole, measured the composition dependence of the macroscopic dielectric constant, which undoubtedly includes contributions from *correlated and nonlocal* fluctuation modes of composition and electrostatic potential within a bulk dielectric. In fact, the applied field-dependent contribution to the density functional derived by Orzechowski *et. al.*⁶⁷ is exactly the second order correction to the macroscopic dielectric constant obtained by Onuki,⁶⁶ highlighting the correspondence between the assumed microscopic constitutive behavior of a fluid and $\partial^2\epsilon/\partial\phi^2$, which is a macroscopic property.

In spite of Beaglehole’s claim, the pervading belief in the above experimental literature is that most chemistry pairs exhibit $\partial^2\epsilon/\partial\phi^2 > 0$, and that field-induced mixing occurs in spite

of this behavior. This is due in part to a number of universal dielectric theories, which predict this behavior for a binary fluid.

One such prediction arises because the dielectric constant of a material is related to its refractive index, n , by $\epsilon = 4\pi n^2/\mu$, where μ is the permeability of the material.²⁸ This implies a binary fluid will have $\partial^2\epsilon/\partial\phi^2 = 8\pi(\partial n/\partial\phi)^2/\mu_0$, which is valid if n is assumed a linear function of the composition and neither fluid possesses a significant magnetic susceptibility, such that its permeability can be replaced with the vacuum permeability, μ_0 . With these assumptions, $\partial^2\epsilon/\partial\phi^2$ should be universally positive. Similarly, the Clausius-Mosotti relation,²⁷ which relates the dielectric constant of a dilute fluid to the molecular polarizability of its species, gives $\partial^2\epsilon/\partial\phi^2 = 18(\alpha'_A - \alpha'_B)^2/(4\pi\rho_0\alpha'_{avg}{}^3)$, where α'_m is the polarizability volume of each species, m , $\alpha'_{avg} = \phi\alpha'_A + (1 - \phi)\alpha'_B$ is the average polarizability volume, and ρ_0 is the number density, again yielding a positive expression.

In spite of these properties of binary dielectric fluids, the free energy defined by Beaglehole (Eq. 3.2), which is correct for a weak electric field, requires $\partial^2\epsilon/\partial\phi^2 < 0$, necessitating additional, composition-dependent contributions to the dielectric constant. For electric fields within the linear regime of the fluid, the sign of $\partial^2\epsilon/\partial\phi^2$ is necessarily predictive of the direction and magnitude of an electric field-induced shift in the stability of the fluid, irrespective of the underlying microscopic phenomena responsible for the shift.

In this work, we employ a recently-developed¹⁷ field theory representation of a coarse-grained polarizable particle model to interrogate the dielectric response of binary mixtures to a uniform applied electric field. In addition to the Van der Waals (VdW) interactions that emerge in the absence of an applied field, which can induce phase separation in binary systems, the polarizable species in the fluid also respond to an external field. We go beyond the mean-field contribution to the dielectric constant that was briefly discussed in Chapter 2, elucidating fluctuation corrections that embed the correlated, nonlocal response of a polarizable fluid to an applied field. In the case of a mixture, it will be seen that the composition dependence of these fluctuation corrections is predictive of changes in miscibility induced by weak electric fields. We further elucidate how the sign and magnitude of the miscibility shift are related to contrast in structure and polarizability of the dielectric fluid components.

The structure of the chapter is as follows: In Section 3.2, a coarse-grained molecular model

of polarizable binary fluids in an applied electric field is introduced and expressed in the form of a statistical field theory. Analytical and numerical methods for computing thermodynamic observables within the field theory are subsequently discussed. Section 3.3 identifies the dielectric displacement, the dielectric constant, and other electrostatic properties as one class of such observables. We also demonstrate that Beaglehole’s expression for the free energy, Eq. 3.2, is appropriate in the linear response (weak applied field) regime of our field theory. Upon examining the composition dependence of the dielectric constant, we show that structural contrast, either due to differences in molecular architecture or differences in the respective range of Gaussian smearing, is necessary for field-induced mixing to occur. In Section 3.4.1, we consider the case of a binary simple fluid, with contrasting polarizabilities assigned to each molecule type. Contrast in ranges for smearing functions is shown to be sufficient for the existence of regimes that admit field-induced mixing. Section 3.4.2 discusses the case of a dielectric polymer blend. In addition to contrasting smearing lengths, field-induced mixing can also be enhanced for large enough differences in the Kuhn lengths of the two polymer species. Section 3.4.3 explores the special case where only one molecule type is a homopolymer, such that the mixture is a polymer solution. We find that the direction of a field-induced shift in the stability envelope can be predicted by simultaneously comparing the smearing length of the chemical species to the Kuhn length of the polymer, along with the dielectric constants of the two pure species; smearing length contrast also influences the field-dependence of miscibility when prescribed. Section 3.5 discusses experimental results from the literature in the context of the predictions made in the preceding sections. We conclude by discussing future prospects for experimental validation of our predictions, as well as potential extensions of the field-theoretic framework to incorporate additional chemistry-specific interactions.

3.2 Field Theory for a Binary Dielectric Fluid in an Applied Electric Field

We again adopt the coarse-grained model and field-theoretic representation for polarizable soft media described in Chapter 2; in the presence of an applied field, each species’ polarizability α_m determines the strength of the polarization response of the bead to the local electric field

at its center of mass. This local electric field is the superposition of the field created by the instantaneous distribution of partial charges on the bead assembly and an externally-applied electric field, \mathbf{E}_0 , which we assume to be uniform.

The present binary system is represented in the canonical ensemble, and consists of n_m molecules of type m in a volume V , where m is either species A or B . A secondary parameter, N_m , specifies the number of beads per molecule of species m . For small molecules, N_m is set to 1, and for polymers, it is the degree of polymerization of species m . We assign induced-dipoles to each bead, so that beads have a polarizability α_m .

To control the compressibility of the fluid and prevent collapse due to long-range electrostatic attractions, a Helfand energy penalty, U_h , is imposed, which has the form

$$\beta U_h = \frac{\zeta}{2\rho_0} \int d\mathbf{r} (\bar{\rho}_A(\mathbf{r}) + \bar{\rho}_B(\mathbf{r}) - \rho_0)^2, \quad (3.3)$$

where $\rho_0 = V^{-1} \sum_m n_m N_m$ is the total bead density, ζ is a parameter that controls the magnitude of the penalty (such that $\zeta \rightarrow \infty$ recovers incompressible behavior), and

$$\bar{\rho}_m(\mathbf{r}) = \sum_{i=1}^{n_m N_m} \Gamma_m(\mathbf{r} - \mathbf{r}_i) \quad (3.4)$$

is the smeared microscopic density of type m beads. Equation 3.3 ensures that local deviations of the total density from ρ_0 are harmonically penalized. In Chapter 2, bead centers of mass and partial charges were smeared by a Gaussian function, $\Gamma(\mathbf{r})$, of width a , which characterized the size of the molecules. Here we assume different smearing lengths for each bead type, such that each bead of type m has its center of mass and dipole partial charges smeared by the Gaussian function, $\Gamma_m(\mathbf{r}) = (2\pi a_m^2)^{-3/2} \exp(-r^2/(2a_m^2))$, which has characteristic width a_m and unit volume integral.

The resulting field theory has the partition function,

$$\mathcal{Z}_E = \frac{\mathcal{Z}_0}{\mathcal{Z}_\phi \mathcal{Z}_w} \int \mathcal{D}\varphi \int \mathcal{D}w e^{-H_E[\varphi, w]}, \quad (3.5)$$

where $\mathcal{Z}_0 = V^{n_A+n_B}/(n_A!n_B!)$ is the ideal gas partition function, and \mathcal{Z}_ϕ and \mathcal{Z}_w are the Gaussian normalization factors defined in Eq. 2.13. The functional integrals denoted by $\int \mathcal{D}\varphi$

and $\int \mathcal{D}w$ are taken over real fields $\varphi(\mathbf{r})$ and $w(\mathbf{r})$.

H_E is a complex-valued effective Hamiltonian, which in CGS electrostatic units has the form,

$$H_E[\varphi, w] = \frac{1}{2} \int d\mathbf{r} \left[\frac{|\nabla\varphi(\mathbf{r})|^2}{4\pi\ell_B} + \frac{\rho_0}{\zeta} w(\mathbf{r})^2 - 2i\rho_0 w(\mathbf{r}) \right] - \frac{\beta V |\mathbf{E}_0|^2}{8\pi} - \sum_m n_m \ln Q_m[w_m]. \quad (3.6)$$

The \mathbf{E}_0 -dependent term in H_E gives the vacuum free energy contribution of the applied field. Although it is of no thermodynamic consequence when considering fluctuations, this term accounts for the non-fluctuating vacuum contribution to the observed permittivity of the fluid. φ is again a fluctuating electrostatic field, and w now corresponds to the Helfand compressibility penalty.

The object Q_m is a single-molecule partition function, which gives the statistical weight of a molecule of type m , interacting with the effective potential field, w_m , defined as,

$$w_m(\mathbf{r}) = -\frac{\alpha_m}{2} |\beta e \mathbf{E}_0 - \Gamma_m * i\nabla\varphi(\mathbf{r})|^2 + \Gamma_m * iw(\mathbf{r}), \quad (3.7)$$

where the symbol $*$ denotes a convolution. For the case that m is a small molecule, Q_m is given by,

$$Q_m[w_m] = \frac{1}{V} \int d\mathbf{r} e^{-w_m(\mathbf{r})}. \quad (3.8)$$

When m is a homopolymer, we adopt the CGC model, such that,

$$Q_m[w_m] = \frac{1}{V} \int d\mathbf{r} q_m(\mathbf{r}, N_m; [w_m]), \quad (3.9)$$

where q_m is a chain propagator that solves the PDE system,

$$\begin{aligned} \frac{\partial}{\partial s} q_m(\mathbf{r}, s; [w_m]) &= \left[\frac{b_m^2}{6} \nabla^2 - w_m(\mathbf{r}) \right] q_m(\mathbf{r}, s; [w_m]) \\ q_m(\mathbf{r}, 0; [w_m]) &= 1, \end{aligned} \quad (3.10)$$

with b_m the Kuhn length of type m monomers.

The object $-i\nabla\varphi$ can be interpreted as a local fluctuation contribution to the electric field

arising from the variable positions and polarization response of the molecular partial charges. For the case of an imposed uniform electric field, φ can be assumed spatially periodic, such that the average local electric field is \mathbf{E}_0 for all configurations of φ sampled by the functional integral, $\int \mathcal{D}\varphi$. This constraint also applies to the functional integral for \mathcal{Z}_φ , so that when no beads are present ($n_A = n_B = 0$), the two φ integrals cancel, and the partition function recovers vacuum behavior, $\mathcal{Z}_E = e^{\beta V |\mathbf{E}_0|^2 / (8\pi)}$. In Section 3.3.3, we show that this constraint can be more rigorously obtained by considering a fluid in the fixed displacement ensemble (*i.e.* between two infinite conducting plates of fixed surface charge density), and performing a Legendre transform to a fixed electric field ensemble, which constrains the electric potential difference between the plates. We also choose w to be periodic, which is appropriate for a bulk fluid.

The Helmholtz free energy is related to the canonical partition function \mathcal{Z}_E by the usual thermodynamic connection formula,

$$\beta \mathcal{A}_E(n_A, n_B, V, T, \mathbf{E}_0) = -\ln \mathcal{Z}_E. \quad (3.11)$$

We note that the applied field vector, \mathbf{E}_0 , which is held fixed for all configurations of the fluid, is included as an additional state variable of the system. We will find that the corresponding conjugate quantity, \mathbf{D} – referred to as the dielectric displacement – will describe the average dielectric behavior of the fluid.

3.2.1 Mean-Field Dielectric Behavior

The simplest approximation for the functional integrals defined in Eq. 3.5 assumes the integrand is sharply peaked about purely imaginary saddle-point configurations, $i\varphi^* = \varphi_0$, where φ_0 is an arbitrary real constant that we choose to be 0 for convenience, and $w^* = 0$, which extremize the action, H_E . Evaluating the integrand at these field configurations, the mean-field free energy is immediately obtained,

$$\beta \mathcal{A}_E(n_A, n_B, V, T, \mathbf{E}_0) = -\ln \mathcal{Z}_0 + H_E[\varphi^*, w^*] = -\ln \mathcal{Z}_0 - \epsilon_{mf} \frac{V \beta |\mathbf{E}_0|^2}{8\pi}, \quad (3.12)$$

where ϵ_{mf} is the mean-field dielectric constant of the fluid:

$$\epsilon_{mf} = 1 + 4\pi\ell_B\rho_0 [\alpha_A\phi + \alpha_B(1 - \phi)], \quad (3.13)$$

with the volume fraction of type A beads defined by $\phi = n_A N_A / (n_A N_A + n_B N_B)$. This expression for ϵ_{mf} is equivalent to a composition weighting of the pure phase mean-field dielectric constants, ϵ_A and ϵ_B . The Helfand compressibility penalty makes no mean-field contribution, since it assumes a homogeneous fluid of density ρ_0 as a reference state, rather than vacuum, which was the case for the excluded volume interaction used in the preceding chapter. We note that apart from this difference at the mean-field level, the interaction specified in Eq. 3.3 is equivalent to prescribing a non-specific excluded volume interaction between beads of magnitude $u = \zeta\rho_0^{-1}$.

This free energy has the same form as the one proposed by Beaglehole (Eq. 3.2), with a dielectric constant that is *linear* in the average composition of the mixture, ϕ , thus admitting no field-induced shift in miscibility. Evidently, it is necessary to consider fluctuation contributions to the dielectric behavior of the fluid to observe an electric field-induced critical point shift.

3.2.2 Extended Gaussian Analysis: Coupled Fluctuation Modes

Beyond the simplest mean-field approximation, one can obtain an analytical expression for the lowest order fluctuation contributions to \mathcal{A}_E by employing a Gaussian approximation. As in the preceding chapter, the Hamiltonian, H_E , is truncated to second order in the Fourier modes of the field fluctuations, $\hat{\varphi}(\mathbf{k}), \hat{w}(\mathbf{k})$, with \mathbf{k} the wavevector, such that the functional integrals in Eq. 3.5 can be represented by a product of independent Gaussian integrals, and \mathcal{Z}_E can be computed analytically.

We begin by computing the second order expansion for Q_m in the field fluctuations, φ and w ; unlike the excluded volume model that was used in the preceding chapter, the present Helfand compressibility interaction admits a vanishing mean-field configuration for w , so there is no need to define the fluctuation contribution ω . Upon distributing the squared electric field term in the effective species field, w_m , given in Eq. 3.7, it proves convenient to define the linear

combination,

$$i\sigma_m(\mathbf{r}) = iw(\mathbf{r}) + \alpha_m\beta e\mathbf{E}_0 \cdot i\nabla\varphi(\mathbf{r}), \quad (3.14)$$

which collects terms that are linear in fields.

w_m can then be rewritten as:

$$w_m(\mathbf{r}) = -\frac{\alpha_m}{2}|\Gamma_m * i\nabla\varphi(\mathbf{r})|^2 + \Gamma_m * i\sigma_m(\mathbf{r}) - \frac{\alpha_m}{2}|\beta e\mathbf{E}_0|^2, \quad (3.15)$$

where terms are listed in descending order of powers of field dependence.

The desired expansion is thus obtained by truncating at linear order in the first term, which is quadratic in φ , and to second order in the second term, which is linear in σ , and thus linear in fields. The latter term is independent of the fields, φ and w , and gives a homogeneous contribution due to the average dielectric response of type- m beads. In Fourier space, the second-order single-molecule partition function is given by,

$$Q_m[w_m] \sim e^{\frac{N_m\alpha_m}{2}|\beta e\mathbf{E}_0|^2} \left\{ 1 - \frac{N_m}{2} \sum_{\mathbf{k} \neq 0} \left[\hat{\Gamma}_m^2(k)\alpha_m k^2 \hat{\varphi}(\mathbf{k})\hat{\varphi}(-\mathbf{k}) + \hat{\Lambda}_m(k)\hat{\sigma}_m(\mathbf{k})\hat{\sigma}_m(-\mathbf{k}) \right] + \dots \right\}, \quad (3.16)$$

where $\hat{\Lambda}_m$ is the single-molecule correlation function for molecules of type, m , defined as:

$$\hat{\Lambda}_m(k) = \begin{cases} \hat{\Gamma}_m^2(k), & \text{small molecule} \\ N_m \hat{\Gamma}_m^2(k) \hat{g}_D(R_{g,m}^2 k^2), & \text{homopolymer} \end{cases}, \quad (3.17)$$

where $\hat{g}_D(x) = (2/x^2)(e^{-x} + x - 1)$ is the Debye function and $R_{g,m} = b_m\sqrt{N_m/6}$ is the bare radius of gyration of polymer chains of type m .

The grouping of linear terms into the effective field, σ_m , which was subsequently carried through the derivation of Eq. 3.16, has an interesting interpretation: whereas the second-order \mathbf{E}_0 -independent electrostatic fluctuations are confined to a single bead, fluctuations due to the Helfand compressibility interaction (manifest as the w field), as well as anisotropic, electric field-dependent fluctuations, are due to correlations between pairings of all the beads of the molecule. These intramolecule bead-bead correlations are collectively quantified by the single-molecule correlation function, $\hat{\Lambda}_m$, which is dependent on both the prescribed smearing length,

and any properties of intramolecular fluctuations that arise due to the molecular architecture of m -type components.

Unlike the previous bead models, which admitted purely uncoupled fluctuation modes at the Gaussian level of analysis, the presence of an applied field here couples the fields φ and w , which is apparent in the cross terms that arise from the product $\hat{\sigma}_m(\mathbf{k})\hat{\sigma}_m(-\mathbf{k})$. It is subsequently convenient to adopt a vector-valued representation for field interactions; we proceed by defining the column vector of field fluctuations, $\mathbf{\Omega} = (\varphi, w)^T$. Combining Eqs. 3.6 and 3.16, the second-order expansion of H_E may be written as,

$$H_E[\varphi, w] \approx H_E[\varphi^*, w^*] + \frac{V}{2} \sum_{\mathbf{k}} \hat{\mathbf{\Omega}}(\mathbf{k}) \cdot [\mathbf{C}_{\mathbf{k}} + \mathbf{Q}_{\mathbf{k}}] \cdot \hat{\mathbf{\Omega}}(-\mathbf{k}), \quad (3.18)$$

where the linear term in w vanishes, due to $w^* = 0$. The explicit, quadratic field-dependent terms in H_E have exact k -space representations, which enter Eq. 3.18 according to the \mathbf{k} -dependent tensor:

$$\mathbf{C}_{\mathbf{k}} = \begin{bmatrix} \frac{k^2}{4\pi\ell_B} & 0 \\ 0 & \frac{\rho_0}{\zeta} \end{bmatrix}, \quad (3.19)$$

and the second-order, single-molecule contribution to the field interactions for each molecular species is summed to give:

$$\mathbf{Q}_{\mathbf{k}} = \rho_0 \begin{bmatrix} \phi Q_{\varphi\varphi}^A + (1-\phi)Q_{\varphi\varphi}^B & \phi Q_{\varphi w}^A + (1-\phi)Q_{\varphi w}^B \\ \phi \bar{Q}_{\varphi w}^A + (1-\phi)\bar{Q}_{\varphi w}^B & \phi Q_{ww}^A + (1-\phi)Q_{ww}^B \end{bmatrix}, \quad (3.20)$$

where \bar{z} denotes the complex conjugate of z . The single-molecule field propagators for a molecule of type m , which enter Eq. 3.20, are given by

$$\begin{aligned} Q_{\varphi\varphi}^m(\mathbf{k}) &= \alpha_m \hat{\Gamma}_m^2(k) k^2 + (\mathbf{k} \cdot \beta e \mathbf{E}_0)^2 \alpha_m^2 \hat{\Lambda}_m(k) \\ Q_{\varphi w}^m(\mathbf{k}) &= -\hat{\Lambda}_m(k) \alpha_m i \mathbf{k} \cdot \beta e \mathbf{E}_0 \\ Q_{ww}^m(\mathbf{k}) &= \hat{\Lambda}_m(k). \end{aligned} \quad (3.21)$$

Approximating the Hamiltonian by its truncated form given in Eq. 3.18, and again invoking the Fourier representation for the normalization factors \mathcal{Z}_φ and \mathcal{Z}_w , we recover a ratio of

independent Gaussian integrals corresponding to each \mathbf{k} value, which may be performed exactly:

$$\mathcal{Z}_E = \mathcal{Z}_0 \prod_{\mathbf{k}} \frac{\int d\hat{\Omega}(\mathbf{k}) e^{-H_E[\varphi, w]}}{\int d\hat{\Omega}(\mathbf{k}) e^{-(V/2) \sum_{\mathbf{k}} \hat{\Omega} \cdot \mathbf{C} \cdot \hat{\Omega}}} \approx \mathcal{Z}_0 e^{\epsilon_{mf} \frac{V\beta|\mathbf{E}_0|^2}{8\pi}} \prod_{\mathbf{k}} \left(\frac{\det(\mathbf{C}_{\mathbf{k}} + \mathbf{Q}_{\mathbf{k}})}{\det \mathbf{C}_{\mathbf{k}}} \right)^{-1/2} \quad (3.22)$$

Applying the thermodynamic connection given in Eq. 3.11 and taking the thermodynamic limit, $\sum_{\mathbf{k}} \rightarrow \frac{V}{(2\pi)^3} \int d\mathbf{k}$,³ the resulting free energy is found to be,

$$\begin{aligned} \beta \mathcal{A}_E(n_A, n_B, V, T, \mathbf{E}_0) = & -\ln \mathcal{Z}_0 - \epsilon_{mf} \frac{V\beta|\mathbf{E}_0|^2}{8\pi} + \frac{V}{2(2\pi)^3} \int d\mathbf{k} \ln \left[\hat{\gamma} \hat{\epsilon}_0 \right. \\ & \left. + (4\pi\ell_B\rho_0)^2 \left(\alpha_A^2 \phi \hat{\Lambda}_A + \alpha_B^2 (1-\phi) \hat{\Lambda}_B + \zeta(\alpha_A - \alpha_B)^2 \phi(1-\phi) \hat{\Lambda}_A \hat{\Lambda}_B \right) \frac{\beta(\mathbf{k} \cdot \mathbf{E}_0)^2}{4\pi\rho_0|\mathbf{k}|^2} \right], \quad (3.23) \end{aligned}$$

where symbols with a hat denote functions that depend on the wavevector magnitude, $k = |\mathbf{k}|$ (*e.g.* $\hat{f} \rightarrow \hat{f}(k)$).

The function $\epsilon_0(k)$ is again the dielectric screening function, here defined as,

$$\hat{\epsilon}_0(k) = 1 + 4\pi\ell_B\rho_0 \left(\alpha_A \phi \hat{\Gamma}_A^2(k) + \alpha_B (1-\phi) \hat{\Gamma}_B^2(k) \right). \quad (3.24)$$

As we noted in the previous chapter, dielectric screening is insensitive to chain architecture effects, with the contribution of each species depending only on its polarizability and its Fourier-transformed smearing function, $\hat{\Gamma}_m(k) = e^{-(a_mk)^2/2}$. The kernel,

$$\hat{\gamma}(k) = 1 + \zeta \left(\phi \hat{\Lambda}_A(k) + (1-\phi) \hat{\Lambda}_B(k) \right), \quad (3.25)$$

gives the strength of w field screening due to the compressibility penalty, and is sensitive to the entire correlation function of each molecule type.

As was the case for the Gaussian free energy given in Eq. 2.40, Eq. 3.23 contains a loop integral that gives the fluctuation correction to the mean-field free energy by summing contributions from each fluctuation mode of wavevector \mathbf{k} . We can again obtain fluctuation corrections to any observable of interest (*e.g.* the dielectric constant) by direct differentiation of the integrand, revealing insight about fluctuation contributions at different length scales and orientations, determined by the magnitude and direction, respectively, of \mathbf{k} .

For example, the composition dependence of the integrand of Eq. 3.23 manifests as an effective χ parameter that can be inferred from the stability limit (spinodal) of the system:

$$\left. \frac{\partial^2 \beta \mathcal{A}_E}{\partial \phi^2} \right|_{\rho_0, V, T, \mathbf{E}_0} = - \left. \frac{\partial^2 \ln \mathcal{Z}_0}{\partial \phi^2} \right|_{\rho_0, V, T, \mathbf{E}_0} - 2V \rho_0 \chi_{eff} = 0, \quad (3.26)$$

such that χ_{eff} quantifies the fluctuation effects that compete with the entropy of mixing. This expression for the spinodal is appropriate when the fluid behaves incompressibly, such that phase separation would give rise to two coexisting phases of contrasting compositions, each with total bead density ρ_0 .

Examining the integrand in Eq. 3.23, the first term inside the logarithm is isotropic and is the product of two contributions, one from the Helfand compressibility interaction and one from electrostatics. The composition dependence of the former term involving $\hat{\gamma}(k)$ gives rise to an effective χ parameter that favors demixing and is nonzero when the two molecules have different correlation functions. It is given by,

$$\chi_h = \frac{1}{8\pi^2 \rho_0} \int_0^\infty dk k^2 \left[\frac{\zeta (\hat{\Lambda}_A - \hat{\Lambda}_B)}{\hat{\gamma}} \right]^2, \quad (3.27)$$

where we have used the identity $\int d\mathbf{k} = 4\pi \int_0^\infty dk k^2$, which is appropriate when the integrand is isotropic. Taking the incompressible ($\zeta \rightarrow \infty$) limit of χ_h recovers an expression that was previously derived in a paper by Fredrickson, Liu, and Bates (FLB),⁶⁸ wherein an unsmeared model was used to interrogate structural influences on miscibility in a homopolymer blend. The contrast in correlation functions was provided by differences in the Kuhn lengths and/or degrees of polymerization of the chains. FLB found that the integral diverges, such that an upper cutoff wavevector must be introduced to render χ_h finite. Even in the present model, which exponentially damps fluctuation modes *via* the smearing functions, the integral in Eq. 3.27 diverges in the incompressible limit. Moreover, choosing a large, but finite value for ζ produces a χ_h that is unphysically large.

Although this χ contribution is of no consequence to the dielectric behavior of the fluid and thus does not enter any of the observables considered in the present article, it is problematic if one is interested in computing phase diagrams, as it renders the mixture unconditionally

unstable, preventing computation of any sensible phase envelope. Moreover, χ_h is composition dependent, such that the critical composition of the fluid is strongly dependent on the value of ζ , overwhelming any other effects that could shift the critical composition. Thus if complete phase diagrams computed with the present field theory are desired, a more sophisticated regularization method to suppress the contribution of χ_h is necessary. A possible approach would be the renormalized one-loop formalism developed by Morse and collaborators for models without electrostatics.⁶⁹

The composition dependence of $\hat{\epsilon}_0$ in the first term of the integrand of Eq. 3.23 gives rise to a χ contribution of a similar form, which is due to contrast in the polarizability and/or the smearing lengths of the two molecules. It is given by,

$$\chi_{vdw} = \frac{(4\pi\ell_B\rho_0)^2}{8\pi^2\rho_0} \int_0^\infty dk k^2 \left[\frac{\alpha_A \hat{\Gamma}_A^2 - \alpha_B \hat{\Gamma}_B^2}{\hat{\epsilon}_0} \right]^2. \quad (3.28)$$

This χ contribution has been previously considered,^{17,70} and it arises from the preference for the more strongly polarizable molecular species to aggregate due to stronger favorable VdW interactions. Like the parameter χ_{VDW} that was determined in Eq. 2.70, χ_{vdw} is dependent on the contrast in polarizability of the two beads, and also depends on the contrast of smearing functions of the two species that is presently imposed. The two are found to correspond when one reverts to an assumption of equal smearing lengths ($a_A = a_B = a$) and assumes a dilute fluid, retaining the leading-order term in bead densities.

As we observed when considering the behavior of the pressure contribution due to induced dipoles, Π_{VDW} , which was depicted Fig. 2.3, we see that the expression for χ_{vdw} in Eq. 3.28 includes a dielectric screening contribution, which enters as $\hat{\epsilon}_0$. We also noted that the full loop integral for Π_{VDW} given in Eq. 2.70 was independent of any molecular architecture effects. Similarly, χ_{vdw} is independent of the correlation functions of the molecules, indicating that it is strictly a property of the bead type pairing.

The final term in the fluctuation integrand of Eq. 3.23 is anisotropic, depending on the angle between the wavevector, \mathbf{k} , and the electric field vector, \mathbf{E}_0 , such that it vanishes when the two vectors are perpendicular. Its presence reduces the rotational invariance (isotropy) of the fluctuation spectrum to a cylindrical symmetry about the electric field direction. This expres-

sion has a complicated dependence on the composition, and is also sensitive to the structure of the molecules, apparent from the presence of the correlation functions, $\hat{\Lambda}_A$ and $\hat{\Lambda}_B$. We defer detailed discussion of the χ contribution associated with this term, *which we will show to determine the direction of an electric field-induced miscibility shift*, to Section 3.3. Nonetheless, it is easily seen that in the absence of an applied electric field, density and electrostatic fluctuations become isotropic and uncoupled, such that they contribute to the miscibility of the fluid only through χ_h and χ_{vdw} , respectively.

Fully-Fluctuating Field-Theoretic Simulations

To ascertain the behavior of the fluid mixture when all orders of fluctuations are permitted, we adopt the CL procedure described Section 2.3.3, replacing the free energy \mathcal{A} and Hamiltonian H with \mathcal{A}_E and H_E , respectively. In addition to the pre-existing natural variables for a binary system in the Canonical ensemble (n_A , n_B , V , and T), the applied field vector \mathbf{E}_0 is an additional fixed quantity that enters as a state variable of \mathcal{A}_E .

In the following section, we will find that direct application of \mathbf{E}_0 derivatives of the free energy given in Eq. 3.11 yields thermodynamic observables that describe the dielectric behavior of the fluid, with corresponding operators appropriate for averaging using a CL simulation procedure. Consequently, the correspondence between the average behavior of a statistical system and its observed physical properties – which is a key motivation for research in the field of statistical thermodynamics – is extended to apply to a fluid’s dielectric properties.

3.3 Dielectric Response

As discussed in the Introduction, the field-dependent shift in the miscibility of a binary fluid arises from the composition dependence of its dielectric response. At the mean-field level we have seen that the dielectric constant is linear in composition, so no change in miscibility is predicted upon the imposition of an electric field. Beyond the mean-field approximation, however, the introduction of an applied field to a binary dielectric fluid gives rise to strongly correlated, coupled fluctuations in the fields, φ and w , which manifest as contributions to the dielectric constant with a nonlinear composition dependence. These fluctuation contributions

therefore determine both the sign and magnitude of any field-induced shift in miscibility.

3.3.1 Dielectric Displacement

The most readily apparent observable for quantifying dielectric behavior in the fixed electric field ensemble is the dielectric displacement, which is obtained by taking an applied field derivative of the free energy, yielding:

$$\mathbf{D} = -\frac{4\pi}{V} \frac{\partial \mathcal{A}_E}{\partial \mathbf{E}_0} \Big|_{n_A, n_B, V, T} = \langle \tilde{\mathbf{D}}[\varphi, w] \rangle. \quad (3.29)$$

Within the field theory, the dielectric displacement is obtained by thermally averaging the corresponding operator, $\tilde{\mathbf{D}}$, which is given by,

$$\tilde{\mathbf{D}}[\varphi, w] = -\frac{4\pi k_B T}{V} \frac{\partial H_E[\varphi, w]}{\partial \mathbf{E}_0} = \mathbf{E}_0 + 4\pi \tilde{\mathbf{P}}[\varphi, w], \quad (3.30)$$

where $\tilde{\mathbf{P}}[\varphi, w]$ is a polarization operator, defined as,

$$\tilde{\mathbf{P}}[\varphi, w] = \frac{\ell_B}{V} \int d\mathbf{r} \sum_m \alpha_m \tilde{\rho}_m(\mathbf{r}; [\varphi, w]) (\mathbf{E}_0 - \Gamma_m * i(\beta e)^{-1} \nabla \varphi(\mathbf{r})). \quad (3.31)$$

The object $\tilde{\rho}_m$ gives the local density of beads from type- m molecules, and is given by,

$$\tilde{\rho}_m(\mathbf{r}) = \frac{n_m}{Q_m V} \begin{cases} e^{-w_m(\mathbf{r})}, & \text{small molecule} \\ \int_0^{N_m} ds q_m(\mathbf{r}, s) q_m(\mathbf{r}, N_m - s) & \text{homopolymer,} \end{cases} \quad (3.32)$$

with the functional dependence of $\tilde{\rho}_m$, Q_m , and q_m on the fields, φ and w , suppressed for a more compact notation.

Applying the thermal average, $\langle \dots \rangle$, to both sides of Eq. 3.30 recovers $\mathbf{D} = \mathbf{E}_0 + 4\pi \mathbf{P}$, which is a well-known relation between displacement, field, and polarization in continuum dielectric theory.²¹ In a parallel plate capacitor setup, bounding a medium with no free charges, the macroscopic dielectric displacement \mathbf{D} corresponds to the unscreened field generated by the charges on the plates. The average field generated by the polarized fluid points in the opposite direction as its average polarization, such that the net electric field within the medium, \mathbf{E} , is

reduced relative to \mathbf{D} . This effect is apparent when \mathbf{D} is instead held fixed and the average field within the medium \mathbf{E} emerges self-consistently. This behavior is discussed in detail in Section 3.3.3.

Rearranging the relation in Eq. 3.30 gives $\mathbf{E}_0 = \tilde{\mathbf{D}} - 4\pi\tilde{\mathbf{P}}$, which has a fixed, non-fluctuating quantity on the left-hand side, and a difference of two fluctuating quantities on the right-hand side, leading to the following interpretation: within the fixed electric field ensemble, the spatially averaged electric field must always equal \mathbf{E}_0 , such that fluctuations in the spatially averaged polarization, which arise from corresponding fluctuations in the configuration of the molecular species of the fluid, must be exactly cancelled by a reconfiguration of the displacement field, and correspondingly the charge on the plates. Connecting the plates to a battery, which was the procedure for the experiments discussed in the Introduction, ensures that this constraint is satisfied by providing a charge bath.

Further insight into these expressions can be obtained from the Gaussian approximation to the field theory. The Gaussian order dielectric displacement is obtained by taking $\partial/\partial\mathbf{E}_0$ of the Gaussian free energy given in Eq. 3.23:

$$\begin{aligned} \mathbf{D} = & \epsilon_{mf}\mathbf{E}_0 - \frac{1}{(2\pi)^3\rho_0} \\ & \times \int d\mathbf{k} \frac{(4\pi\ell_B\rho_0)^2 \left(\alpha_A^2\phi\hat{\Lambda}_A + \alpha_B^2(1-\phi)\hat{\Lambda}_B + \zeta(\alpha_A - \alpha_B)^2\phi(1-\phi)\hat{\Lambda}_A\hat{\Lambda}_B \right) \frac{\mathbf{k}\mathbf{k}}{\tilde{\gamma}|\mathbf{k}|^2} \cdot \mathbf{E}_0}{\hat{\epsilon}_0 + (4\pi\ell_B\rho_0)^2 \left(\alpha_A^2\phi\hat{\Lambda}_A + \alpha_B^2(1-\phi)\hat{\Lambda}_B + \zeta(\alpha_A - \alpha_B)^2\phi(1-\phi)\hat{\Lambda}_A\hat{\Lambda}_B \right) \frac{\beta(\mathbf{k}\cdot\mathbf{E}_0)^2}{4\pi\rho_0\tilde{\gamma}|\mathbf{k}|^2}}. \end{aligned} \quad (3.33)$$

The integrand of the loop integral in Eq. 3.33 appears as a ratio of two expressions: in the numerator is a term that is linear in the applied field, evidently specifying a bare fluctuation contribution due to the applied field from second-order field fluctuations. The presence of terms both with and without the Helfand compressibility parameter, ζ , implies contributions from a combination of purely electrostatic ($\varphi\varphi$) and coupled electrostatic-density (φw) modes. Additionally, the terms in this expression depend on the single-molecule correlation functions, $\hat{\Lambda}_m$, indicating a sensitivity of the dielectric behavior of the fluid to molecular architecture. In the denominator appears the entire argument of the logarithm in the fluctuation integral of the Gaussian free energy, Eq. 3.23, specifying a wavevector-dependent screening of fluid response to

an applied field. Evidently, fluctuation corrections to the dielectric displacement are screened by the nonlocal bare dielectric function of the fluid, $\hat{\epsilon}_0(k)$, modified by a self-consistent contribution that is $O(E_0^2)$ and depends on both fluid structure and architecture.

This complicated dependence of the dielectric displacement on coupled fluctuation modes is in contrast to other Gaussian-order observables, such as χ_{vdw} (Eq. 3.28), which arises purely from electrostatic fluctuations, and consequently only experiences screening due to the bare dielectric function, $\hat{\epsilon}_0$. We can understand this qualitative difference by examining the character of second-order field correlations due to the beads of the fluid, which are collectively enumerated by the \mathbf{k} -dependent tensor \mathbf{Q}_k , defined in Eq. 3.20. The off-diagonal elements of \mathbf{Q}_k , which correspond to coupled φw correlations, vanish as $\mathbf{E}_0 \rightarrow 0$. Evidently, at Gaussian order, no such couplings exist in the absence of an applied field.

3.3.2 Linear Dielectric Behavior and the Dielectric Constant

The dielectric displacement can be generally expressed as a nonlinear function of the applied field, valid for all magnitudes of \mathbf{E}_0 . However, we can obtain a simpler expression for the dielectric response of the fluid by assuming \mathbf{E}_0 is small in magnitude. In this regime, the dielectric displacement is linear in the applied field, such that the two can be related by a quantity, ϵ , referred to as the dielectric constant.²¹ This object is particularly useful for connecting the predictions of the present theory to physically realized mixtures, as dielectric constants have been tabulated for a wide variety of dielectric fluids and polymers. Moreover, the composition dependence for the dielectric constant of binary mixtures was directly measured in two of the experimental papers discussed in the Introduction (Refs. 22,23). Further, as discussed by Beaglehole,²³ the response of a binary fluid to a weak applied electric field is completely specified by its dielectric constant, such that Eq. 3.2 is exact, and the composition dependence of the dielectric constant necessarily dictates any field-induced shift in miscibility.

Holding all non-electrostatic state variables of \mathcal{A}_E constant and adopting the simplified notation $\mathcal{A}_E(\mathbf{E}_0)$ for the free energy, we can relate a binary fluid in the presence of a field to

the same system in the absence of a field by thermodynamic integration:

$$\mathcal{A}_E(\mathbf{E}_0) = \mathcal{A}_E(\mathbf{0}) + \int_0^{|\mathbf{E}_0|} dE \left. \frac{\partial \mathcal{A}_E}{\partial \mathbf{E}_0} \right|_{\mathbf{E}_0 = E \hat{\mathbf{E}}_0} \cdot \hat{\mathbf{E}}_0 = \mathcal{A}_E(\mathbf{0}) - \frac{V}{4\pi} \int_0^{|\mathbf{E}_0|} dE \mathbf{D}(E \hat{\mathbf{E}}_0) \cdot \hat{\mathbf{E}}_0, \quad (3.34)$$

where $\hat{\mathbf{E}}_0 \equiv \mathbf{E}_0/|\mathbf{E}_0|$ is a unit vector giving the electric field direction, and we have chosen a path of integration that lies parallel to the applied electric field vector, which can be traversed by integrating over the field magnitude, parametrized as the scalar-valued dummy variable, E . Noting that the fluid carries no net polarization in the absence of an applied field, such that \mathbf{D} identically vanishes in the limit $\mathbf{E}_0 \rightarrow 0$, the linear response formula for \mathbf{D} as a function of some weak applied field \mathbf{E} can be written as,

$$\mathbf{D}(\mathbf{E}) = \left. \frac{\partial \mathbf{D}}{\partial \mathbf{E}_0} \right|_{\mathbf{E}_0 = \mathbf{0}} \cdot \mathbf{E} + O(E^2). \quad (3.35)$$

Inserting this expression for \mathbf{D} into Eq. 3.34, the thermodynamic integration can be performed analytically, yielding,

$$\mathcal{A}_E(\mathbf{E}_0) = \mathcal{A}_E(\mathbf{0}) - \frac{V}{8\pi} \left. \frac{\partial \mathbf{D}}{\partial \mathbf{E}_0} \right|_{\mathbf{E}_0 = \mathbf{0}} : \mathbf{E}_0 \mathbf{E}_0 + O(E_0^3). \quad (3.36)$$

If the fluid exhibits isotropic dielectric behavior such that $\partial \mathbf{D} / \partial \mathbf{E}_0 = \epsilon \mathbf{I}$, where ϵ is a scalar and \mathbf{I} is the identity tensor, the expression for the free energy further simplifies:

$$\mathcal{A}_E(\mathbf{E}_0) = \mathcal{A}_E(\mathbf{0}) - \epsilon \frac{V}{8\pi} |\mathbf{E}_0|^2 + O(E_0^3), \quad (3.37)$$

such that ϵ is the *dielectric constant* of the fluid, given by,

$$\epsilon = \frac{1}{3} \text{Tr} \left. \frac{\partial \mathbf{D}}{\partial \mathbf{E}_0} \right|_{\mathbf{E}_0 = \mathbf{0}} = -\frac{4\pi}{3V} \text{Tr} \left. \frac{\partial^2 \mathcal{A}_E}{\partial \mathbf{E}_0 \partial \mathbf{E}_0} \right|_{\mathbf{E}_0 = \mathbf{0}}, \quad (3.38)$$

and the form proposed by Beaglehole (Eq. 3.2) is recovered. The dielectric constant may be also be inserted into Eq. 3.35, obtaining the relation,

$$\mathbf{D} = \epsilon \mathbf{E}, \quad (3.39)$$

which is a well known property of linear, isotropic dielectric materials.²¹

The associated field-theoretic operator for the dielectric constant of a fluid is computed according to Eq. 2.43:

$$\begin{aligned}\tilde{\epsilon}[\varphi, w] &= \frac{k_B T}{3} \text{Tr} \left(-\frac{4\pi}{V} \frac{\partial^2 H_E[\varphi, w]}{\partial \mathbf{E}_0 \partial \mathbf{E}_0} + \frac{V}{4\pi} \text{cov}(\beta \tilde{\mathbf{D}}[\varphi, w], \beta \tilde{\mathbf{D}}[\varphi, w]) \right)_{\mathbf{E}_0=\mathbf{0}} \\ &= \epsilon_{mf} - \frac{(i)^2 4\pi \ell_B}{3V} \sum_m \alpha_m^2 \int d\mathbf{r} \tilde{\rho}_m(\mathbf{r}; [\varphi, w]) |\Gamma_m * \nabla \varphi(\mathbf{r})|^2 - \frac{4\pi \beta V}{3} |\tilde{\mathbf{P}}[\varphi, w]|_{\mathbf{E}_0=\mathbf{0}}^2, \quad (3.40)\end{aligned}$$

which is appropriate when the fluid exhibits isotropic dielectric behavior. Due to this isotropy, all the diagonal elements of the tensor-valued expression that enters $\text{Tr}(\dots)$ will thermally average to the same value (each giving the relationship between D_j and $E_{0,j}$ for a different Cartesian direction j), so that only one of these elements is required to compute $\tilde{\epsilon}$. However, since a 3-dimensional CL simulation of the dielectric fluid includes all three of these independently-fluctuating quantities, taking the average defined by $(1/3)\text{Tr}(\dots)$ reduces the variance of $\tilde{\epsilon}$ by a factor of $3^{-1/2}$ with no additional computational cost.

When the behavior of the fluid is anisotropic, one can similarly define an operator for the *dielectric susceptibility tensor* given by

$$\begin{aligned}\tilde{\chi}_e[\varphi, w] &= \frac{(\epsilon_{mf} - 1)}{4\pi} \mathbf{I} - 4\pi \beta V \tilde{\mathbf{P}}[\varphi, w] \tilde{\mathbf{P}}[\varphi, w]_{\mathbf{E}_0=\mathbf{0}} \\ &\quad - \frac{(i)^2 \ell_B}{V} \sum_m \alpha_m^2 \int d\mathbf{r} \tilde{\rho}_m(\mathbf{r}; [\varphi, w]) \Gamma_m * \nabla \varphi(\mathbf{r}) \Gamma_m * \nabla \varphi(\mathbf{r}). \quad (3.41)\end{aligned}$$

The factor of the identity tensor, \mathbf{I} , is subtracted away because the standard literature definition for $\chi_e = \langle \tilde{\chi}_e \rangle$ neglects the vacuum contribution.²¹ In the limit $\mathbf{E}_0 \rightarrow \mathbf{0}$, the average displacement, $\langle \tilde{\mathbf{D}} \rangle$, vanishes, as does the non-fluctuating vacuum contribution to $\tilde{\mathbf{D}}$, so that $\tilde{\mathbf{D}} \rightarrow 4\pi \tilde{\mathbf{P}}$, and the covariance in the top line of Eq. 3.40 is replaced by the latter term. We have also neglected a term proportional to the dyadic, $(\partial Q_m / \partial \mathbf{E}_0)(\partial Q_m / \partial \mathbf{E}_0)$, since it gives a correlation contribution that vanishes in the thermodynamic limit ($V \rightarrow \infty$).

As an alternative approach, one can estimate the dielectric constant operator by invoking

the relation, $\mathbf{D} \approx \epsilon \mathbf{E}_0$, for an \mathbf{E}_0 of small magnitude, E_0 :

$$\tilde{\epsilon}[\varphi, w] \sim \frac{\hat{\mathbf{z}} \cdot \tilde{\mathbf{D}}[\varphi, w]|_{\mathbf{E}_0 = E_0 \hat{\mathbf{z}}}}{E_0} + O(E_0), \quad (3.42)$$

where $\hat{\mathbf{z}}$ is a unit vector describing the direction of the applied field vector. This approximate method is found to admit a lower variance due to CL-generated noise, as well as smaller errors due to the choice of finite Δt , compared to the exact expression defined in Eq. 3.40.

In practice, we find that it takes orders of magnitude longer simulation time to compute ϵ from its exact linear response behavior given by the expression in Eq. 3.40, compared to the estimate provided by Eq. 3.42. Nevertheless, the two methods attain the expected agreement when errors are rendered small by proper parametrization of each numerical procedure. We consequently use the latter approach to compute ϵ for the systems considered in Sections 3.4.1-3.4.3.

When this approach is used, error in the measured value of ϵ will arise from CL-generated noise, as well as the weak nonlinear response that enters Eq. 3.42; the latter can be estimated by expressing \mathbf{D} , evaluated at $\mathbf{E}_0 = E_0 \hat{\mathbf{z}}$, as a Taylor series expansion about $\mathbf{E}_0 = \mathbf{0}$, retaining the first 2 non-zero terms:

$$D_z(E_0) \sim E_0 D'_z(0) + \frac{1}{2!} E_0^2 D''_z(0) + O(E_0^3) \sim E_0 \epsilon + \frac{1}{2} E_0^2 \frac{\partial \epsilon}{\partial E_{0,z}} + O(E_0^3), \quad (3.43)$$

with $D_z(E) \equiv \hat{\mathbf{z}} \cdot \mathbf{D}|_{\mathbf{E}_0 = E \hat{\mathbf{z}}}$ an E -dependent function defined for convenience.

Inserting this expansion for D_z into Eq. 3.42, the error due to nonlinear response in the measured dielectric constant will be given by,

$$\Delta \epsilon \sim \frac{1}{2!} E_0 \frac{\partial \epsilon}{\partial E_{0,z}} + O(E_0^2). \quad (3.44)$$

The approximation, $\epsilon \approx \epsilon_a(E_0) \equiv D_z(E_0)/E_0$, will thus have the leading order error contribution, δ_ϵ , which can then be estimated using a finite difference by measuring \mathbf{D} at two different field magnitudes, E_0 and $E_0 + \Delta E$:

$$\delta_\epsilon \equiv \left| \frac{E_0}{2} \frac{\partial \epsilon}{\partial E_{0,z}} \right| \sim \frac{E_0}{2} \left| \frac{\epsilon_a(E_0 + \Delta E) - \epsilon_a(E_0)}{\Delta E} + O\left(\frac{E_0}{\Delta E}\right) + O(\Delta E) \right|, \quad (3.45)$$

evidently implying an optimal $\Delta E \sim E_0^{1/2}$ that minimizes the sum of the two contributions to the residual.

Although δ_ϵ does not provide a strict upper bound for the error (*i.e.* when all terms of the series for D_z in Eq. 3.43 have the same sign, we will have $|\Delta\epsilon| > \delta_\epsilon$), it is useful for determining the magnitude of the nonlinear response error that enters Eq. 3.42.

Equations 3.40 and 3.41 are *exact* field operators for the dielectric constant and dielectric susceptibility of the model. Within the Gaussian approximation, the average dielectric constant is similarly computed by inserting the Gaussian free energy (Eq. 3.23) into Eq. 3.38, resulting in

$$\epsilon = \epsilon_{mf} - \frac{(4\pi\ell_B\rho_0)^2}{6\pi^2\rho_0} \int_0^\infty \frac{dk k^2}{\hat{\gamma}\hat{\epsilon}_0} \left[\alpha_A^2\phi\hat{\Lambda}_A + \alpha_B^2(1-\phi)\hat{\Lambda}_B + \zeta\phi(1-\phi)(\alpha_A - \alpha_B)^2\hat{\Lambda}_A\hat{\Lambda}_B \right]. \quad (3.46)$$

Evidently, fluctuation corrections to the dielectric constant of a polarizable binary fluid are universally *negative* in sign, corresponding to a depression relative to the mean-field value. Comparing this expression to the Gaussian dielectric displacement, given in Eq. 3.33, it can be seen that the final $O(E_0^2)$ term in the denominator has been discarded, so that screening occurs only through the zero-field dielectric function $\hat{\epsilon}_0$. The assumption of linear dielectric response is thus equivalent to assuming that externally-driven, (applied) field-dependent fluctuation modes are small in magnitude relative to field-independent, thermally excited fluctuations. It is worth noting that Eq. 3.46 is equivalent to the $k \rightarrow 0$ limit of Eq. 28 in Ref. 70, wherein a homopolymer blend of equal-length, conformationally symmetric chains was considered with single-molecule correlation functions $\hat{\Lambda}_A = \hat{\Lambda}_B = N\hat{g}_D\hat{\Gamma}^2$.

In the incompressible ($\zeta \rightarrow \infty$) limit, no local fluctuations in the total density of the fluid are permitted, and the dielectric constant in the Gaussian approximation simplifies to

$$\epsilon = \epsilon_{mf} - \frac{(4\pi\ell_B\rho_0)^2\phi(1-\phi)(\alpha_A - \alpha_B)^2}{6\pi^2\rho_0} \int_0^\infty dk k^2 \frac{\hat{\Lambda}_A\hat{\Lambda}_B}{\hat{\gamma}_\infty\hat{\epsilon}_0}, \quad (3.47)$$

with the kernel $\hat{\gamma}_\infty \equiv \phi\hat{\Lambda}_A + (1-\phi)\hat{\Lambda}_B$, which accounts for steric screening effects due to incompressibility. In this limiting case the only remaining fluctuation correction is proportional to the polarizability contrast $(\alpha_A - \alpha_B)^2$ and the factor $\phi(1-\phi)$, which vanishes when the fluid

is a pure phase ($\phi = 0$ or 1). Evidently, an induced-dipole fluid requires either total density or composition fluctuations in order to admit fluctuation contributions to the dielectric constant. Single component induced-dipole fluids, which permit neither, thus exhibit simple mean-field dielectric behavior in the Gaussian approximation.

Based on this property of induced-dipole fluids, in the following sections we will prescribe the polarizability of each molecular species, α_m , by assuming that its mean-field dielectric constant, $1 + 4\pi\ell_B\alpha_m\rho_0$, is equal to its fluctuation-corrected pure-phase dielectric constant ϵ_m . In other words, we assume that α_m is everywhere replaced by the expression $(\epsilon_m - 1)/(4\pi\ell_B\rho_0)$, and dependence on the Bjerrum length, ℓ_B , exactly cancels. Any deviation from this assumption for a pure-phase fluid can be understood as a consequence of our choice of a finite value for ζ , which permits small fluctuation corrections to ϵ_m .

Although the experimental systems considered in the references discussed in the Introduction generally include at least one molecular species with a significant *permanent dipole*, our simple model embeds only induced-dipole behavior. In applying the theory to permanent dipole systems, it should be understood that the value for ϵ_m used to parameterize α_m embeds mean-field contributions from both the polarizability and permanent dipole of the molecular species.⁷¹ In such instances, α_m can be interpreted as a renormalized or effective polarizability. We also note that the polarizability contribution to the dielectric constant of a fluid is temperature-independent, whereas its dipole contribution is proportional to $\beta \sim 1/T$.⁷¹ Consequently, this approach for illuminating the dielectric behavior of a binary fluid is only appropriate for the temperature at which the dielectric constant of each component was measured.

Linear Response Regime

To identify the magnitude of nonlinear dielectric response in the fluid, it is instructive to perform an expansion of the dielectric displacement about its linear response contribution, $\mathbf{D} \approx \epsilon\mathbf{E}_0$. In the Gaussian approximation, given by Eq. 3.33, non-linear response arises from the electric field dependence of the latter term in the denominator of the integrand; Taylor expanding yields,

$$\mathbf{D} \sim \left[\epsilon_{mf} - \frac{1}{2\pi^2\rho_0} \int_0^\infty dk k^2 \frac{\hat{v}}{\hat{\gamma}\hat{\epsilon}_0} \sum_{j=0}^\infty \frac{\left(\frac{-\hat{v}}{\hat{\gamma}\hat{\epsilon}_0} \frac{\beta|\mathbf{E}_0|^2}{4\pi\rho_0} \right)^j}{2j+3} \right] \mathbf{E}_0, \quad (3.48)$$

where we have assumed the summand of the series is less than 1 for all values of \mathbf{k} , ensuring convergence, and used the identity, $\int d\mathbf{k}(\mathbf{k} \cdot \mathbf{E}_0/|\mathbf{k}|)^{2n} = 4\pi(2n+1)^{-1} \int_0^\infty dk k^2 |\mathbf{E}_0|^{2n}$, to integrate out the orientation dependence of each summand. The kernel, \hat{v} , gives the wavevector-dependent, unscreened fluctuation contribution to the dielectric susceptibility of the fluid, and is defined as,

$$\hat{v}(k) = (4\pi\ell_B\rho_0)^2 \left(\alpha_A^2 \phi \hat{\Lambda}_A(k) + \alpha_B^2 (1-\phi) \hat{\Lambda}_B(k) + \zeta(\alpha_A - \alpha_B)^2 \phi(1-\phi) \hat{\Lambda}_A(k) \hat{\Lambda}_B(k) \right). \quad (3.49)$$

We note that discarding $j \neq 0$ terms of the summation in Eq. 3.48 recovers linear dielectric behavior, $\mathbf{D} = \epsilon \mathbf{E}_0$, where ϵ is the Gaussian-order dielectric constant defined in Eq. 3.46.

Inspecting the expansion defined in Eq. 3.48, one can infer a dimensionless parameter,

$$\delta \equiv \max_k \left(\frac{\hat{v}(k)}{\hat{\gamma}(k)\hat{\epsilon}_0(k)} \right) \frac{\beta |\mathbf{E}_0|^2}{4\pi\rho_0}, \quad (3.50)$$

which gives the magnitude of contributions to the dielectric displacement from nonlinear response (we neglect the factor of $(2j+3)^{-1}$, since the ratio of consecutive summands approaches a form in the $j \rightarrow \infty$ limit that is insensitive to this prefactor). Thus, we can say that a fluid is expected to respond linearly to an applied field, \mathbf{E}_0 , when the field-dependent fluctuation contribution is small relative to the field-independent, internally-generated fluctuations.

Even in the incompressible limit, δ has a complicated dependence on the composition of the fluid and the wavevector magnitude, k . However, we can obtain an upper bound by determining by inspection that the expression $\hat{v}/(\hat{\gamma}\hat{\epsilon}_0)$ is monotonically decreasing with k :

$$\delta \leq \frac{(\epsilon_A - \epsilon_B)^2}{\min(\epsilon_A, \epsilon_B)} \frac{N_A N_B}{\min(N_A, N_B)} \frac{\beta |\mathbf{E}_0|^2}{8\pi\rho_0}. \quad (3.51)$$

The dependence on N_A and N_B arises because the correlation function, $\hat{\Lambda}_m$, approaches N_m as $k \rightarrow 0$.

As an example, we consider a generic binary fluid with pure-component dielectric constants $\epsilon_A = 10.0$ and $\epsilon_B = 2.0$, and assume a bead number density of $\rho_0 = 10^{28} \text{ m}^{-3} = 10^{22} \text{ cm}^{-3}$, which is typical for a small molecule liquid. The experiments discussed in the Introduction that measured the critical points of simple binary fluids, with $N_A = N_B = 1$, used electric field

strengths of up to $20 \text{ MV/m} \approx 667 \text{ statvolt/cm}$. At room temperature, with this electric field strength, one obtains $\delta \leq 2.75 \times 10^{-4}$, indicating $|\mathbf{E}_0|$ is well within the linear response regime, in spite of the seemingly large electric field magnitude. Similarly, Wirtz and Fuller³³ considered polymer solutions with molecular weights that corresponded to $1000 \leq N \leq 10,000$, at a field strength of $0.5 \text{ MV/m} \approx 16.68 \text{ statvolt/cm}$. Assuming the same dielectric constant pair and bead number density as in the preceding paragraph, with the choice of $N = 10,000$, we obtain $\delta \leq 1.722 \times 10^{-3}$, again indicating a negligible contribution from nonlinear dielectric response.

3.3.3 Dielectric Fluid in a Fixed Displacement Field

In the preceding section, we introduced a field theory description for a binary dielectric fluid, in the presence of a fixed uniform applied electric field. We presently consider instead a binary, induced-dipole fluid that lies between two infinite, parallel capacitor plates, which have a surface charge density, $\pm\sigma_0$. We define the unit vector, $\hat{\mathbf{z}}$, to be perpendicular to the plates, such that the displacement field between the plates is given by $\mathbf{D}_0 = 4\pi\sigma_0\hat{\mathbf{z}}$. If the positively charged plate lies at $z = 0$, with the negatively charged plate at $z = L$, we can adopt a piecewise representation to specify the displacement field over all space:

$$\mathbf{D}(\mathbf{r}) = \begin{cases} \mathbf{0}, & z < 0 \\ \mathbf{D}_0, & 0 < z < L \\ \mathbf{0}, & z > L, \end{cases} \quad (3.52)$$

and can similarly compute a scalar-valued function, ρ_f , for the free charge density at all points in space, according to the identity $\rho_f = (4\pi e)^{-1}\nabla \cdot \mathbf{D}$:²¹

$$\rho_f(\mathbf{r}) = \frac{|\mathbf{D}_0|}{4\pi e} (\delta(z) - \delta(z - L)) = \frac{\sigma_0}{e} (\delta(z) - \delta(z - L)), \quad (3.53)$$

where δ is the Dirac delta function.

In addition to the free charges present on the plates, the paired partial charges of each bead type, with valence $\pm\delta q_m$, contribute to a microscopic bound charge density function, defined

within the medium:

$$\bar{\rho}_b(\mathbf{r}) = \sum_m \sum_{i=1}^{A/B 2n_m} (-1)^i \delta q_m \Gamma_m(\mathbf{r} - \mathbf{r}_{m,i}), \quad (3.54)$$

such that charges with odd indices will be negative, and the charge pairs of each of the n_m beads of type m contribute to $\bar{\rho}_b$ according to the smearing function, Γ_m , centered at their location, $\mathbf{r}_{m,i}$. Each bead's partial charges are bonded to its center of mass by a harmonic potential of strength, K , but otherwise freely translate.

The electrostatic potential energy is obtained from the bare Coulomb interaction:

$$\begin{aligned} \beta U_{el} &= \frac{\ell_B}{2} \int d\mathbf{r} \int d\mathbf{r}' \frac{[\rho_f(\mathbf{r}) + \bar{\rho}_b(\mathbf{r})][\rho_f(\mathbf{r}') + \bar{\rho}_b(\mathbf{r}')] }{|\mathbf{r} - \mathbf{r}'|} \\ &= \frac{\ell_B}{2} \int d\mathbf{r} \int d\mathbf{r}' \frac{\bar{\rho}_b(\mathbf{r})\bar{\rho}_b(\mathbf{r}')}{|\mathbf{r} - \mathbf{r}'|} + \ell_B \int d\mathbf{r} \int d\mathbf{r}' \frac{\rho_f(\mathbf{r})\bar{\rho}_b(\mathbf{r}')}{|\mathbf{r} - \mathbf{r}'|} + \frac{\beta V}{8\pi} |\mathbf{D}_0|^2, \end{aligned} \quad (3.55)$$

where expanding the quadratic term in the numerator of the first integral yields terms due to the pairwise interactions of the beads, the interactions of the beads with the surface charge on the plates, and the vacuum electrostatic potential energy of the plates, respectively.

We assign the same non-electrostatic properties to the beads as in the preceding section, such that the corresponding field theory for this particle model in the Canonical ensemble will have the partition function,

$$\mathcal{Z}'_D = \frac{\mathcal{Z}_0}{\mathcal{Z}_\psi \mathcal{Z}_w} \int \mathcal{D}\psi \int \mathcal{D}w e^{-H'_D[\psi, w]}, \quad (3.56)$$

where \mathcal{Z}_ψ has the same form as \mathcal{Z}_φ – defined in Eq. 2.13 – but with no restrictions placed on the domain of integration, $\int \mathcal{D}\psi$.

The associated effective Hamiltonian is given by,

$$\begin{aligned} H'_D[\psi, w] &= \frac{1}{2} \int d\mathbf{r} \left[\frac{|\nabla\psi(\mathbf{r})|^2}{4\pi\ell_B} + \frac{\rho_0}{\zeta} w(\mathbf{r})^2 - 2i\rho_0 w(\mathbf{r}) \right] \\ &+ \frac{\beta V |\mathbf{D}_0|^2}{8\pi} - \sum_m n_m \ln Q'_m [i\Gamma_m * \psi, i\Gamma_m * w], \end{aligned} \quad (3.57)$$

with Q'_m a single-molecule partition function, which computes the statistical weight of a type- m bead that interacts with the smeared chemical potential field, $i\Gamma_m * w$. The bead's partial

charges fluctuate about its center of mass, and interact with the total local electric potential, which sums contributions due to pair interactions with other smeared charges, and due to the free charges on the capacitor plates:

$$\psi_{m,tot}(\mathbf{r}) = i\Gamma_m * \psi(\mathbf{r}) + \ell_B \int d\mathbf{r}' \frac{\rho_f(\mathbf{r}')}{|\mathbf{r} - \mathbf{r}'|}, \quad (3.58)$$

where ψ is dimensionless, such that the product, $e^{-1}\psi$, returns a field with units of electric potential.

In Chapter 2, it was shown that a multipole expansion could be performed, such that the interaction of the bead's partial charges with the local electric potential could be approximated by a parameter, $\alpha_m = (\delta q_m)^2/K$ – called the polarizability – which interacts with the effective local electric field, given by,

$$\mathbf{E}_{m,tot}(\mathbf{r}) = -(\beta e)^{-1} \nabla \psi_{m,tot}(\mathbf{r}) = \mathbf{D}_0 - (\beta e)^{-1} \Gamma_m * i \nabla \psi(\mathbf{r}), \quad (3.59)$$

at the bead's center of mass.

Adopting this approximation, Q'_m can immediately be replaced with Q_m , defined in Eq. 3.8, for a small molecule interacting with the effective chemical potential field,

$$w_m(\mathbf{r}) = i\Gamma_m * w(\mathbf{r}) - \frac{\alpha_m}{2} |\mathbf{E}_{m,tot}(\mathbf{r})|^2. \quad (3.60)$$

The Helmholtz free energy in the fixed displacement ensemble is subsequently obtained from the thermodynamic connection,

$$\beta \mathcal{A}_D(n_A, n_B, V, T, \mathbf{D}_0) = -\ln \mathcal{Z}'_D. \quad (3.61)$$

Boundary Conditions and Macroscopic Polarization

If we assume the separation between the charged plates, L , is large, we can restrict our analysis to the region near the center of the medium, far from either plate, where the fluid exhibits bulk behavior. Since the charged plates are not connected to a battery, no restrictions have yet been placed on ψ , and it is free to attain non-periodic configurations – corresponding to a nonvanish-

ing contribution to the average electric field – in addition to admitting inhomogeneities due to local fluctuations of the fluid. It is instructive to segregate these two respective contributions to ψ according to:

$$i\psi(\mathbf{r}) = i\varphi(\mathbf{r}) + 4\pi\beta e\mathbf{P} \cdot \mathbf{r}, \quad (3.62)$$

where φ is a periodic function that accounts for local perturbations to the electric potential due to fluctuations of the fluid, and the latter term has the form of a ramp, accounting for the spatially averaged electric field generated by a fluid with macroscopic polarization density, \mathbf{P} . With this substitution, the local effective electric field experienced by type- m beads becomes:

$$\mathbf{E}_{m,tot}(\mathbf{r}) = \mathbf{D}_0 - 4\pi\mathbf{P} - (\beta e)^{-1}\Gamma_m * i\nabla\varphi(\mathbf{r}). \quad (3.63)$$

Extending this substitution to the form of the functional integral over ψ defined in Eq. 3.56, the partition function can be reexpressed as:

$$\mathcal{Z}'_D = \frac{\mathcal{Z}_0}{\mathcal{Z}_\psi \mathcal{Z}_w} \int d\mathbf{P} \int \mathcal{D}\varphi \int \mathcal{D}w e^{-H'_D[\psi,w]}, \quad (3.64)$$

such that the macroscopic polarization density and the local perturbations in the electric potential, φ , are treated as distinct fluctuating objects.

If we define a macroscopic polarization per molecule, $\mathbf{p} \equiv \rho_0^{-1}\mathbf{P}$, the Canonical partition function can be rewritten as,

$$\begin{aligned} \mathcal{Z}'_D = & \frac{\mathcal{Z}_0 \rho_0}{\mathcal{Z}_\psi \mathcal{Z}_w} \int d\mathbf{p} \int \mathcal{D}\varphi \int \mathcal{D}w (z_A[w_A])^{n_A} (z_B[w_B])^{n_B} \\ & \times e^{-\int (|\nabla\varphi|^2 + |\beta e\mathbf{D}_0|^2)/(8\pi\ell_B) - \rho_0 \int (w^2/(2\zeta) - iw)}, \end{aligned} \quad (3.65)$$

with $z_m[w_m] = Q_m[w_m] \exp(4\pi\rho_0\beta|\mathbf{p}|^2/2)$, which highlights that \mathbf{P} -dependent contributions to \mathcal{Z}'_D scale exponentially with particle number.

In the thermodynamic limit, the integral over \mathbf{P} in the partition function becomes sharply peaked, and the free energy may be evaluated at a fixed, equilibrium value of the polarization density, \mathbf{P}^* , according to,

$$\beta\mathcal{A}_D(n_A, n_B, V, T, \mathbf{D}_0) = -\ln \mathcal{Z}_D, \quad (3.66)$$

where \mathcal{Z}_D is the associated Canonical partition function, given by,

$$\begin{aligned}\mathcal{Z}_D &= \frac{\mathcal{Z}_0}{\mathcal{Z}_\varphi \mathcal{Z}_w} \int \mathcal{D}\varphi \int \mathcal{D}w e^{-H_D[\varphi, w]}, \\ H_D[\varphi, w] &= \frac{1}{2} \int d\mathbf{r} \left[\frac{|\nabla\varphi(\mathbf{r})|^2}{4\pi\ell_B} + \frac{\rho_0}{\zeta} w(\mathbf{r})^2 - 2i\rho_0 w(\mathbf{r}) \right] \\ &\quad - \sum_m n_m \ln Q_m[w_m] + \frac{\beta V}{8\pi} (|\mathbf{D}_0|^2 - |4\pi\mathbf{P}^*|^2),\end{aligned}\quad (3.67)$$

and \mathbf{P}^* satisfies,

$$\left\langle \frac{\partial H_D[\psi, w]}{\partial \mathbf{P}} \Big|_{\mathbf{P}=\mathbf{P}^*} \right\rangle = 0. \quad (3.68)$$

Here, $\langle \dots \rangle$ denotes an ensemble average with the weighting, e^{-H_D} .

The condition for \mathbf{P}^* is found to be,

$$\mathbf{P}^* = \left\langle \frac{\ell_B}{V} \int d\mathbf{r} \sum_m \alpha_m \tilde{\rho}_m(\mathbf{r}; [\varphi, w]) \mathbf{E}_{m, tot}(\mathbf{r}) \right\rangle = \frac{(\epsilon_{mf} - 1)}{4\pi\epsilon_{mf}} \mathbf{D}_0 + \langle \tilde{\mathbf{P}}_{fl}[\varphi, w] \rangle, \quad (3.69)$$

where ϵ_{mf} is the mean-field dielectric constant, and the operator,

$$\tilde{\mathbf{P}}_{fl}[\varphi, w] = -\frac{e}{\epsilon_{mf}V} \int d\mathbf{r} \sum_m \alpha_m \tilde{\rho}_m(\mathbf{r}; [\varphi, w]) \Gamma_m * i\nabla\varphi(\mathbf{r}), \quad (3.70)$$

gives the fluctuation contribution to the polarization.

Unlike the field theory described in Section 3.2, which constrains the average electric field within the medium to be \mathbf{E}_0 , irrespective of the behavior of the fluid, the present framework separately includes a contribution to the average electric field from the macroscopic polarization density, \mathbf{P}^* , which is nonfluctuating, but which nevertheless depends on the average behavior of the fluctuating fluid. Consequently, Eq. 3.69 can be said to give a *self-consistent* condition for the average polarization density. A simulation of the present field theory would thus require a fixed-point iteration, in which a “guess” for \mathbf{P}^* is chosen, and then its value is updated according to Eq. 3.69, where the righthand side is evaluated at the current value of \mathbf{P}^* – requiring a full CL calculation – yielding a new value of \mathbf{P}^* .

Dielectric Behavior in Fixed \mathbf{D} Ensemble

Drawing analogy to the average displacement vector considered in Section 3.3, one can compute the average electric field in the fixed displacement ensemble by taking a \mathbf{D}_0 derivative of the free energy. The associated operator is found to be,

$$\tilde{\mathbf{E}}[\varphi, w] = \frac{4\pi k_B T}{V} \frac{\partial H_D[\varphi, w]}{\partial \mathbf{D}_0} = \mathbf{D}_0 - 4\pi \left(\mathbf{P}^* + \tilde{\mathbf{P}}_{fl}[\varphi, w] - \langle \tilde{\mathbf{P}}_{fl}[\varphi, w] \rangle \right) = \frac{\mathbf{D}_0}{\epsilon_{mf}} - 4\pi \tilde{\mathbf{P}}_{fl}[\varphi, w]. \quad (3.71)$$

Repeating the thermodynamic integration procedure that lead to Eq. 3.37, and noting that the average electric field can be related to a weak displacement field according to the linearization, $\mathbf{E} \equiv \langle \tilde{\mathbf{E}}[\varphi, w] \rangle \sim \epsilon^{-1} \mathbf{D}_0 + O(D_0^2)$ – where we have assumed isotropic behavior ($\partial \mathbf{E} / \partial \mathbf{D}_0 \sim \epsilon^{-1} \mathbf{I}$) – one obtains:

$$\mathcal{A}_D(\mathbf{D}_0) \sim \mathcal{A}_D(\mathbf{0}) + \epsilon^{-1} \frac{V\beta |\mathbf{D}_0|^2}{8\pi} + O(D_0^3) \sim \mathcal{A}_D(\mathbf{0}) + \epsilon \frac{V\beta |\mathbf{E}|^2}{8\pi} + O(D_0^3), \quad (3.72)$$

yielding the form for the free energy proposed by Debye and Kleboth.²²

The apparent dielectric constant, ϵ , that enters Eq. 3.72 is defined according to:

$$\begin{aligned} \frac{1}{\epsilon} &= \frac{4\pi}{3V} \text{Tr} \left. \frac{\partial^2 \mathcal{A}_D}{\partial \mathbf{D}_0 \partial \mathbf{D}_0} \right|_{\mathbf{D}_0=\mathbf{0}} \\ &= \frac{1}{\epsilon_{mf}} + \left\langle \frac{4\pi\beta V \epsilon_{mf}}{3} |\tilde{\mathbf{P}}_{fl}[\varphi, w]|^2 + \frac{4\pi\ell_B(i)^2}{3\epsilon_{mf}V} \int d\mathbf{r} \sum_m \alpha_m^2 \tilde{\rho}_m(\mathbf{r}; [\varphi, w]) |\Gamma_m * \nabla \varphi(\mathbf{r})|^2 \right\rangle. \end{aligned} \quad (3.73)$$

In the limit of vanishing displacement, the macroscopic polarization, \mathbf{P}^* , also vanishes, and the thermal average in Eq. 3.73 may be computed with a single CL calculation. This expression differs from the dielectric constant in a fixed \mathbf{E} ensemble (Eq. 3.40) – even though the two field theories become identical in the limit of vanishing external fields – because the two expressions enumerate the response of the fluid to weak fields with differing associated electrostatic boundary conditions. We do note, however, that this expression for the dielectric constant admits agreement with Eq. 3.40 if expanded to second order in electrostatic fluctuations, φ .

Legendre Transform to Fixed Electric Field Ensemble

If the plates are then connected to a battery that requires the electric potential drop between them to be $\bar{\psi}$, the average electric field within the medium will subsequently be fixed at:

$$\mathbf{E}_0 = \frac{\bar{\psi}}{L} \hat{\mathbf{z}}. \quad (3.74)$$

For a given configuration of the fields φ and w , the charges on the plates couple to the potential drop imposed by the battery, such that the displacement field identically couples to the applied electric field. Consequently, \mathbf{D}_0 will adopt a value that minimizes the sum of the free energy of the medium and the potential energy due to coupling with \mathbf{E}_0 , giving rise to the following Legendre transform:

$$\mathcal{A}_E = \min_{\mathbf{D}_0} \left(\mathcal{A}_D(\mathbf{D}_0) - \frac{V}{4\pi} \mathbf{D}_0 \cdot \mathbf{E}_0 \right), \quad (3.75)$$

which is satisfied by,

$$\mathbf{D}_0^* - \mathbf{E}_0 = \left\langle \frac{4\pi\ell_B}{V} \int d\mathbf{r} \sum_m \alpha_m \tilde{\rho}_m \mathbf{E}_{m,tot}(\mathbf{r}) \right\rangle. \quad (3.76)$$

Combining Eqs. 3.69 and Eq. 3.76, one obtains the condition:

$$\mathbf{E}_0 = \mathbf{D}_0^* - 4\pi\mathbf{P}^* = \left\langle \tilde{\mathbf{E}}[\varphi, w] \right\rangle, \quad (3.77)$$

which recovers the expected relation, $\mathbf{D} = \mathbf{E} + 4\pi\mathbf{P}$, and equivalently constrains the macroscopic electric field to the value \mathbf{E}_0 .

The field theory described in Section 3.2 is then immediately obtained by the substitution,

$$\mathcal{A}_E(n_A, n_B, V, T, \mathbf{E}_0) = \mathcal{A}_D(n_A, n_B, V, T, \mathbf{D}_0^*) - \frac{V}{4\pi} \mathbf{E}_0 \cdot \mathbf{D}_0^*, \quad (3.78)$$

which eliminates dependence on \mathbf{D}_0 .

3.3.4 Field-Dependent Miscibility Contributions

Returning to the fixed electric field ensemble, one can ascertain the field-induced shift in miscibility by combining the definition of χ_{eff} given in Eq. 3.26 with the linearized form for the free energy of a fluid in an electric field, Eq. 3.37, which is appropriate for an incompressible fluid in the presence of a weak electric field:

$$\chi_E = \frac{1}{2} \frac{\partial^2 \epsilon}{\partial \phi^2} \frac{\beta |\mathbf{E}_0|^2}{8\pi\rho_0}. \quad (3.79)$$

The observable $(\partial^2 \epsilon / \partial \phi^2)$ is obtained from a 4th order derivative of \mathcal{A}_E , due to the two \mathbf{E}_0 derivatives that enter the definition of ϵ . After some simplification, it is given by:

$$\frac{\partial^2 \epsilon}{\partial \phi^2} = \left\langle \frac{\partial^2 \tilde{\epsilon}[\varphi, w]}{\partial \phi^2} - 2\beta\rho_0 V \text{cov} \left(\frac{\partial \tilde{\epsilon}[\varphi, w]}{\partial \phi}, \tilde{\mu}_c[\varphi, w] \right) + (\beta\rho_0 V)^2 \text{cov}(\tilde{\epsilon}[\varphi, w], \tilde{\mu}_c[\varphi, w], \tilde{\mu}_c[\varphi, w]) \right\rangle, \quad (3.80)$$

with the composition derivatives of the dielectric constant operator found to be

$$\begin{aligned} \frac{\partial \tilde{\epsilon}[\varphi, w]}{\partial \phi} &= 4\pi\ell_B\rho_0(\alpha_A - \alpha_B) \\ &\quad - \frac{4\pi(i)^2}{3V} \int d\mathbf{r} \left[\frac{\tilde{\rho}_A(\mathbf{r}; [\varphi, w])}{\phi} |\Gamma_A * \nabla\varphi(\mathbf{r})|^2 - \frac{\tilde{\rho}_B(\mathbf{r}; [\varphi, w])}{1-\phi} |\Gamma_B * \nabla\varphi(\mathbf{r})|^2 \right] \\ &\quad - \frac{8\pi\beta V}{3} \left(\frac{|\tilde{\mathbf{P}}_A[\varphi, w]|^2}{\phi} + \frac{\tilde{\mathbf{P}}_A[\varphi, w] \cdot \tilde{\mathbf{P}}_B[\varphi, w]}{\phi(1-\phi)} - \frac{|\tilde{\mathbf{P}}_B[\varphi, w]|^2}{1-\phi} \right) \\ \frac{\partial^2 \tilde{\epsilon}[\varphi, w]}{\partial \phi^2} &= \frac{8\pi\beta V}{3} \left(\frac{|\tilde{\mathbf{P}}_A[\varphi, w]|^2}{\phi^2} - 2 \frac{\tilde{\mathbf{P}}_A[\varphi, w] \cdot \tilde{\mathbf{P}}_B[\varphi, w]}{\phi(1-\phi)} + \frac{|\tilde{\mathbf{P}}_B[\varphi, w]|^2}{(1-\phi)^2} \right), \end{aligned} \quad (3.81)$$

where $\tilde{\mathbf{P}}_m$ denotes the contribution of m type beads to the volume-averaged polarization of the fluid, and is defined as:

$$\tilde{\mathbf{P}}_m[\varphi, w] = \frac{ie\alpha_m}{V} \int d\mathbf{r} \tilde{\rho}_m(\mathbf{r}[\varphi, w]) \Gamma_m * \nabla\varphi(\mathbf{r}). \quad (3.82)$$

We have also defined the operator $\tilde{\mu}_c$ appearing in Eq. 3.80 as

$$\tilde{\mu}_c[\varphi, w] = -k_B T \left(\frac{\ln Q_A[w_A]}{N_A} - \frac{\ln Q_B[w_B]}{N_B} \right), \quad (3.83)$$

which gives the contrast in the chemical potential per bead between molecules. Evidently, μ_c is an *exchange* chemical potential that prescribes the chemical equilibrium condition for a binary system with two coexisting incompressible phases, each with fixed total bead density, ρ_0 .

Equation 3.80 thus in principle provides a route for directly computing $\epsilon''(\phi) \equiv \partial^2 \epsilon / \partial \phi^2$ in a CL field-theoretic simulation. We note, however, that substituting the full expression for $\tilde{\epsilon}$ into the latter term of this operator yields a term that is the product of a prefactor that is $O(V^3)$, and a fluctuating object with mean value that is $O(V^{-3})$. This large prefactor amplifies noise by a factor of V^2 relative to the stochastic behavior of $\tilde{\epsilon}$, which already amplifies noise by a factor of V compared to first-order operators. Proper sampling of the operator for $\epsilon''(\phi)$ is thus prohibitively expensive, requiring several orders of magnitude more simulation time, compared to $\tilde{\epsilon}$, to adequately average out noise. We have therefore elected to compute $\epsilon''(\phi)$ by numerical differentiation of estimates of $\epsilon(\phi)$ obtained from CL simulations.

An alternative approach is to invoke the Gaussian approximation. Applying Eq. 3.79 to the incompressible, Gaussian order dielectric constant given in Eq. 3.47, the following field-dependent miscibility contribution is obtained:

$$\chi_E = \frac{(\epsilon_{mf,A} - \epsilon_{mf,B})^2}{6\rho_0^2\pi^2} \times \int_0^\infty dk k^2 \frac{\hat{\Lambda}_A \hat{\Lambda}_B}{\hat{\gamma}_\infty \hat{\epsilon}_0^2} \left[\frac{\hat{\epsilon}_A \hat{\epsilon}_B}{\hat{\epsilon}_0} - \frac{(\hat{\Lambda}_A - \hat{\Lambda}_B) (\hat{\epsilon}_A \hat{\Lambda}_A \phi^2 - \hat{\epsilon}_B \hat{\Lambda}_B (1 - \phi)^2)}{\hat{\gamma}_\infty^2} \right] \frac{\beta |\mathbf{E}_0|^2}{8\pi}, \quad (3.84)$$

where $\hat{\epsilon}_m = 1 + 4\pi\ell_B\rho_0\alpha_m\hat{\Gamma}_m^2$ is the bare dielectric function for a pure fluid of type m molecules with density ρ_0 , related to its mean-field value by $\epsilon_{mf,m} = \hat{\epsilon}_m(0)$. The form of this object illuminates two different fluctuation contributions to miscibility. The first term is strictly positive, corresponding to a field-induced demixing contribution for any choice of parameters, while the latter has a signed dependence on the single-molecule correlation functions, $\hat{\Lambda}_m$, the dielectric functions, $\hat{\epsilon}_m$, and the composition. Depending on the sign of the latter term throughout the spectrum of wavevectors k , these two contributions will either compete, or will both favor field-induced demixing.

In particular, the last term depends on the difference of the two correlation functions, $\hat{\Lambda}_A - \hat{\Lambda}_B$. If both molecular components have the same single-molecule correlation function,

$\hat{\Lambda}_A = \hat{\Lambda}_B = \hat{\Lambda}$, the latter term vanishes, and the expression simplifies considerably:

$$\chi_E = \frac{((\epsilon_{mf,A} - \epsilon_{mf,B})^2 \beta |\mathbf{E}_0|^2)}{6\rho_0^2 \pi^2} \frac{1}{8\pi} \int_0^\infty dk k^2 \frac{\hat{\Lambda} \hat{\epsilon}_A \hat{\epsilon}_B}{\hat{\epsilon}_0^3}, \quad (3.85)$$

predicting field-induced demixing for any prescribed electrostatic properties.

Alternatively, if there exists strong contrast in the molecular structure of the two molecular components – and consequently their correlation functions – the latter term does not vanish. Instead, there exist regimes within the fluctuation spectrum for which one of the two correlation functions is dominant. If we break A , B symmetry of the expression in Eq. 3.84, and we arbitrarily choose $\hat{\Lambda}_A$ to be dominant, such that $\hat{\Lambda}_A \gg \hat{\Lambda}_B$, the expression inside [...] in Eq. 3.84 reduces to

$$\hat{\epsilon}_A \left(\frac{\hat{\epsilon}_B}{\hat{\epsilon}_0} - 1 \right), \quad (3.86)$$

which is negative when $\alpha_A > \alpha_B$.

Evidently, field-induced mixing is possible when the stronger dielectric component is also the one which dominates the steric environment of the fluid over the fluctuation modes that make the largest contribution to dielectric behavior.

We can interpret this result by considering the form of the dielectric constant in Eq. 3.47: the numerators of the prefactor and integrand together give the contribution from a field-dependent net repulsion between A and B beads. This repulsion arises from a field-enhancement of the attractive VdW interactions between beads, which induce demixing by favoring aggregation of the more strongly polarizable beads. This enhancement of VdW attractions occurs because the average unperturbed configuration of individual beads is now a polarized state, rather than an isotropic one, favoring aligned orientations of the beads' dipoles, which increases the statistical weight of configurations for which the dipole-dipole pair interaction is attractive.

However, when one considers the contribution from the function, $\hat{\gamma}_\infty$, the field-induced alignment of dipoles becomes screened by the steric environment of the fluid, and the field-enhancement of VdW attractions is reduced relative to an unscreened state. If the molecule type that has the larger polarizability also has a sufficiently dominant correlation function, the free energy contribution from field-enhancement of VdW attractions will be maximized

when the fluid is mixed, such that molecules with a weaker correlation function are present, and the value of $\hat{\gamma}_\infty$ is reduced. If instead the more strongly polarizable molecular component has the weaker correlation function, both the bare field-enhanced VdW contribution and the contribution from $\hat{\gamma}_\infty^{-1}$ are maximized in a phase-separated state, and the latter term in [...] in Eq. 3.84 becomes positive.

We note that the simplified form in Eq. 3.86 is only valid for wavevectors that give $\hat{\Lambda}_A \gg \hat{\Lambda}_B$, and does not hold for the entire domain of integration. Thus, this expression is only instructive if it corresponds to values of k that are not rendered small by the prefactor of [...] in Eq. 3.84. As this prefactor depends on the product of correlation functions, $\hat{\Lambda}_A \hat{\Lambda}_B$, the weighting it imposes on k values is highly dependent on the structural properties assigned to each molecular component.

3.4 Results

3.4.1 Binary Dielectric Simple Fluid

In the simplest case of a binary small molecule mixture, the correlation functions, $\hat{\Lambda}_A$ and $\hat{\Lambda}_B$, are replaced by the smearing functions, $\hat{\Gamma}_A^2$ and $\hat{\Gamma}_B^2$, respectively. As described above, field-induced mixing can occur when the stronger dielectric species admits a stronger correlation behavior. Consequently, we presently choose the A species to possess the larger dielectric constant, and also assign it the smaller smearing length, such that $\hat{\Gamma}_A^2$ is more slowly decaying in k , and $\hat{\Gamma}_A^2 > \hat{\Gamma}_B^2$ for all values of k . A smaller smearing length corresponds to stronger correlations because it indicates a bead that is more “point-like”, permitting correlations at smaller wavelengths (larger values of k).

In Fig. 3.1, we have chosen $\epsilon_B = 2.0$, and selected a different value for ϵ_A in each of the two plots. $\partial^2\epsilon/\partial\phi^2$ is plotted as a function of composition, for 3 different values of the smearing length contrast. These plots all have a similar shape, giving a large positive value of $\partial^2\epsilon/\partial\phi^2$ when the A volume fraction is smaller; as ϕ increases, the curve changes sign, at a composition we will call ϕ_0 , and then adopts negative values that are much smaller in magnitude than the positive values found when $\phi < \phi_0$. Field-induced mixing is less likely to occur at smaller values of ϕ because in this regime, $\hat{\gamma}_\infty$, which weights the steric screening according to the

volume fraction of each species, more heavily weights the weaker correlation function, $\hat{\Lambda}_B$. Consequently, demixing carries a weaker penalty due to screening of the VdW interaction, and the effect is insufficient to overcome the bare preference for demixing in the numerator of Eq. 3.47. A fluid can evidently be said to exhibit field-induced mixing if $\phi_c > \phi_0$, where ϕ_c is the critical composition of the fluid.

Unsurprisingly, Fig. 3.1 shows that field-induced mixing ($\partial^2\epsilon/\partial\phi^2 < 0$) occurs over a broader range of compositions when the contrast in the smearing lengths is larger. The range of k values for which Eq. 3.86 is valid can be identified by taking the ratio of the two smearing functions:

$$\frac{\hat{\Gamma}_B^2(k)}{\hat{\Gamma}_A^2(k)} = [e^{-(a_B^2 - a_A^2)k^2}] \ll 1, \quad (3.87)$$

such that the integrand of Eq. 3.84 is negative for $k \gtrsim (a_B^2 - a_A^2)^{-1/2}$. However, for sufficiently large wavevector magnitudes, $k \gtrsim a_B^{-1}$, the presence of $\hat{\Lambda}_B = \hat{\Gamma}_B^2$ in the prefactor of [...] in Eq. 3.84 exponentially damps the integrand, such that its contribution to the loop integral is reduced in weight. For there to exist a range of k values that satisfies $(a_B^2 - a_A^2)^{-1/2} < k < a_B^{-1}$ – such that the weighting of the integrand in Eq. 3.84 decays more slowly in k^2 than the ratio in Eq. 3.87, and Eq. 3.86 is recovered – it is necessary to choose $a_A/a_B < 2^{-1/2} \approx 0.707$.

Although this cutoff is not very sharp, due to the soft behavior of the Gaussian smearing functions (evident in the $a_A/a_B = 0.8$ curves in Fig. 3.1, which still admit a window of field-induced mixing), and its value, $2^{-1/2}$, is specific to the present choice of Gaussian smearing functions as a regularization procedure, it is expected to also exist in models that use alternative regularization methods, wherein sharper functional forms are chosen for $\hat{\Lambda}_A$ and $\hat{\Lambda}_B$. In such a system, field-induced mixing would still require the existence of a length-scale for which A molecules have a dominant correlation function, but for which fluctuations are not significantly suppressed by $\hat{\Lambda}_B$, implying some critical ratio of length-scales for the two bead types that is necessary for there to exist any k that satisfies both of these conditions.

Additionally, choosing a larger value for ϵ_A also shifts the field-induced mixing regime to a broader range of compositions. We can understand this effect by examining the expression in Eq. 3.86; when ϵ_A is larger, the ratio in the first term of (...) is reduced relative to -1 , increasing the magnitude of (...), and the prefactor, $\hat{\epsilon}_A$, is also increased, such that this contribution

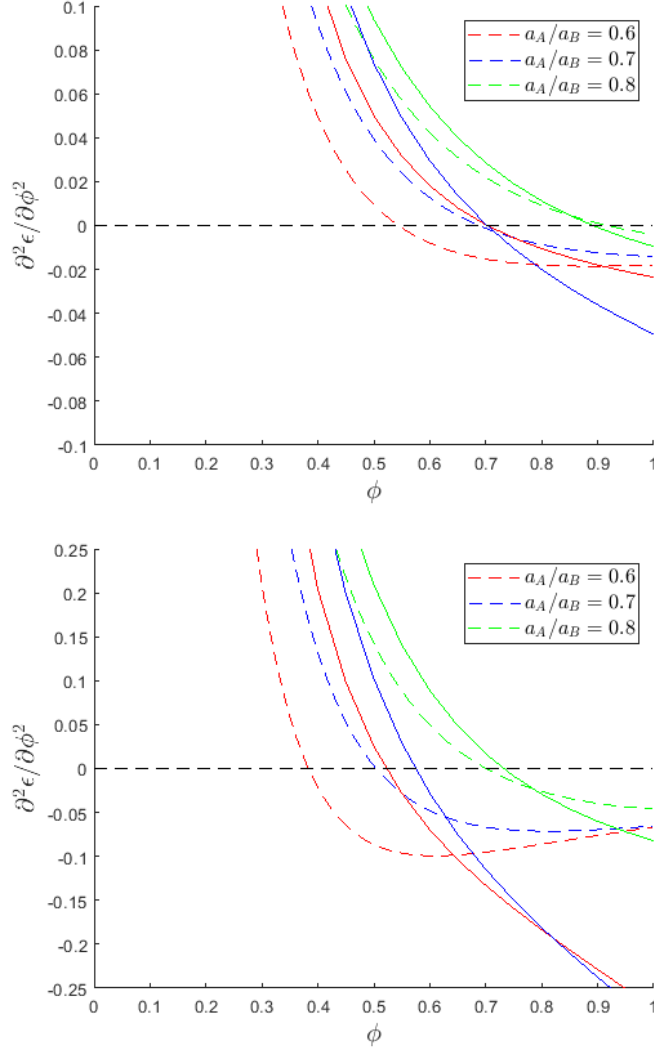


Figure 3.1: Plots of $\partial^2\epsilon/\partial\phi^2$ vs A bead volume fraction for a binary simple fluid, with average bead density $\rho_0 a_B^3 = 2.0$. The dashed curves were computed in the incompressible limit using the Gaussian approximation, and the solid curves were obtained from numerically differentiating $\epsilon(\phi)$ data computed in CL, with Helfand compressibility parameter $\zeta = 250$. The dielectric constant pairs are (**top**) $\epsilon_A = 8.0$, $\epsilon_B = 2.0$ and (**bottom**) $\epsilon_A = 15.0$, $\epsilon_B = 2.0$. The dashed line at $\partial^2\epsilon/\partial\phi^2 = 0$ is added to more easily identify where the curves change sign. The window of compositions that admit field-induced mixing ($\partial^2\epsilon/\partial\phi^2 < 0$) can be widened by increasing either the dielectric contrast or the contrast in smearing lengths.

to the integrand, which favors mixing, is increased in weight. Within the conceptualization of field-enhanced VdW interactions discussed in the previous section, we can make the following argument: increasing ϵ_A increases the net preference for A beads to aggregate at the unscreened fluctuation level – however, it does so indiscriminately, such that the magnitude of χ_E is increased, regardless of sign, and no preference for mixing or demixing is imparted. On the other hand, the presence of the dielectric function, $\hat{\epsilon}_0$, in the denominator of Eq. 3.47 indicates dielectric screening of these field-enhanced VdW interactions, such that the favorable VdW interactions in the A -rich branch are now more strongly screened by the larger dielectric function – relative to a single mixed phase – resulting in a stronger net penalty for demixing.

3.4.2 Dielectric Homopolymer Blend

If we instead choose each molecular component to be a homopolymer, the correlation function for a type- m chain will be given by $\hat{\Lambda}_m = N_m \hat{g}_D(N_m b_m^2 k^2 / 6) \hat{\Gamma}_m^2$, introducing the Kuhn lengths, b_A and b_B , as an additional species-dependent length-scale that can contrast the two molecule types, as well as the unperturbed radii of gyration of the chains, $R_{g,A}$ and $R_{g,B}$, where $R_{g,m} = b_m(N_m/6)^{1/2}$. These length-scales will give rise to multiple regimes within the integrand of Eq. 3.84, and the behavior of the correlation functions at each of these corresponding regimes for the wavevector magnitude, k , will determine the form of $\hat{\gamma}_\infty$, and thus the sign of χ_E .

At low k , such that $k \lesssim \min(R_{g,A}^{-1}, R_{g,B}^{-1})$, corresponding to wavelengths that are larger than the greater of the two radii of gyration, the k -dependent functions that enter each correlation function are approximately 1, such that $\hat{\Lambda}_m = N_m$, and each chain behaves as a point particle consisting of N_m beads. Again adopting the convention, $\epsilon_A > \epsilon_B$, choosing $N_A \gg N_B$ would evidently recover field-induced mixing in this regime. However, since the loop integral for χ_E in Eq. 3.84 includes a factor of k^2 in the integrand, the weight of the contribution of this regime is $O([\min(R_{g,A}^{-1}, R_{g,B}^{-1})]^3)$. For typical sizes of polymers, this weight becomes small, and the contribution of this regime can be neglected. The intermediate regime defined by $\min(R_{g,A}^{-1}, R_{g,B}^{-1}) \lesssim k \lesssim \max(R_{g,A}^{-1}, R_{g,B}^{-1})$ can similarly be neglected when $O([\max(R_{g,A}^{-1}, R_{g,B}^{-1})]^3)$ is also small.

When $k \gg \max(R_{g,A}^{-1}, R_{g,B}^{-1})$, the Debye functions, \hat{g}_D , within each correlation function approach the asymptotic behavior $\hat{g}_D(x) \sim 2/x$, such that the correlation functions become

$\hat{\Lambda}_m = 12(b_mk)^{-2}\hat{\Gamma}_m^2$, and the behavior of the fluid becomes invariant to the degree of polymerization of each chain. The intermediate regime that lies between the present one, which concerns the character of fluctuations that are on the monomer length-scale, and the previous low- k regime, i.e. due to fluctuations on the length-scale of the entire chain, admits a crossover between the two limiting behaviors that is dependent on the lengths of the chains. However, the relative weight of this contribution can be reduced by increasing the length of each chain, as indicated by the curves plotted in Fig. 3.2. For sufficiently long chains, the dielectric behavior of the fluid is seen to become independent of both chain lengths, such that it is also invariant to their ratio.

The asymptotic form for the Debye function in this regime gives correlation functions that decay algebraically in the product b_mk . Choosing $b_A < b_B$ ensures that this contribution is larger for the more strongly polarizable A -type monomers, and in the case of equal smearing lengths ($a_A = a_B = a$), remains larger as $k \rightarrow \infty$. Taking the ratio of the two correlation functions gives $\hat{\Lambda}_B/\hat{\Lambda}_A = b_A^2/b_B^2$, which is independent of k , unlike the ratio of dissimilar smearing functions, given in Eq. 3.87, which decays exponentially in k^2 . Evidently, for equal monomer smearing lengths, it is not possible to enter a regime that has $\hat{\Lambda}_A \gg \hat{\Lambda}_B$, unless one chooses $b_A \ll b_B$, which would only be appropriate in the case B -type chains exhibit rod-like behavior. Consequently, comparing the top image of Fig. 3.3, which plots $\partial^2\epsilon/\partial\phi^2$, to that of Fig. 3.1 reveals a weaker field-induced mixing effect when comparing curves with the same ratio of lengths. Evidently, conformational asymmetry is a sufficient contribution to structural contrast to give rise to field-induced mixing, but admits a weaker dependence on the ratio of respective length-scales. This difference would be even more pronounced if the Gaussian smearing functions were replaced with functions that more sharply depended on (a_mk) .

When $b_A \gtrsim a$, the contributions to χ_E that give rise to field-induced mixing occur for values of k that have $\hat{\Gamma}^2 = O(0.1)$, such that these fluctuations are not strongly damped. If instead, one chooses $a > b_B$, such that the smearing length of the monomers exceeds their Kuhn lengths, these modes become significantly more damped, and as indicated by the middle image of Fig. 3.3, admit much weaker field-induced mixing. A chain that could be characterized by such a large smearing length would likely have bulky sidearms, which would greatly increase the length-scale over which fluctuations are “smeared out”, with a likely increase in the Kuhn

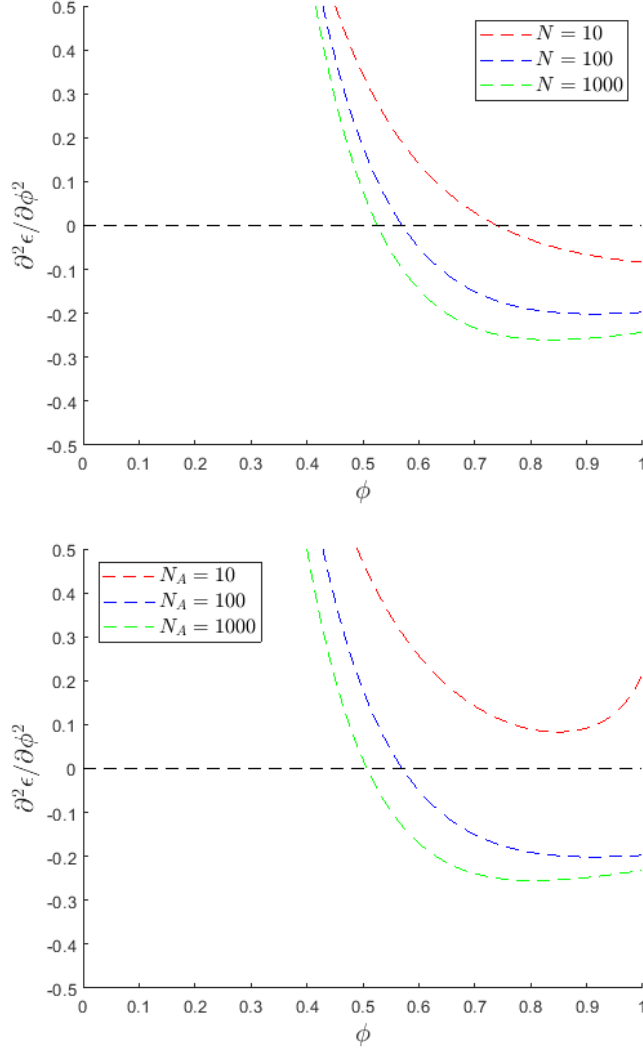


Figure 3.2: Plots of $\partial^2 \epsilon / \partial \phi^2$ vs A bead volume fraction for a homopolymer blend with average bead density $\rho_0 b_B^3 = 14.70$, Kuhn length ratio $b_A / b_B = 0.5$, equal smearing lengths $a_A / b_B = a_B / b_B = 0.408$, dielectric constant pairs $\epsilon_A = 10.0$, $\epsilon_B = 2.0$, computed in the incompressible with the Gaussian approximation. The length of the A -type chain is varied, with (**top**) equal-length chains ($N_A = N_B = N$) or with (**bottom**) fixed B -type chain length ($N_B = 100$). For small values of N_m , the low- k regime contributes significantly to the dielectric behavior of the blend, such that $\partial^2 \epsilon / \partial \phi^2$ admits strong N_m -dependence. As N_m are increased, the weight of the low- k regime is decreased, and invariance to N_m is eventually recovered.

length of the monomers, relative to an architecture with fewer or leaner sidearms.

In the final plot of Fig. 3.3, contrast in the smearing lengths of the monomers is introduced, such that $a_A < a_B$, which enhances field-induced mixing relative to the top image. Evidently, field-induced mixing would be most prominent in homopolymer blends for which the more strongly polarizable monomer has a shorter Kuhn length, and none or fewer sidearms, such that the corresponding single-chain correlation function of this chain, $\hat{\Lambda}_A$, admits stronger correlation behavior at the monomer length-scale.

We also note that because this dielectric behavior is invariant to chain lengths, the relative lengths of the two chains can be used to specify the critical composition without altering the dielectric behavior of the polymer blend. Consequently, one could imagine an experimental system for which the sign of the field-induced critical point shift can be selected by a simple adjustment in the relative lengths of the two chain types.

3.4.3 Dielectric Homopolymer Solution

If only one molecular component of a binary fluid is chosen to be a polymer, the mixture can be classified as a polymer solution, such that the small molecule component acts as a solvent. For this section, we replace the designations A and B with P and S , which correspond to the polymer and solvent, respectively. We also define the degree of polymerization, N , and Kuhn length, b , of the chain without any subscript, since the solvent does not have any such properties.

For this system, we have the correlation functions, $\hat{\Lambda}_P = N\hat{g}_D(Nb^2k^2/6)\hat{\Gamma}_P^2$ and $\hat{\Lambda}_S = \hat{\Gamma}_S^2$, such that the multiple length-scales associated with the polymer chain will have corresponding regimes for the value of k , analogous to the polymer blend system discussed in the previous section.

We again ignore the low- k regime, due to its negligible contribution to χ_E for typical values of N , and consider the monomer length-scale, which has $k \sim b^{-1}$. In this regime, the correlation function of the chain recovers the asymptotic form, $\hat{\Lambda}_P \sim 12(bk)^{-2}\hat{\Gamma}_P^2$. If no smearing length contrast is assumed, such that $a_P = a_S = a$, the ratio of correlation functions has the form

$$\frac{\hat{\Lambda}_P}{\hat{\Lambda}_S} = \frac{12}{(bk)^2}, \quad (3.88)$$

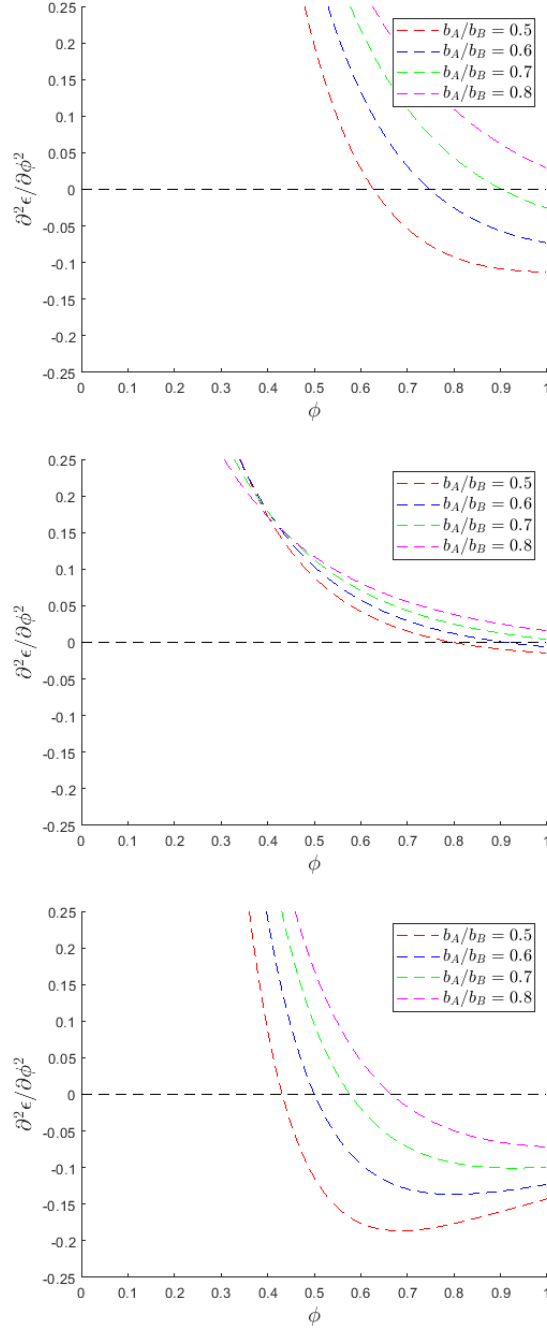


Figure 3.3: Plots of $\partial^2\epsilon/\partial\phi^2$ vs A bead volume fraction of a homopolymer blend with average bead density $\rho_0 b_B^3 = 14.70$, chain lengths $N_A = N_B = 100$, dielectric constant pairs $\epsilon_A = 8.0$, $\epsilon_B = 2.0$, computed in the incompressible limit with the Gaussian approximation. The smearing length pairs are (**top**) $a_A/b_B = a_B/b_B = 0.408$, (**middle**) $a_B/b_B = a_B/b_B = 1.225$, and (**bottom**) $a_A/b_B = 0.286$, $a_B/b_B = 0.408$. Increasing conformational asymmetry gives stronger field-induced mixing; increasing the smearing length damps this behavior, and mixing is suppressed for $a > b_A$. Smearing length contrast ($a_A < a_B$) enhances mixing.

which decays algebraically with k . Unlike the ratios of correlation functions discussed in the preceding sections, this ratio can be small or large, depending on the value of k . This is due to the conformational entropy of the chain, which suppresses fluctuations for $k \gtrsim 2\sqrt{3}b^{-1}$, such that screening at high k is due purely to the solvent, but admits a stronger correlation contribution for $k \lesssim 2\sqrt{3}b^{-1}$, such that the contribution from the solvent molecules can be neglected at sufficiently small k .

Each of these regimes will admit their own range of k values for which Eq. 3.86 becomes correct – where in each case, the A -type component is replaced with the component that has the dominant correlation function – such that the respective miscibility contributions of the two regimes will have opposite sign. Although it is not obvious which regime will have the larger contribution when $a \sim b$, we can adjust the relative weight of each regime by our choice of smearing length.

If $a \gtrsim b$, the smearing function suppresses the high- k , solvent-dominated regime ($\hat{\Lambda}_S > \hat{\Lambda}_P$), such that field-induced mixing can occur when $\epsilon_P > \epsilon_S$. In the top image of Fig. 3.4, increasing the smearing length shifts ϕ_0 to smaller polymer volume fractions, but appears to saturate around $\phi = 0.25$. Evidently, this is the limit of completely suppressing the competing demixing contribution from the $\hat{\Lambda}_S > \hat{\Lambda}_P$ regime. As shown in the lower image, ϕ_0 can be shifted further to the left by also introducing smearing length contrast between the monomers and the solvent, with $a_P < a_S$.

If we instead assume $a \lesssim b$, the beads of the fluid become more point-like in their behavior, and larger values of k are permitted to contribute to the integrand in Eq. 3.84. Since $\hat{\Lambda}_S > \hat{\Lambda}_P$ for all $k > 2\sqrt{3}b^{-1}$, choosing smaller values of the smearing length extends the solvent-dominant regime to larger values of k , increasing its weight. For sufficiently small values of a , this regime dominates in weighting relative to the previous lower- k regime, and field-induced mixing can occur if $\epsilon_S > \epsilon_P$.

In the top image of Fig. 3.5, the composition dependence of $\partial^2\epsilon/\partial\phi^2$ is plotted for a polymer solution system with $\epsilon_S > \epsilon_P$ and no smearing length contrast. As the smearing length is decreased, ϕ_0 shifts to the right (smaller solvent volume fractions), corresponding to a broader range of compositions at which the fluid will admit field-induced mixing. In the bottom image, smearing length contrast is prescribed, with $a_S < a_P$, which shifts ϕ_0 in favor of mixing.

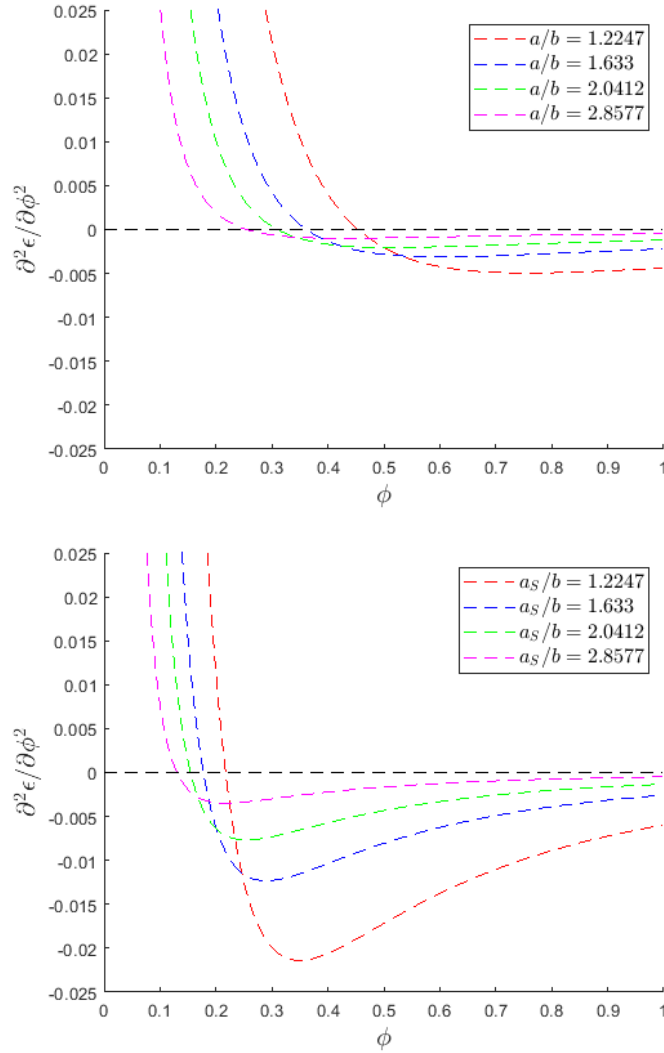


Figure 3.4: Plots of $\partial^2\epsilon/\partial\phi^2$ vs polymer volume fraction for a homopolymer solution with average bead density $\rho_0 b^3 = 7.35$, chain length $N = 100$, dielectric constant pairs $\epsilon_P = 8.0$, $\epsilon_S = 2.0$, computed in the incompressible limit using the Gaussian approximation. The smearing length ratios are **(top)** $a_P/a_S = 1.0$, and **(bottom)** $a_P/a_S = 0.7$. When $\epsilon_P > \epsilon_S$, larger smearing lengths suppress the k regime that would otherwise favor field-induced demixing, permitting field-induced mixing at smaller ϕ values. Introducing smearing length contrast, such that $a_P < a_S$, further shifts the curves in favor of mixing.

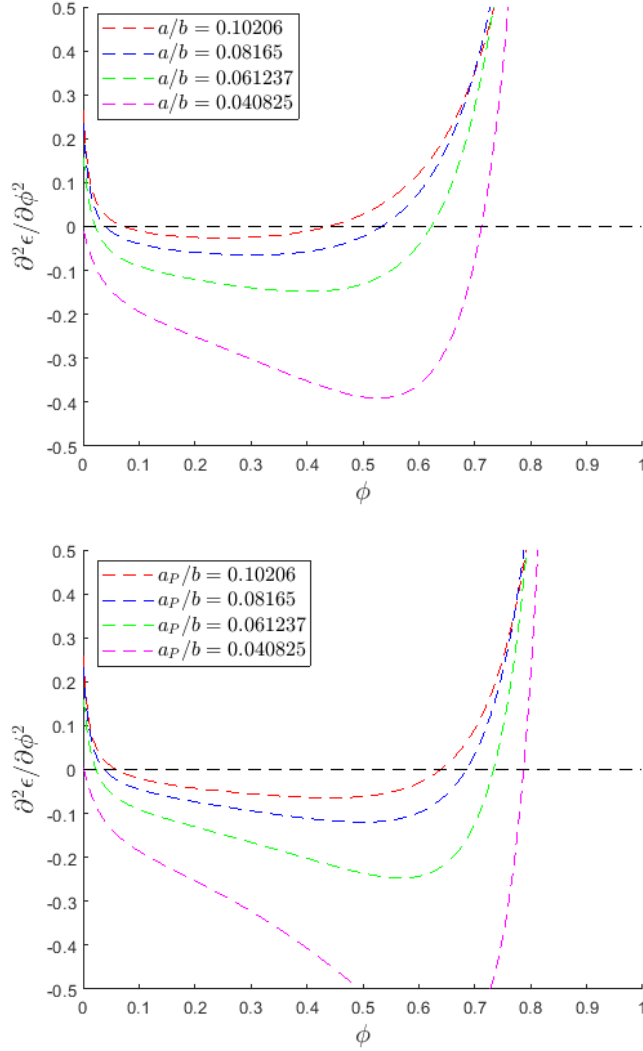


Figure 3.5: Plots of $\partial^2\epsilon/\partial\phi^2$ vs polymer volume fraction for a homopolymer solution with average bead density $\rho_0 b^3 = 147.0$, chain length $N = 100$, dielectric constant pairs $\epsilon_P = 2.0$, $\epsilon_S = 8.0$, computed in the incompressible limit using the Gaussian approximation. The smearing length ratios are **(top)** $a_S/a_P = 1.0$, and **(bottom)** $a_S/a_P = 0.7$. When $\epsilon_P < \epsilon_S$, choosing smaller smearing lengths increases the k -space volume of the regime that favors mixing, permitting field-induced mixing at greater ϕ values. Introducing smearing length contrast, such that $a_S < a_P$, further shifts the curves in favor of mixing.

3.5 Discussion

In the present chapter, we have considered the dielectric properties of binary soft fluids, which we modeled using a field theory for polarizable molecular species in the presence of a uniform applied electric field, \mathbf{E}_0 . By taking an \mathbf{E}_0 derivative of the free energy given in Eq. 3.11, we obtained the dielectric displacement, \mathbf{D} , which included fluctuation contributions that could be analyzed either analytically, using a Gaussian fluctuation approximation, or numerically, using an approximation-free complex Langevin procedure. By means of these techniques, we have illuminated corrections to the simple linear dielectric behavior predicted at the mean-field level.

Beyond the full form for the dielectric displacement, which has a nonlinear dependence on \mathbf{E}_0 , we identified a linear response formula, appropriate for sufficiently small electric field magnitudes. This relates field and displacement according to $\mathbf{D} = \epsilon\mathbf{E}_0$, and we identified the prefactor, ϵ , as the dielectric constant. Leveraging this expression for \mathbf{D} in tandem with thermodynamic integration, we reproduced the form of the free energy proposed by Beaglehole (Eq. 3.2), which relates the free energy of a fluid in the presence of an applied field to its free energy in the absence of a field, and which prescribes the correspondence between the composition dependence of a binary fluid’s dielectric constant and any shift in the miscibility of the fluid due to the introduction of a weak applied electric field.

In the linear response regime, we defined an effective Flory chi parameter, χ_E , which quantifies the electric field-dependent contribution to the tendency for demixing of the fluid, according to Eq. 3.79. Since the mean-field contribution to the dielectric constant is linear in composition, χ_E arises entirely from electric field-mediated fluctuations in both structure and electrostatic potential within the fluid. Within the Gaussian approximation, the expression for χ_E , Eq. 3.84, is proportional to the square of the contrast in polarizability of the two molecule types, with contributions from two competing terms. The first term favors demixing for any choice of properties of the fluid. The second term has a signed dependence on the *contrast* of the k -dependent single-molecule correlation functions, $\hat{\Lambda}_A$ and $\hat{\Lambda}_B$, and vanishes when $\hat{\Lambda}_A = \hat{\Lambda}_B$.

Without specifying functional forms for the correlation functions, we identified the inequality $\hat{\Lambda}_A > \hat{\Lambda}_B$, where we have chosen A to be the more polarizable bead type, as a necessary condition for field-induced mixing to occur. Choosing a particular physical system of interest informs the

structure of $\hat{\Lambda}_{A/B}$ and leads to physically-based conditions for the observation of field-induced mixing.

We first considered a binary small molecule mixture. The Gaussian-smearred point particles admit no correlation effects due to any inherent molecular structure unless contrasting smearing lengths are specified. Choosing a smaller smearing length for A -type (more polarizable) beads gives $\hat{\Lambda}_A > \hat{\Lambda}_B$ for all values of k , and is thus a requirement for field-induced mixing. Upon computing χ_E , we found that increasing either the dielectric contrast or the smearing length contrast both enhanced field-induced mixing.

For field-induced mixing to occur, we also identified the inequality, $a_A/a_B < 2^{-1/2} \approx 0.707$, as a loose requirement for the ratio of the bead smearing lengths; the constraint arises because structural contrast between beads is due to the same Gaussian smearing functions that regularize the theory by suppressing fluctuations below the diameter of the beads. If, as an example, we replace each Gaussian smearing function with the function $\hat{\eta}_m(k) \equiv e^{-(a_m k)^4}$ – which has the form of a Boltzmann-weighted anharmonic potential – the inequality becomes $a_A/a_B < 2^{-1/4} \approx 0.841$. Evidently, the sensitivity of χ_E to contrast in bead sizes is highly dependent on the choice of regularization procedure, but we can generally say that the qualitative behavior depicted in Fig. 3.1 will occur if there exists a length-scale for which only A -type molecules admit a significant contribution to pair correlations.

For the small molecule systems considered by Debye and Kleboth,²² as well as Beaglehole,²³ the field-induced critical point shift was studied, yielding field-induced mixing, and the composition dependence of the dielectric constant $\epsilon(\phi)$ was measured. In each case, the authors concluded that $\epsilon''(\phi)$ was positive at the respective critical composition of each system, which in both cases was $\phi_c \approx 0.4$. However, the resolution of ϕ values sampled in each study was limited, and it is not obvious where, if at all, the $\epsilon(\phi)$ curves possess a point of inflection.

In Fig. 3.6 we have compared the $\epsilon(\phi)$ data measured in Ref. 22 for the system nitrobenzene–2,2,4-trimethylpentane to data computed by the present field theory, wherein we have chosen the same pure phase dielectric constants, a bead density of $\rho_0 = 1 \times 10^{-28} \text{ m}^{-3} = 10 \text{ nm}^{-3}$, a smearing length for B -type beads of $a_B = 3.0 \text{ \AA}$, and the modest smearing length contrast, $a_A/a_B = 0.8$. We note qualitative agreement in the shape of the two curves, but emphasize that the resolution of the experimental curve is insufficient to ascertain the behavior near $\phi = 0.4$.

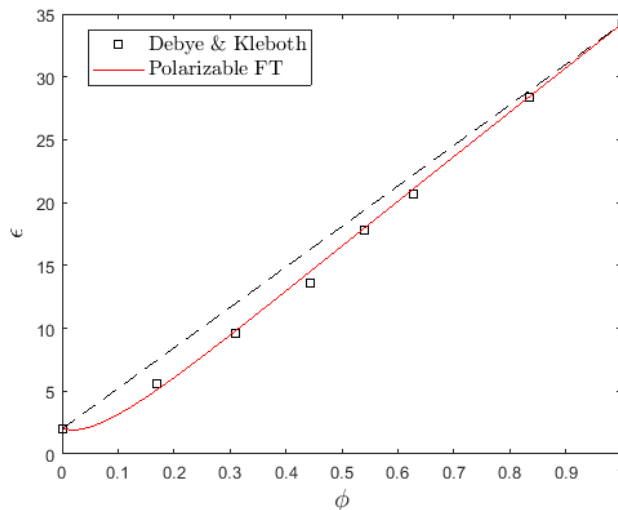


Figure 3.6: Dielectric constant vs volume fraction of nitrobenzene in 2,2,4-trimethylpentane. The black squares are plotted from data tabulated by Debye and Kleboth,²² and the red line is generated from the present field theory in the Gaussian approximation, with dielectric constant pairs $\epsilon_A = 34.2$, $\epsilon_B = 2.0$, density $\rho_0 a_B^3 = 0.27$, smearing length contrast $a_A/a_B = 0.8$, in the incompressible limit.

In the aniline-cyclohexane system considered by Beaglehole,²³ no such qualitative correspondence exists between our field theory and his $\epsilon(\phi)$ measurements; in particular, his curve appears to adopt a large, positive curvature near $\phi = 0.7$, in contrast to the qualitative behavior identified in Fig. 3.1. There evidently exists in this binary system a chemistry-specific interaction that influences the dielectric behavior of the fluid. We propose hydrogen bonding (H -bonding) as one such possible interaction, due to the ability of aniline to H -bond to itself;⁷² in contrast, the system considered by Debye and Kleboth exhibits no H -bonding behavior.

The next system we considered was a homopolymer blend. For sufficiently large molecular weight of each chain type ($N_m \sim 100$), the dielectric behavior of the blend becomes insensitive to the length of each chain, and arises from fluctuation modes near the monomer length-scale and smaller. In the absence of smearing length contrast, the ratio of the single-molecule correlation functions is independent of k , such that conformational asymmetry ($b_A < b_B$) can give rise to field-induced mixing, but is weaker than the effect of smearing length contrast.

In a pair of studies,^{31,32} Kriisa and Roth have measured the electric field-induced critical point shift of the LCST polymer blend system, Poly(vinyl methyl ether)-Polystyrene, observing a shift favoring mixing. Conversely, Lee and collaborators have measured the shift in critical point of an LCST²⁹ and of a UCST³⁰ polymer blend system – each containing Poly(vinylidene

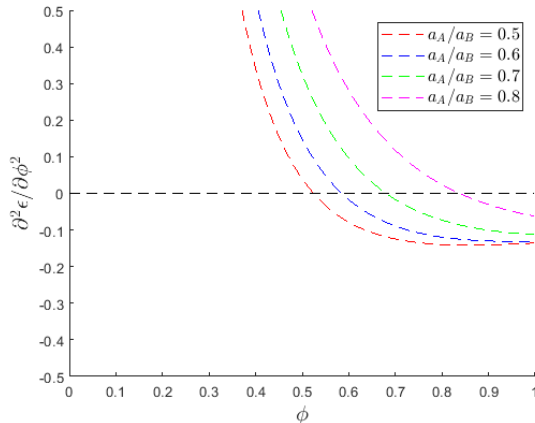


Figure 3.7: Plots of $\partial^2\epsilon/\partial\phi^2$ vs A monomer volume fraction for a homopolymer blend with no conformational asymmetry ($b_A = b_B$), B smearing length $a_B/b_B = 0.408$ average bead density $\rho_0 b_B^3 = 14.70$, chain lengths $N_A = N_B = 100$, dielectric constant pairs $\epsilon_A = 15.0$, $\epsilon_B = 2.0$, computed in the incompressible limit using the Gaussian approximation.

fluoride) as one of its components – and instead observed a field-induced shift in favor of demixing for both systems.

Comparing the results of each group to the observations made in Section 3.4.2, we note that both used chains with molecular weights corresponding to $N_m = O(1000)$, such that the dielectric behavior would be expected to be independent of chain length. Given the strong asymmetry required to obtain field-induced mixing according to the curves in Fig. 3.3, it is unlikely that this effect is responsible for the observations made by Kriisa and Roth. In fact, given the nearly identical literature values for the Kuhn lengths of the two monomer chemistries – ($b_{PVME} = 0.69 \text{ nm}$)⁷³ and ($b_{PS} = 0.68 \text{ nm}$)⁷⁴ – structural contrast in this system would have to entirely arise due to differences in the high- k behavior of the two species. In Fig. 3.7, $\epsilon''(\phi)$ is computed for a homopolymer blend system with $b_A = b_B$; the system admits only a small window of field-induced mixing at large volume fractions of the A monomers, even when a strong contrast in smearing lengths is prescribed. From this we conclude that the field-induced mixing behavior observed by Kriisa and Roth is due to an interaction that was not included in the present field theory.

Although Kriisa and Roth did not measure an $\epsilon(\phi)$ curve for their polymer blend system, such a curve has previously been measured for other systems with a H -bonding component, namely several water-containing binary systems.^{24–26} In each case a significant increase in

the dielectric constant relative to linear mixing for high water volume fractions was observed, with a corresponding negative curvature in $\epsilon(\phi)$. Additionally, in Ref. 26, a simple model that accounted for H -bonding contributions to the dielectric constant of H_2O -DMSO *via* strong, orientation-dependent “dipole correlations” between the molecules predicted this behavior, giving good quantitative agreement with experiment. We hypothesize that a measurement of $\epsilon(\phi)$ for PVME-PS will also yield negative curvature, such that the behavior observed by Kriisa and Roth is consistent with the free energy expression proposed by Beaglehole (Eq. 3.2).

Conversely, neither system considered by Lee and collaborators admits H -bonding, with the LCST behavior observed in the Poly(vinylidene fluoride)-Poly(1,4-butylene adipate) system they considered²⁹ believed to arise from a weak association due to the carbonyl oxygen of the PBA ester.⁷⁵ Evidently, if this association influences the dielectric behavior of a PVDF-PBA blend, it is insufficient to give rise to field-induced mixing. The field-induced demixing they observed in each system is consistent with our observation of Fig. 3.3, which admits no field-induced mixing in a weakly asymmetric system. Although PVDF is known to be piezoelectric,³¹ such that its preferred conformation has a significant \mathbf{E}_0 -dependence, it is unclear at present how this property affects the dielectric and/or demixing behavior of PVDF-containing mixtures.

The final system we discussed was a polymer solution. We again concluded that the behavior of the solution becomes independent to the molecular weight of the polymer for $N \gtrsim 100$, and instead is due to fluctuations at the monomer length-scale or smaller. Specifically, we found that the ratio of correlation functions of the two molecule types specifies a wavevector magnitude, $k = 2\sqrt{3}b^{-1}$, below which the polymer segments dominate the correlation behavior of the solution, and above which the solvent dominates. When no contrast in smearing length was prescribed, the relative weight of each regime could be adjusted by changing the bead smearing length. Choosing larger smearing lengths selectively suppresses the solvent-dominant higher k modes, and field-induced mixing can occur if $\epsilon_P > \epsilon_S$. On the other hand, choosing smaller smearing lengths increases the high k cutoff that determines the weight of the solvent-dominant regime, and field-induced mixing can instead occur if $\epsilon_S > \epsilon_P$.

Wirtz and Fuller³³ considered the field-induced critical point shift of two polymer solution systems, one the UCST Polystyrene-Cyclohexane system, and one the LCST Poly(*p*-chlorostyrene)-ethylcarbitol system, and also measured the orientation-dependent scattering

function of each solution in the presence of an electric field. In each case, they found field-induced mixing, as well as the appearance of an anisotropy in the scattering function of the phase-separated fluid, indicating coarsening of the isotropic droplets into grains that are aligned with the electric field vector. This is consistent with the form for the Gaussian free energy computed in the present model (Eq. 3.23), which penalizes fluctuation modes that have $\mathbf{k} \cdot \mathbf{E}_0 \neq 0$.

In the first system considered by Wirtz and Fuller, there is weak dielectric contrast ($\epsilon_{PS} = 2.5$, $\epsilon_{CH} = 2.0$),⁷⁶ with $\epsilon_P > \epsilon_S$. Although one could repeat the calculations in Fig. 3.4 with this dielectric constant pair and choose a smearing length sufficiently large to give field-induced mixing at the critical composition they observed, $\phi_c = 0.04$, such a smearing length would be unrealistically large relative to the Kuhn length of PS. It is more likely that the contribution of χ_E to the miscibility of PS/CH depends on atomic scale local structural details, which are not captured by our soft spherical bead model. Such contributions would also exist in other systems with larger dielectric contrast, but we might hope that in such cases their contribution to χ_E would be swamped by the larger scale fluctuation phenomena captured by our polarizable model.

In the second PC/EC system studied by Wirtz and Fuller, the solvent is the component with the larger dielectric constant. In accordance with Fig. 3.5, their observation of field-induced mixing is consistent with behavior predicted by the model, provided our choice of $a \lesssim 0.1b$ is faithful to the high k behavior of the monomers and the solvent.

3.5.1 Concluding Remarks

We have presented a dielectric theory of liquids based on a field theory for polarizable species, where molecules are represented by spherically symmetric, softly repelling beads that are optionally connected to form continuous Gaussian chains when a dielectric polymer is desired. We considered binary dielectric fluid mixtures with this model and examined the composition dependence of the dielectric constant of three classes of mixtures. The sign of the second derivative of the dielectric constant was shown to dictate the shift in the miscibility of the fluid in the presence of a weak applied electric field. The theory further provides insight into the microscopic factors that determine this shift, namely the contrast in polarizability of the fluid components and the contrast in their wavevector k -dependent single-molecule correlation

functions, $\hat{\Lambda}_{A/B}$.

It is clear from the comparison with experimental literature data in the previous section that our theory at best provides only qualitative guidelines for when a mixture of fluids should exhibit electric field-induced mixing vs. demixing. This can be traced to a number of significant limitations of the model: it does not account for atomic scale structure and harsh repulsions, it does not include permanent dipoles, and it does not allow for specific interactions such as hydrogen bonds. Nonetheless, it is the only theory of which we are aware that attempts a *microscopic* rather than phenomenological description of electric field effects on thermodynamic stability and does provide some guidance for the design of systems with desired field-induced mixing or demixing behavior.

Some predictions of our theory remain untested experimentally. For example, our calculations of χ_E predict field-induced mixing for volume fractions of the more strongly polarizable species that are above a threshold value, ϕ_0 . Below ϕ_0 , field-induced demixing is predicted. We therefore anticipate that an aprotic system that exhibits field-induced mixing at its critical point, ϕ_c (such as the one considered by Debye and Kleboth²²), can be made to instead demix in the presence of an electric field by choosing a volume fraction of the stronger dielectric that is significantly smaller than ϕ_c , and then repeating the experiment. For the same reason, a homopolymer blend (without *H*-bonds) that exhibits field-induced mixing is expected to demix if the molecular weight of the higher dielectric constant polymer is increased sufficiently, such that the critical composition of the blend is brought below ϕ_0 .

H-bonds, and other strong, localized electrostatic associations between molecules, contribute to the dielectric behavior of a fluid; it was found that consideration of the dipole correlations between molecules was sufficient to faithfully compute the contribution of *H*-bonding effects to the $\epsilon(\phi)$ curve for a *H*₂*O*-DMSO system.²⁶ As such, anisotropic dipolar couplings – including *H*-bonds – indicate an attractive direction to proceed in improving the molecular detail present in the polarizable field theory, permitting more sophisticated predictions of the dielectric behavior of fluids.

Additional molecular detail would necessarily enter within the structure of the single-molecule partition function, Q_m . The lack of dipole correlations in the present field theory is a consequence of the truncated multipole expansion that gives rise to each α_m , which ap-

proximates the behavior of a bead’s paired partial charges by an isotropic interaction with the local electric field at the bead’s center of mass. Any bead polarizability model that similarly depends isotropically on the local electric field will necessarily meet the same shortcomings.

We suggest three possible modifications to Q_m that embed the anisotropy necessary for dipolar couplings to emerge: in one such method, the unapproximated form for Q_m defined in Chapter 2 is used, which integrates over the position of the bead center of mass, as well as the vector, \mathbf{s} , which gives the displacement of the bead’s partial charges relative to its center of mass, and implicitly requires that they fluctuate symmetrically. This explicit representation of the partial charges grants access to multipole modes of all orders.

As a second method, one can instead relax the latter constraint, such that each partial charge of valence $\pm\delta q_m$ is tethered to the bead center of mass by an independent spring of strength K , and has displacement vector \mathbf{s}_\pm that is integrated over. Performing a multipole expansion about the bead center of mass, up to the order of the quadrupole moment – which is appropriate when K is large relative to variations in the local electric field – the \mathbf{s}_\pm integrals can be performed analytically, and one obtains:

$$\begin{aligned}
Q_m[\varphi, w] &\sim \frac{1}{V} \int d\mathbf{r} e^{-i\Gamma_m * w + (\alpha_m/2)\Gamma_m * \nabla i\varphi \cdot \mathbf{B} \cdot \Gamma_m * \nabla i\varphi - (1/2)(\frac{\delta q_m}{K}\Gamma_m * \nabla^2 i\varphi)^2} + O(K^{-4}) \\
\mathbf{B}(\mathbf{r}) &= \mathbf{I} + \left(\frac{\delta q_m}{K}\right)^2 \Gamma_m * \nabla^2 i\varphi(\mathbf{r}) \Gamma_m * \nabla \nabla i\varphi(\mathbf{r}),
\end{aligned} \tag{3.89}$$

where $\alpha_m = 2(\delta q_m)^2/K$ is the isotropic part of the polarizability.

This expression for Q_m permits calculation of a single-bead partition function that is anisotropically coupled to the local variation in the electric field, while retaining the form of a single integral over space, making it ideal for analysis using the Gaussian approximation derived in Section 3.2.2 – or alternatively, the higher-order expansion performed by Grzetic and collaborators.^{70,71}

3.5.2 Water Molecule and General Atomistic Single-Molecule Constructions

In a third method, one can construct charge-neutral n -mers of charged beads, which each separately interact with the fields, φ and w . Due to its ubiquity in soft matter systems, and the strongly anisotropic molecular structure that permits it to participate in hydrogen bonding,

H₂O is an obvious choice for introduction to an electrostatic field theory *via* an atomistically-derived single-molecule partition. Imposing the bond angle θ_{HOH} and O–H bond lengths b_{OH} , the partition function for water is found to be:

$$Q_{H_2O}[\varphi, w] = \frac{1}{4\pi^2 V} \int d\mathbf{r} \int_0^\pi d\eta \int_0^{2\pi} d\phi \int_0^\pi d\theta \sin(\theta) e^{-\nu_O(\mathbf{r}) - \nu_H[\mathbf{r} + \mathbf{r}_+(\eta, \phi, \theta)] - \nu_H[\mathbf{r} + \mathbf{r}_-(\eta, \phi, \theta)]}, \quad (3.90)$$

where the function,

$$\mathbf{r}_\pm(\eta, \phi, \theta) = b_{OH} \begin{bmatrix} \sin(\theta) \cos(\theta_{HOH}/2) \pm \cos(\eta) \cos(\theta) \sin(\theta_{HOH}/2) \\ \pm \sin(\eta) \sin(\theta_{HOH}/2) \\ \cos(\theta) \cos(\theta_{HOH}/2) \mp \cos(\eta) \sin(\theta) \sin(\theta_{HOH}/2) \end{bmatrix}, \quad (3.91)$$

gives the instantaneous bond vector between the O atom and each H atom.

In Eq. 3.90, ϕ and θ are the azimuthal and zenith angle, respectively, for a spherical coordinate system that describes the orientation of the molecule's H–O–H angle bisector, denoted by the unit vector $\hat{\mathbf{r}}_0$, with the O atom placed at the origin; η gives the angle of rotation of the molecule about $\hat{\mathbf{r}}_0$, and its domain of integration in Eq. 3.90 is restricted to $[0, \pi]$ because the periodicity property $\mathbf{r}_+(\nu, \phi, \theta) = \mathbf{r}_-(\nu + \pi, \phi, \theta)$, combined with the indistinguishability of the two H atoms, yields a degenerate set of configurations when $\pi \leq \eta \leq 2\pi$. On the other hand, the spherical angles ϕ and θ must be integrated over the entire unit sphere, since each octant explored by $\hat{\mathbf{r}}_0$ yields unique H atom positions in space. The bond vector function is defined with the reference $\mathbf{r}_\pm(0, 0, 0) = b_{OH}(\pm \sin(\theta_{HOH}/2), 0, \cos(\theta_{HOH}/2))^T$, so that the molecule is in the xz plane and $\hat{\mathbf{r}}_0$ lies along the positive z axis when all angles are 0.

The fields,

$$\begin{aligned} \nu_H(\mathbf{r}) &= i\Gamma_H * [w + (\delta q_{H_2O})\varphi(\mathbf{r})] + (\alpha_H/2)|\Gamma_H * \nabla\varphi(\mathbf{r})|^2 \\ \nu_O(\mathbf{r}) &= i\Gamma_O * [w(\mathbf{r}) - 2(\delta q_{H_2O})\varphi(\mathbf{r})] + (\alpha_O/2)|\Gamma_O * \nabla\varphi(\mathbf{r})|^2 \end{aligned} \quad (3.92)$$

give the effective potential experienced by each atom type, and $\Gamma_{H/O}$ is a Gaussian smearing function with width $a_{H/O}$, so that each atom type is optionally assigned a different smearing length. $\alpha_{H/O}$ are the induced-dipole polarizabilities assigned to each atom type, and are related

to water’s molecular polarizability according to $2\alpha_H + \alpha_O = \alpha_{H_2O}$. The net partial charge δq_{H_2O} is related to the literature dipole moment of H_2O by $\mu_{H_2O} = 2(\delta q_{H_2O})b_{OH} \cos(\theta_{HOH}/2)$.

One can further define a general form for a single-molecule partition function of a molecule consisting of p atoms, connected by fixed bonds with fixed bond angles:

$$Q_a[\varphi, w] = \frac{1}{8\pi^2 V} \int d\mathbf{r} \int_0^{2\pi} d\eta \int_0^{2\pi} d\phi \int_0^\pi d\theta \sin(\theta) e^{-\sum_{j=1}^p \nu_j[\mathbf{r} + \mathbf{r}_j(\eta, \phi, \theta)]}, \quad (3.93)$$

where the three integrated angles are the same as in Eq. 3.90, and the vector $\hat{\mathbf{r}}_0$ must be again chosen relative to the structure of the molecule. The function

$$\mathbf{r}_j(\eta, \phi, \theta) = \mathbf{R}_z(\phi) \cdot \mathbf{R}_y(\theta) \cdot \mathbf{R}_z(\eta) \cdot \mathbf{r}_j^0, \quad (3.94)$$

gives the separation vector between atom j and the reference position \mathbf{r} , according to the molecule’s instantaneous orientation. The tensor-valued functions $\mathbf{R}_{y/z}(\psi)$ are *rotation matrices*, defined so that the linear operation $\mathbf{s} = \mathbf{R}_{y/z}(\psi) \cdot \mathbf{t}$ yields a new vector \mathbf{s} that has been rotated, relative to the vector \mathbf{t} , about the Cartesian y or z axis by an angle ψ , and $\mathbf{r}_j^0 = \mathbf{r}_j(0, 0, 0)$ gives the vector between atom j and the position \mathbf{r} when the molecule is at the reference orientation, $\hat{\mathbf{r}}_0 = \hat{\mathbf{z}}$. The effective field experienced by atom j is written as:

$$\nu_j(\mathbf{r}) = i\Gamma_j * [w(\mathbf{r}) + (\delta q_j)\varphi(\mathbf{r})] + (\alpha_j/2)|\Gamma_j * \nabla\varphi(\mathbf{r})|^2, \quad (3.95)$$

with Γ_j a Gaussian of width a_j that smears the j th atom; if the atoms’ partial charges δq_j violate the constraint $\sum_{j=1}^p \delta q_j = 0$, the molecule will carry a total net charge, and consequently will behave as an electrolyte.

Apart from the trivial $p = 1$ molecule that recovers a simple spherical bead partition function, the form of Q_a for a $p = 2$ “dumbbell molecule” is another special case of Eq. 3.93, which can be equivalently identified by a single-step Markov process that joins two spherically symmetric atoms with a rigid link. Since the bond transition probability function associated with a rigid link has a closed-form Fourier representation, one can compute Q_a for a dumbbell

molecule according to the spectral representation:

$$Q_a[\varphi, w] = \sum_{\mathbf{k}} \hat{q}_1(-\mathbf{k}) j_0(b_{12}k) \hat{q}_2(\mathbf{k}), \quad (3.96)$$

where b_{12} is the specified bond length between the two atoms, $j_0(x) = \sin(x)/x$ is the spherical Bessel function, and each \hat{q}_j gives a Fourier transform of the Boltzmann-weighted effective field experienced by the j th atom:

$$\hat{q}_j(\mathbf{k}) = \frac{1}{V} \int d\mathbf{r} e^{-\nu_j(\mathbf{r}) - i\mathbf{k}\cdot\mathbf{r}}. \quad (3.97)$$

By exploiting the high symmetry of the dumbbell molecule, the Fourier representation for Q_a in Eq. 3.96, circumventing the need for explicit orientational degrees of freedom. This form for Q_a can be computed in near linear time, leveraging the Fast Fourier Transform algorithm to compute each \hat{q}_j , with computational cost proportional to $M \ln(M)$.

For a molecule with $p > 2$, there will necessarily be at least one atom with multiple bonds, breaking its spherical symmetry with respect to linking location, and consequently requiring explicit enumeration of the molecule's orientation in space when computing Q_a .

Despite its high dimensionality, this structure for Q_a provides a powerful general framework from which to build atomistic molecular models of arbitrary complexity. Provided the molecule is a rigid body, with fixed bond lengths and angles, the partition function will retain the form specified in Eq. 3.93, in nearly all cases requiring computation of a 6-dimensional integral. It is worth noting, however, that each of the angular integrals can be performed using a quadrature method, permitting high accuracy in the computed value of Q_a with a relatively small set of associated basis functions. Additionally, the dumbbell model described in Eq. 3.96 provides an attractive compromise between molecular detail and computational efficiency, admitting anisotropic electrostatic behavior due to the atoms' explicit charges, while retaining the desirable accuracy of a spectral representation.

We also note that a single-molecule partition function of the form given in Eq. 3.93 imparts molecules with anisotropic steric properties, such that packing effects will emerge, due to the molecule's preference for obtaining a position and orientation that minimize the sum of poten-

tials experienced by its beads. When an applied electric field is introduced, the molecule will prefer to align its net dipole with the field, and the competition of these effects will give rise to new contributions to χ_E .

Chapter 4

Field Effects in Phase-Separating Block Copolymer Systems

4.1 Background

The self-assembly of block copolymers (BCPs) has been a long-standing subject of interest due to the emergence of periodically repeating ordered microphases with features on the nanometer length scale.⁷⁷ This behavior has made BCPs an attractive platform for industrial production of materials and devices requiring placement of small repeating structures,⁷⁸ including semiconductor devices,^{79,80} nanoporous membranes,^{81,82} and other tunable functional nanomaterials.^{78,83}

The BCP phase behavior can be faithfully captured by a coarse-grained molecular model of continuous Gaussian chains combined with self-consistent field theory (SCFT). SCFT is a mean-field approach^{3,35} that is particularly efficient for dense, high-molar-mass polymer melts. Although it fails to reproduce certain features near the order-disorder transition,⁸⁴ SCFT is highly reliable for assessing the stability of copolymer microphases at intermediate to strong segregation strengths.^{3,85}

The expected (lowest free energy) structure of the simplest AB diblock copolymer system can be determined within the SCFT framework by specifying two system parameters: volume fraction of A monomers (f) and an effective segregation strength parameter (χN). The latter is

the product of a Flory parameter (χ) and the diblock degree of polymerization (N), and is sensitive to the chemistry of the two constituent monomers, the temperature, and the molar mass of the BCP.^{35,77} It is currently predicted by SCFT and experimentally confirmed that seven phases compete for relative stability in this two-dimensional parameter space: disordered (DIS), lamellar (LAM), hexagonal-packed cylinders (HEX), BCC spheres, FCC/HCP spheres, the gyroid Ia $\bar{3}$ d cubic network phase (GYR), and the orthorhombic Fddd network phase (O⁷⁰).^{1,2,35,43–47} Knowledge of SCFT phase diagrams for both simple and complex BCPs has provided powerful guidance for materials design, interrogation, and application.

Of continuing interest is the effect of an applied electric field (\mathbf{E}_0) on the ordered structure in a BCP system. The tendency for BCP microphase structures to elongate or align along the direction of an applied electric field^{37,38} has attracted attention as a potential experimental or industrial technique for enhancing or controlling the self-assembly process. For example, leveraging this alignment effect has been identified as a strategy for overcoming surface-air and surface-surface interactions to produce novel, perforated nanomaterials in directed self-assembly (DSA) applications.⁸⁶ Electric fields have also been identified as a means of enhancing the kinetics of the BCP self-assembly process,⁸⁷ greatly increasing the throughput potential of an industrial DSA workflow. Some other methods for aligning microstructures during the self-assembly process include application of magnetic fields,^{88–90} localized annealing using high-performance photonic devices,^{91,92} and epitaxial prepatterning.⁷⁸

The driving force for alignment of BCP microphases in an electric field is posited to be the dielectric inhomogeneity in phase-separated BCP systems; the introduction of an applied electric field breaks the rotational invariance of bulk ordered structures, preferentially acting upon interfaces for which \mathbf{E}_0 has a component out-of-plane.^{36,93} This broken-symmetry effect permits BCP nanostructures to exhibit anisotropic dielectric properties, even when purely isotropic behavior is prescribed at the monomer length scale.⁹⁴ Within the SCFT framework, a simple extension can be made to include the effect of an applied electric field. The electrostatic property of the system is specified by an inhomogeneous macroscopic dielectric constant, obtained from a linear constitutive relation between prescribed monomer dielectric constants and local volume fractions.

This modified SCFT formalism is inspired by an earlier model, wherein nonelectrostatic

contributions to the behavior of the BCP melt are represented by a Ginzburg-Landau (GL) free energy functional that depends on an inhomogeneous composition field; the composition-dependence of the dielectric constant then biases this free energy when electrostatics are introduced. Using this formalism, Andelman and collaborators identified an electric field-induced phase transition in lamella-forming BCP thin films⁶⁴ and later reported the role of ionic impurities in altering the magnitude of field necessary to induce such a transition.⁹⁵ The latter has also more recently been studied using a full SCFT representation.⁹⁶

This linear mixing rule for describing dielectric behavior of a BCP melt was later implemented within a full SCFT formalism, including several papers by Matsen^{40,42,97} that address the self-assembly of BCPs confined to a thin gap between two charged plates. Among other novel results, Matsen’s work identifies electric fields as a promising methodology for manufacture of perforated thin films by reorienting ordered cylindrical or lamellar structures perpendicular to the confinement. Matsen’s work further demonstrates the efficacy and extensibility of the present SCFT model as a procedure for identifying stability limits, kinetic pathways,⁴⁰ and other properties and phenomena of interest. The full SCFT formalism has been shown to agree with the simpler GL model in the weak segregation regime.⁹⁸

In another set of studies,^{39,41} Schick and collaborators performed similar investigations, considering in detail the thermodynamic character of electric field-induced phase transitions in dielectric BCP systems. They identified several stable phases that exist for a cylinder-forming thin-film system, arising from competition between surface-wetting energy and dielectric response.⁴¹

More recently, Zvelindovsky and collaborators combined the electrostatic formalism with a dynamical SCFT framework to investigate the kinetic pathways of electric field-induced phase transitions and structure reorientations.^{99–103} In one study,¹⁰² this group used a dynamical extension of the GL model employed by Andelman to simulate the large-scale time-dependent rearrangement of defective lamellar structures subjected to an electric field. In striking agreement with experimental observations,¹⁰⁴ their results identified two healing mechanisms, one arising from the reorientation of locally ordered grains and one a “nucleation and growth” pathway – corresponding to the growth of perfectly aligned regions, with associated migrating boundaries that overrun the misaligned grains – and illuminated the role of segregation

strength in selecting between them. In a later study,¹⁰⁵ they also identified a third mechanism in their simulations, “selective disordering” – wherein misaligned grains will melt into a disordered state, before recrystallizing as the aligned microstructure – which has been observed in experiments.^{106, 107}

In the present study, we use the full SCFT model to compute the complete diblock phase diagram for a bulk melt subjected to an external electric field, including all seven phases found in the field free state.⁴⁶ The field and temperature are treated as constant, with the implied assumption that any heating due to the conductivity of the melt will be mitigated by thermostatting. We assume purely dielectric constituent segments, a uniform applied electric field, and equal statistical segment lengths. We extend a previously-derived variable-cell updating method,¹⁰⁸ which permits the simulation cell shape and size to evolve to a stress-free configuration in tandem with solving the mean-field equations. In doing so, this approach automatically computes the commensurate unit-cell configuration for each morphology considered, permitting the free energy comparisons necessary for constructing the phase diagram of equilibrium morphologies. We show that the systems considered possess an orientation-sensitive free energy penalty arising from dielectric contrast, as described by Schick,³⁶ which selectively disfavors mesostructures that do not have an interface-free axis to align along the electric field vector. We show that this phenomenon has the effect of deforming phase boundaries of the diblock copolymer phase diagram, and in particular, preferentially stabilizing the O⁷⁰ network phase relative to the GYR network phase, permitting access to the former structure at larger values of χN for intermediate field strengths.

4.2 Theory and Model

4.2.1 Dielectric Block Copolymer: Field-Theoretic Representation

We employ a field theory model based on a coarse-grained description of an incompressible, monodisperse melt of n diblock copolymer chains, with a contact Flory-Huggins repulsion, χ , between dissimilar chain segments.³ We invoke the continuous Gaussian chain model and assume a locally isotropic dielectric response of the constituent segments. In the SCFT framework, this leads to an electric field-induced shift of the effective potential felt by a segment of

species j (A or B):

$$w_j^{eff}(\mathbf{r}) = w_j(\mathbf{r}) - \frac{\beta \epsilon_j \epsilon_0}{2\rho_0} |\nabla \psi(\mathbf{r})|^2, \quad (4.1)$$

where $w_j(\mathbf{r})$ is the auxiliary chemical potential field experienced by segments of type j due to non-electrostatic effects (immiscibility and incompressibility); its form is specified by the exchange field-theoretic formalism of Model E, described in Ref. 3. ϵ_0 is the vacuum permittivity, ϵ_j is the dielectric constant of type j segments, and $\psi(\mathbf{r})$ is the local electrostatic potential, such that $-\nabla\psi$ represents the local electric field experienced by a segment at position \mathbf{r} , and the latter term of Eq. 4.1 is the electrostatic potential energy per segment, expressed in SI electrostatic units.

To determine the electric potential, we account for the heterogeneous dielectric response resulting from inhomogeneities in species densities and solve the differential form of Gauss' law in the absence of unbound charge:

$$\nabla \cdot [\epsilon(\mathbf{r})\nabla\psi(\mathbf{r})] = 0 \quad (4.2)$$

where $\epsilon(\mathbf{r})$ is a dielectric profile, defined by a simple linear constitutive coupling to species densities:

$$\epsilon(\mathbf{r}) = \frac{1}{\rho_0} \sum_{j=A,B} \epsilon_j \tilde{\rho}_j \left(\mathbf{r}; \left[w_A^{eff}, w_B^{eff} \right] \right). \quad (4.3)$$

Here $\tilde{\rho}_j$ is the segment density operator for the j th segment species, presented in Eq. 4.12 in the following section. The imposed incompressibility condition requires a uniform total segment number density, ρ_0 , at each position, \mathbf{r} , such that $\tilde{\rho}_A(\mathbf{r}) + \tilde{\rho}_B(\mathbf{r}) = \rho_0$. We note that Eqs 4.2 and 4.3 together give a self-consistent condition for electric potential, ψ . As we demonstrated in Chapter 2, this *ad hoc* model can be equivalently obtained from a consistent microscopic origin by taking the incompressible, unsmeared (point dipole) limit of a general model of polarizable chain segments with self-consistently treated induced-dipoles on each segment.

In addition to a shift in the effective potential field that alters the microphase free energies, the introduction of an applied electric field also induces morphological distortions of the phase

structures. Consequently, some symmetries associated with the unperturbed candidate phase are broken, and equilibrium domain spacing becomes orientation-dependent. The unit cell shape and size must therefore be self-consistently optimized in the presence of the field to eliminate internal elastic stresses:

$$\tilde{\boldsymbol{\sigma}}[w_A^{eff}, w_B^{eff}, \mathbf{h}] = \mathbf{0}, \quad (4.4)$$

where $\tilde{\boldsymbol{\sigma}}$, defined in Eq. 4.14 in the following section, is the internal stress for a BCP melt subject to the effective chemical potential fields w_A^{eff} and w_B^{eff} within a periodically repeated arbitrary parallelepiped cell defined by the shape tensor \mathbf{h} .¹⁰⁸ For ease of notation, we retain the designations associated with the classical unperturbed morphologies, in contrast to other works, such as Ref. 109, wherein the authors define a distinct “ellipsoid” phase, corresponding to the reduced symmetry microstructure associated with a distorted BCC morphology.

4.2.2 Single-Chain Operators

The monomer density, $\tilde{\rho}_j$, and internal stress, $\tilde{\boldsymbol{\sigma}}$, operators that enter the field theory can be computed from the single-chain partition function, Q . In the present unit cell, which is described by the shape tensor, \mathbf{h} , it is convenient to adopt the cell-scaled coordinate, $\mathbf{x} \in [0, 1]^3$, related to the dimensional position in space by $\mathbf{r} = \mathbf{h} \cdot \mathbf{x}$. In this coordinate system, Q may be written in the scale-invariant form:

$$Q[w_A^{eff}, w_B^{eff}, \mathbf{g}] = \int d\mathbf{x} q(\mathbf{x}, 1), \quad (4.5)$$

where the chain propagator, q , solves the modified anisotropic diffusion equation

$$\begin{aligned} \frac{\partial}{\partial s} q(\mathbf{x}, s) &= [R_g^2 \nabla_{\mathbf{x}} \cdot \mathbf{g}^{-1} \cdot \nabla_{\mathbf{x}} - W(\mathbf{x}, s)] q(\mathbf{x}, s) \\ q(\mathbf{x}, 0) &= 1 \quad s \in [0, 1], \end{aligned} \quad (4.6)$$

and $\mathbf{g} = \mathbf{h} \cdot \mathbf{h}$ is the metric tensor associated with the simulation cell. The volume of the cell is related to \mathbf{h} according to $V = \det \mathbf{h}$.

The length-scale $R_g = b\sqrt{N/6}$ is the bare radius of gyration of a conformationally symmetric BCP with statistical segment length $b = b_A = b_B$, and N is the degree of polymerization. W

gives the local field experienced by the segment at contour position s ,

$$W(\mathbf{x}, s) = \begin{cases} W_A^{eff}(\mathbf{x}) & s < f \\ W_B^{eff}(\mathbf{x}) & s \geq f \end{cases}, \quad (4.7)$$

where the cell-scaled species fields are related to their dimensional counterparts by $W_j^{eff}(\mathbf{x}) = Nw_j^{eff}(\mathbf{r})$.

The internal stress operator can be computed from Q according to:

$$\tilde{\boldsymbol{\sigma}}[w_A^{eff}, w_B^{eff}, \mathbf{h}] = -\frac{2nkT}{V} \mathbf{h} \cdot \frac{\partial \ln Q[w_A^{eff}, w_B^{eff}, \mathbf{g}]}{\partial \mathbf{g}} \cdot \mathbf{h} - \varepsilon_0 \bar{\epsilon} \mathbf{E}_0 \mathbf{E}_0, \quad (4.8)$$

where $\bar{\epsilon}$ is the average macroscopic dielectric constant, defined as

$$\bar{\epsilon} \equiv \frac{1}{V} \int d\mathbf{r} \epsilon(\mathbf{r}) = \epsilon_A f + \epsilon_B (1 - f), \quad (4.9)$$

such that the latter term in Eq. 4.8 cancels the homogeneous electrostatic contribution to the internal stress.

Using a technique detailed by Villet *et al.*,¹⁸ one may apply the derivative $\frac{\partial}{\partial \mathbf{g}}$ to Eq. 4.6 and arrive at a PDE that results in the following expression for the internal stress operator:

$$\tilde{\boldsymbol{\sigma}} [w_A^{eff}, w_B^{eff}, \mathbf{h}] = \frac{nkT}{V} \int d\mathbf{x} \left[\mathbf{h} \cdot \tilde{\boldsymbol{\Sigma}}(\mathbf{x}) \cdot \mathbf{h} + \sum_{j=A,B} \frac{\partial W_j^{eff}(\mathbf{x})}{\partial \mathbf{h}} \cdot \mathbf{h} \tilde{\phi}_j(\mathbf{x}) \right] - \varepsilon_0 \bar{\epsilon} \mathbf{E}_0 \mathbf{E}_0. \quad (4.10)$$

$\tilde{\boldsymbol{\Sigma}}$ can be interpreted as a local, cell-scaled, single-chain contribution to the internal stress and is given by

$$\tilde{\boldsymbol{\Sigma}}(\mathbf{x}) = \frac{2}{Q} \int_0^1 ds q(\mathbf{x}, s) (R_g^2 \mathbf{g}^{-1} \cdot \nabla_{\mathbf{x}} \nabla_{\mathbf{x}} \cdot \mathbf{g}^{-1}) q^\dagger(\mathbf{x}, 1 - s), \quad (4.11)$$

where q^\dagger is a complementary propagator, which solves Eq. 4.6, with $W(\mathbf{x}, s)$ replaced by $W^\dagger(\mathbf{x}, s) \equiv W(\mathbf{x}, 1 - s)$. Similarly, $\tilde{\phi}_j$ is a cell-scaled volume fraction operator, defined as

$$\tilde{\phi}_j(\mathbf{x}) = \frac{1}{Q} \int_0^1 ds u_j(s) q(\mathbf{x}, s) q^\dagger(\mathbf{x}, 1 - s) = \frac{1}{\rho_0} \tilde{\rho}_j \left(\mathbf{r}; [w_A^{eff}, w_B^{eff}] \right) \quad (4.12)$$

with u_j a function that selects the limits of integration according to the identity of the desired species, j :

$$u_j(s) = \begin{cases} \Theta(f - s) & j = A \\ \Theta(s - f) & j = B \end{cases}, \quad (4.13)$$

where Θ is the Heaviside function. The latter expression of Eq. 4.12 identifies the connection to the segment density operator described in the preceding section.

Substituting Eq. 4.1 into the expression for W_j^{eff} and noting that only the electrostatic term contributes a non-vanishing response to changes in the cell shape tensor, \mathbf{h} , we arrive at a final expression for the stress operator:

$$\tilde{\boldsymbol{\sigma}} [w_A^{eff}, w_B^{eff}, \mathbf{h}] = \frac{nkT}{V} \int d\mathbf{x} \mathbf{h} \cdot \tilde{\boldsymbol{\Sigma}}(\mathbf{x}) \cdot \mathbf{h} + \tilde{\boldsymbol{\sigma}}_{el}[\psi], \quad (4.14)$$

where $\tilde{\boldsymbol{\sigma}}_{el}$ is an *electrostatic internal stress* contribution, given by:

$$\tilde{\boldsymbol{\sigma}}_{el}[\psi] = \frac{\varepsilon_0}{V} \int d\mathbf{r} \epsilon(\mathbf{r}) \nabla\psi(\mathbf{r}) \nabla\psi(\mathbf{r}) - \varepsilon_0 \bar{\epsilon} \mathbf{E}_0 \mathbf{E}_0. \quad (4.15)$$

4.2.3 SCFT Procedure

Our SCFT procedure thus requires simultaneously relaxing the field configurations of the polymer melt (w_A, w_B) to the saddle-points specified in the exchange-mapped auxiliary field theory,^{3,110} optimizing the shape and size of the periodic cell (\mathbf{h}) to a zero-stress configuration (Eq. 4.4) via the variable-cell method,¹⁰⁸ and determining the electric potential (ψ) self-consistently by solving Eq. 4.2 with appropriate boundary conditions. We solve the latter by enforcing periodic boundary conditions in the *local, internally-generated electric field*, $\mathbf{E}_{int} \equiv -\nabla\psi - \mathbf{E}_0$, and requiring $\int d\mathbf{r} \mathbf{E}_{int} = \mathbf{0}$, which is appropriate for a dielectric material in a fixed applied electric field. We note that although this condition is not sufficient to specify $\int d\mathbf{r} \psi$, it is sufficient to specify the local electric field, $-\nabla\psi$, which enters Eq. 4.1.

As discussed by Schick,³⁶ the introduction of an applied electric field to an inhomogeneous dielectric medium imparts an orientation sensitivity: configurations that violate the condition $\mathbf{E}_0 \cdot \nabla\epsilon = 0$ (*i.e.* that \mathbf{E}_0 is in the plane of any and all dielectric interfaces) will reduce the local electric field magnitude, resulting in a free energy penalty. It can be shown that this

free energy penalty, which we define to be the difference in the electrostatic free energy for the inhomogeneous polymer melt and the corresponding term for the homogeneous (disordered) state with the same composition, is given by

$$\Delta F_{el} = \frac{\varepsilon_0}{2} \int d\mathbf{r} \epsilon(\mathbf{r}) [|\mathbf{E}_0|^2 - |\nabla\psi(\mathbf{r})|^2] = \frac{\varepsilon_0}{2} \int d\mathbf{r} \epsilon(\mathbf{r}) |\mathbf{E}_{int}(\mathbf{r})|^2 = -\frac{\varepsilon_0}{2} \int d\mathbf{r} \psi_{int}(\mathbf{r}) [\nabla\epsilon(\mathbf{r}) \cdot \mathbf{E}_0], \quad (4.16)$$

where ψ_{int} is the internally-generated contribution to the electric potential, defined by $-\nabla\psi_{int} = \mathbf{E}_{int}$. The form of the latter term of Eq. 4.16 emphasizes that ΔF_{el} vanishes when $\nabla\epsilon \cdot \mathbf{E}_0 = 0$. Consequently, we will find that the introduction of an applied electric field to a BCP melt induces elongation of ordered structures – and in some cases drives phase transitions to aligned structures – to reduce this free energy penalty.

In the weak segregation regime, the density profile for each monomer, $\tilde{\rho}_j$, is weakly inhomogeneous. Making the substitution $-\nabla\psi = -\nabla\psi_{int} + \mathbf{E}_0$ into Eq. 4.2, and solving the resulting PDE for ψ_{int} to leading order in the perturbation, $\Delta\rho = \tilde{\rho}_A - \rho_0 f$, the following asymptotic expression is obtained for the electrostatic free energy penalty,

$$\begin{aligned} \Delta F_{el} &\sim \frac{\kappa}{2} \int d\mathbf{r} \int d\mathbf{r}' \frac{(\nabla\tilde{\rho}_A(\mathbf{r}) \cdot \mathbf{E}_0)(\nabla\tilde{\rho}_A(\mathbf{r}') \cdot \mathbf{E}_0)}{\rho_0^2 |\mathbf{r} - \mathbf{r}'|} + O\left(\left[\frac{\Delta\rho}{\rho_0}\right]^3\right) \\ \kappa &\equiv \frac{\varepsilon_0(\epsilon_A - \epsilon_B)^2}{4\pi\bar{\epsilon}}, \end{aligned} \quad (4.17)$$

where we have used the property, $\nabla\tilde{\rho}_A = -\nabla\tilde{\rho}_B$, which is required by incompressibility.

We note that Eq. 4.17 appears in numerous previous studies that employ this electrostatic formalism (*e.g.* Refs. 38,64), and is proportional to the square of the dielectric contrast between monomer species. Evidently, the dielectric response of a BCP melt in the weak segregation regime is specified by the single parameter, κ , such that the responses of systems with differing dielectric constant pairs may be collapsed to a common curve by a simple rescaling of \mathbf{E}_0 . We therefore limit our calculations to a single pair of dielectric constants, with the understanding that the simulations must be repeated for other dielectric constant pairs when quantitative accuracy is required beyond the weak segregation regime.

4.3 Results and Discussion

4.3.1 Orientation-Dependent Dielectric Response

The orientation sensitivity imparted by an applied electric field has a symmetry-breaking property: for a fixed applied electric field, the free energy of a polymer mesostructure becomes sensitive to its orientation relative to the electric field vector, \mathbf{E}_0 . In comparing free energies of competing phases, we choose the relative lattice orientation of a given mesostructure that minimizes its overall free energy response, as a bulk polymer melt can be expected to freely self-assemble in such a manner to attain this minimum in an applied electric field.

For the case of lamellae (LAM) and hexagonally packed cylinders (HEX), this optimal orientation is trivial to deduce:^{36,111} each phase has at least one axis of dielectric uniformity, and can align such that the condition $\mathbf{E}_0 \cdot \nabla\epsilon = 0$ is everywhere satisfied – with the result that the free energy response, defined in Eq. 4.18 below, is 0. For structures without a uniform axis, this condition is not satisfied for any orientation of the microphase. The determination of the optimal orientation of the structure is thus made numerically while accounting for the self-consistent morphological response. Although this orientation sensitivity has been considered for the BCC phase,¹¹¹ it has yet to be explored in other 3D morphologies. The network phases shown to be stable by SCFT for a field-free diblock system, (O⁷⁰)⁴³ and (GYR),⁴⁶ consist of complicated arrangements of species interfaces, and the preferred orientation of each mesostructure in a uniform applied electric field is not immediately obvious.

To interrogate the orientation-dependence of each network phase, a simple sweep was performed: the electric field magnitude was held constant, and the free energy response (Eq. 4.18) of the phase was calculated as a function of the relative orientation of the uniform applied electric field. The free energy response is defined to be

$$\Delta F(\theta, \phi) = F(\theta, \phi) - F_0 + \frac{\epsilon_0 \bar{\epsilon} V}{2} |\mathbf{E}_0|^2 \quad (4.18)$$

where θ and ϕ specify the polar and azimuthal angles, respectively, of the orientation of the electric field vector on the unit sphere. $F(\theta, \phi)$ is the mean-field (SCFT) free energy of a given phase, subject to the applied electric field \mathbf{E}_0 , F_0 is the free energy of each phase in

the absence of an applied electric field, and the final term in Eq. 4.18 removes the dielectric response contribution to the free energy for a homogeneous mixed state.

In Fig. 4.1, we plot the intensive free energy response of the GYR and O^{70} phases in an electric field as a function of θ and ϕ . These results indicate that the GYR phase has a preferred (lowest free energy) electric field orientation of $\theta = \tan^{-1} \sqrt{2} \approx 0.955$, $\phi = \pi/4$, corresponding to the [111] direction, and the O^{70} phase has a preferred orientation of $\theta = 0$, which corresponds to the [001] direction.

The values on the scale bars for the contour plots in Fig. 4.1 show another important difference between the two structures: the free energy response varies little ($\sim 0.5\%$) as a function of electric field orientation for the GYR phase, whereas it changes by a factor of 5 for the O^{70} phase. Since the GYR phase belongs to a cubic crystal system, group-theoretic arguments demand that its linear response (*i.e.*, $E_0 \rightarrow 0$) be precisely isotropic,¹¹² and we can understand the weak anisotropy displayed in Fig. 4.1 as arising from the *nonlinear response* resulting from a *self-consistent* morphological distortion. On the other hand, the O^{70} phase is orthorhombic and admits a much stronger anisotropy in dielectric response that is finite in the linear response regime. One consequence of this anisotropy is that the free energy response of the O^{70} phase at its preferred orientation is smaller than that of GYR by $\sim 10^{-3}kT/n$, indicating a relative destabilization of the GYR phase.

This apparent anisotropic response to an applied field can be characterized by a tensor-valued dielectric constant, ϵ , which will be related to the free energy of the melt by,

$$F(\theta, \phi) = F_0 - \frac{\epsilon_0 V}{2} \mathbf{E}_0 \mathbf{E}_0 : \epsilon. \quad (4.19)$$

If we further segregate the isotropic dielectric behavior of the DIS phase, defining the tensor-valued correction, $\Delta\epsilon = \epsilon - \bar{\epsilon}\mathbf{I}$, Eq. 4.18 can be written as,

$$\Delta F(\theta, \phi) = -\frac{\epsilon_0 V}{2} \mathbf{E}_0 \mathbf{E}_0 : \Delta\epsilon, \quad (4.20)$$

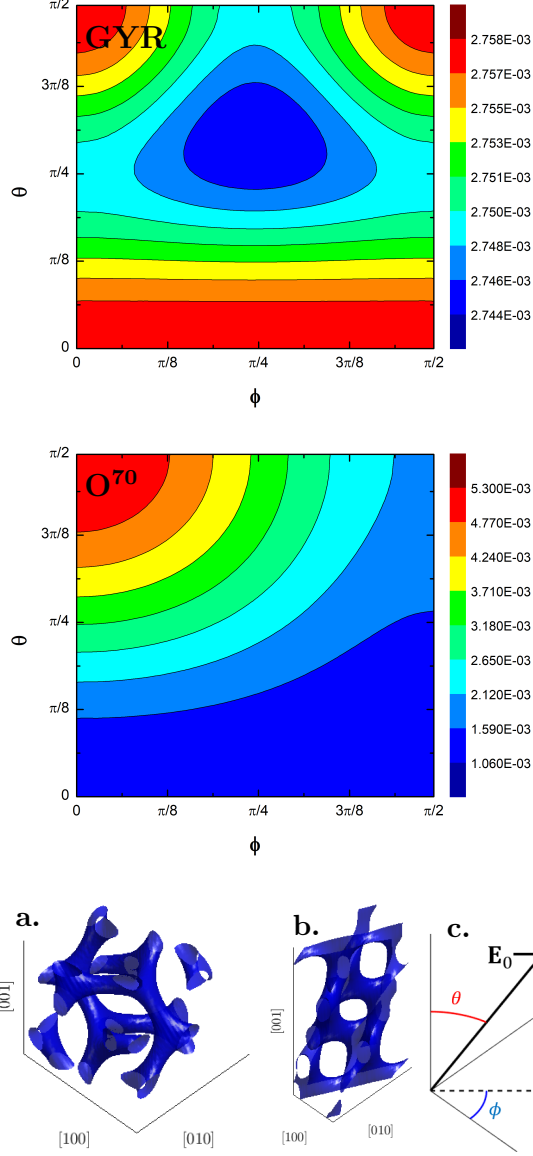


Figure 4.1: Intensive free energy response $[\beta\Delta F(\theta, \phi)/n]$ of GYR (top) and O^{70} (middle) phases at electric field strength $E_0[nkT/(\epsilon_0 V)]^{-1/2} = 0.25$ for the diblock system of $f = 0.4$, $\chi N = 14.0$ and $\epsilon_A = 1.0$, $\epsilon_B = 4.0$. The images on the bottom row are 3D renders of the GYR (a.) and O^{70} (b.) unit cells and their corresponding lattice directions, along with a schematic (c.) depicting the correspondence between the angles (θ and ϕ) and the orientation of the field as applied to the two structures.

which is equivalently identified as a condition for each element of $\Delta\epsilon$:

$$\Delta\epsilon_{ij} = -\frac{2\Delta F(\theta, \phi)}{E_{0i}E_{0j}\epsilon_0 V}, \quad (4.21)$$

where the components of the electric field vector are obtained *via* the usual transformation from a spherical coordinate system:

$$\begin{aligned} E_{0x} &= |\mathbf{E}_0| \sin(\theta) \cos(\phi) \\ E_{0y} &= |\mathbf{E}_0| \sin(\theta) \sin(\phi) \\ E_{0z} &= |\mathbf{E}_0| \cos(\theta). \end{aligned} \quad (4.22)$$

For each of the two network phases, the elements of $\Delta\epsilon$ can be estimated from the $F(\theta, \phi)$ data shown in Fig. 4.1, by enforcing Eq. 4.21 at each ordered pair (θ, ϕ) that was sampled, and performing a least-squares fit:

$$\Delta\epsilon^{O^{70}} \approx \begin{bmatrix} -0.1695 & 0.0003 & 0.0014 \\ 0.0003 & -0.0647 & 0.0011 \\ 0.0014 & 0.0011 & -0.0346 \end{bmatrix} \quad \Delta\epsilon^{GYR} \approx \begin{bmatrix} -0.0883 & 0.0005 & 0.0005 \\ 0.0005 & -0.0883 & 0.0005 \\ 0.0005 & 0.0005 & -0.0883 \end{bmatrix}. \quad (4.23)$$

Neglecting the small magnitude off-diagonal elements of each $\Delta\epsilon$, the negative sign of the diagonal elements of both dielectric constant tensors indicates that they give the magnitude of an orientation-dependent free energy penalty due to the applied field. Whereas all the diagonal elements of $\Delta\epsilon^{GYR}$ are the same, up to the number of significant digits shown, the diagonal elements of $\Delta\epsilon^{O^{70}}$ admit significant contrast between each other, indicating the expected anisotropy. Additionally, $\Delta\epsilon_{zz}^{O^{70}}$ is smaller in magnitude than each diagonal element of $\Delta\epsilon^{GYR}$ by more than a factor of two. This confirms that the stronger anisotropy of the O^{70} phase allows it to reduce its associated free energy penalty, reorienting such that \mathbf{E}_0 points along its unit cell's z axis, yielding a value for ΔF that is smaller than the corresponding quantity for any orientation of the GYR phase.

To illuminate the scaling of this anisotropy effect, we compute the free energy for each network phase at two different electric field orientations, as a function of electric field magnitude,

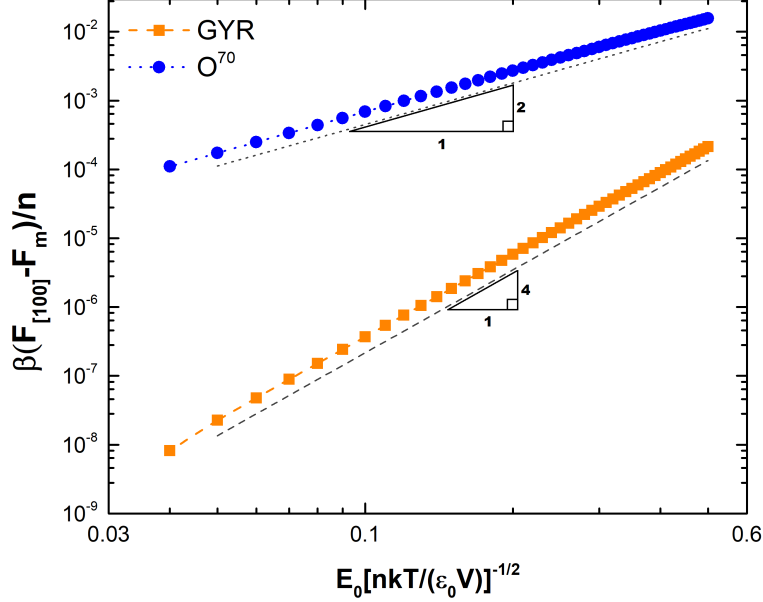


Figure 4.2: Difference in intensive free energy between two \mathbf{E}_0 orientations as a function of dimensionless field strength for the diblock system of $f = 0.4$, $\chi N = 14.0$ and $\epsilon_A = 1.0$, $\epsilon_B = 4.0$. The [100] direction is chosen for each phase as a disfavored orientation of \mathbf{E}_0 , and the other is chosen to minimize the intensive free energy (F_m) for each corresponding phase structure. The dashed line has a slope of 4 and the dotted line has a slope of 2.

E_0 , and plot the difference. We choose the [100] direction as an arbitrary direction that is disfavored for both phases and compare to the preferred orientation of each respective phase. The scaling identified in Fig. 4.2 indicates that the leading order term of this free energy difference varies as E_0^4 for the GYR phase and E_0^2 for the O^{70} phase. This indicates that the leading-order contribution to anisotropic dielectric response in the GYR phase must arise from nonlinear response, whereas the anisotropy of the O^{70} phase has a non-vanishing linear response contribution.

4.3.2 Diblock Phase Stability in an Applied Electric Field

We proceed by investigating the effect of the orientation-dependent dielectric response on the free energy competition that determines phase stability and order-order-transition boundaries. Fig. 4.3 shows the intensive SCFT free energy of GYR and each neighboring phase as a function of electric field magnitude, for values of f , χN at which GYR is most stable in the absence of a field. Since the free energy response is zero for both HEX and LAM in this SCFT framework, both network phases are eventually disfavored with sufficiently large electric fields. However,

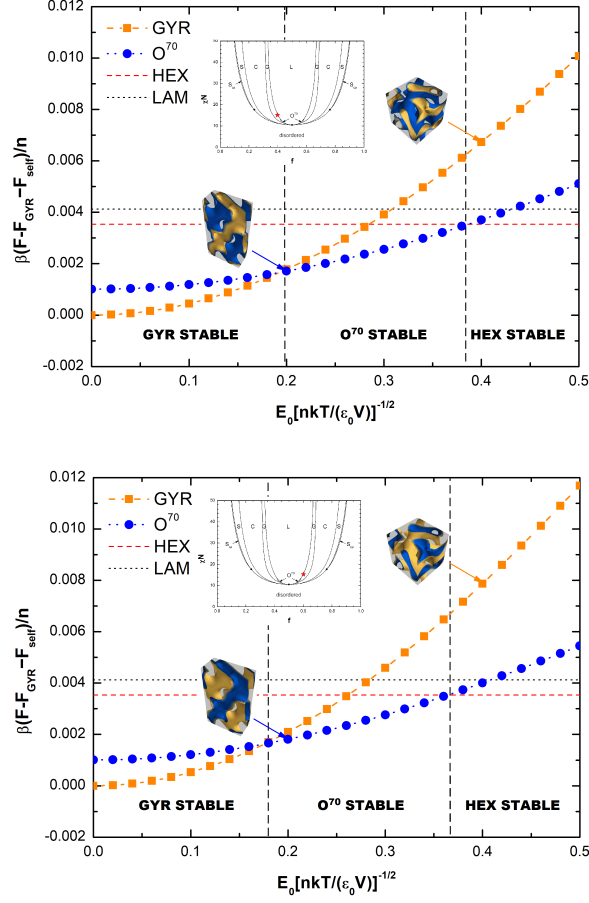


Figure 4.3: Free energy per molecule, $\beta F/n$, for the GYR and O^{70} phases, along with the HEX and LAM phases for reference, at their preferred orientations, as a function of dimensionless electric field strength, $E_0[nkT/(\epsilon_0 V)]^{-1/2}$. The BCP parameters are $f = 0.4$ (top) and $f = 0.6$ (bottom), at $\chi N = 14.0$ and $\epsilon_A = 1.0$, $\epsilon_B = 4.0$. F_{GYR} is the free energy of the GYR phase in the absence of an applied electric field and $F_{self} = -(\bar{\epsilon}\epsilon_0 V/2)E_0^2$ removes the bulk dielectric response of the mixed phase. The GYR phase is most stable at $E_0 = 0$, but there is an intermediate range of E_0 values for which O^{70} is favored.

due to the stronger dielectric response of GYR over O^{70} , we also find a large window of electric field strengths within which the O^{70} phase is predicted to have the lowest free energy.

In Fig. 4.4, we plot the phase diagrams for diblock copolymer systems in the absence of an electric field (top) and in the presence of an electric field with dimensionless magnitude of (middle) 0.25 and (bottom) 0.4. When an external electric field is introduced, the axially uniform LAM and HEX phases and the disordered phase are favored, such that the phase boundaries for both the order-disorder transitions (ODTs) and the order-order transitions (OOTs) shift to enlarge the stability regions corresponding to these structures.

The O^{70} -GYR phase boundary, which divides the network region of stability, is shifted by

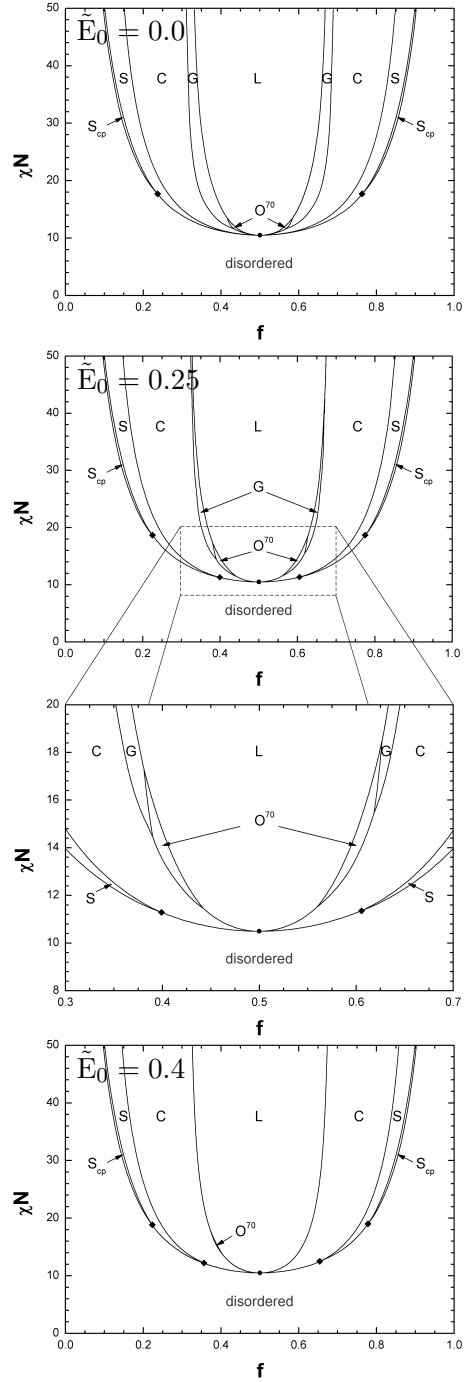


Figure 4.4: Diblock phase diagrams for $\tilde{E}_0 \equiv E_0[nkT/(\epsilon_0 V)]^{-1/2} = 0$ (top), 0.25 (middle two panels), and 0.4 (bottom), with $\epsilon_A = 1.0$, $\epsilon_B = 4.0$. The critical point (dot) is unaffected by the introduction of an applied electric field. However, the triple points (diamonds) shift to larger χN values and additional triple points emerge. The phase labels are: FCC spheres (S_{cp}), BCC spheres (S), hexagonal-packed cylinders (C), lamellar (L), Ia $\bar{3}$ d double gyroid cubic network (G), and orthorhombic Fddd network (O^{70}).

the electric field in favor of the O^{70} phase, a signature of the preferential destabilization of the GYR phase that was demonstrated in Fig. 4.3. To emphasize this shift, we also show an inset for the weak-segregation regime in the phase diagram with $E_0 [nkT/(\varepsilon_0 V)]^{-1/2} = 0.25$ in Fig. 4.4, third panel. This result may be of particular interest, since the O^{70} phase is predicted by SCFT to be thermodynamically stable only at weak segregation strength, and has only been obtained experimentally within a narrow temperature range.⁴⁵ Near the ODT, thermal fluctuations are expected to strongly perturb the phase diagram, and if sufficiently strong, perhaps eliminate¹⁹ the O^{70} region of thermodynamic stability when no electric field is present. The use of an electric field to shift the O^{70} -GYR phase boundary to larger segregation strengths may therefore prove to be a viable protocol for realizing the equilibrium stabilization of O^{70} at lower temperatures, where thermal fluctuations are weaker.

We note that in the present mean-field scheme, order-disorder transitions are also modified by the applied electric field if $f \neq 0.5$. However, the mean-field critical point lying at $f = 0.5$ is unaffected by the electric field due to the lack of dielectric response of both the LAM and DIS phases, in contrast with experimental predictions.¹¹³ Evidently, a full treatment of composition fluctuations in tandem with an applied electric field is required to properly describe sensitivity of the ODT to applied fields.

At asymmetric ($f \neq 0.5$) compositions and in the absence of an electric field, SCFT predicts a narrow window of sphere-phase stability at the ODT. Under an applied electric field, DIS-HEX-BCC triple-points are predicted to appear; the electric field selectively destabilizes the BCC phase, so that there exists a segregation strength $\chi_{TP}N > \chi_c N$, where χ_{TP} is the triple point and χ_c is the critical point, below which the BCC phase is not thermodynamically stable. Below $\chi_{TP}N$, the ODT is predicted to be a first-order direct HEX-DIS transition. For the same reason, one can identify triple points (not marked on the phase diagram), delineating a χN window away from which direct LAM-HEX transitions emerge without intervening O^{70} or GYR phases.

Another important feature of the phase diagrams shown in Fig. 4.4 is the emergence of asymmetry about the vertical line passing through $f = 0.5$ (*i.e.* asymmetry in transposition of A and B monomer species) when an electric field is introduced. It can be seen that the previously discussed changes in the features of the phase diagram that emerge as a consequence

of dielectric response (e.g. a narrower network phase window of stability) are more exaggerated on the large f side of the plot. For this side of the phase diagram, the B monomer (which we have selected to possess the larger dielectric constant of the two species) is the minority species, such that the average dielectric constant of a melt of this composition, $\bar{\epsilon}$, is smaller than for the composition corresponding to the opposing side of the phase diagram. As a consequence, the dielectric response of the melt, \mathbf{E}_{int} , is larger in magnitude, and the corresponding electrostatic free energy penalty, given by Eq. 4.16, is larger, consistent with the scaling predicted by the asymptotic form for ΔF_{el} derived in Eq. 4.17. This effect is also evident in Fig. 4.3, wherein the plot of free energy response at $f = 0.6$ indicates a stronger destabilization of the network phases, and the phase transitions from GYR to O^{70} , then from O^{70} to HEX, occur at smaller electric field magnitudes.

In designing an experiment that leverages the phase behavior of a BCP melt in an electric field, one would ideally want to choose an architecture for which the monomer species with the larger dielectric constant is the less abundant of the two. Doing so permits access to the desired effects with an electric field that is smaller in magnitude, reducing the demands of the experimental setup (e.g. a wider gap in a parallel-plate capacitor setup may be used) and reducing the risk that the strength of the field exceeds the dielectric breakdown limit of the monomer species.

Finally, we provide a rough estimate about the physical electric field strength by translating the dimensionless electric field strength $E_0[nkT/(\epsilon_0V)]^{-1/2} = 0.25$ into a value in real units. We consider a BCP melt of intermediate chain concentration ($nR_g^3V^{-1} = 1.0$) and the radius of gyration $R_g = 10.0$ nm, operating in a parallel plate capacitor set-up at temperature $T = 200$ °C. For such a system, the dimensionless electric field strength (specified in the middle phase diagram of Fig. 4.4) corresponds to a field strength of $E_0 = 6.79$ kV/mm, which is an order of magnitude below the dielectric breakdown strength of many common monomer chemistries and is well within physically realizable experimental values. This simple calculation supports the feasibility of applied electric fields as a modality for shifting phase boundaries and obtaining morphologies such as the O^{70} phase that might be otherwise difficult to access in bulk BCP systems.

4.4 Conclusion

We have presented a study of the equilibrium self-assembly of microphases of a BCP melt in the presence of a uniform applied electric field, \mathbf{E}_0 . We assumed linear dielectric response in individual polymer chain segments and constructed a heterogeneous dielectric profile, ϵ , from a linear constitutive relation. The electrostatic potential is coupled to the melt configuration by self-consistently enforcing Gauss' law for an inhomogeneous dielectric (Eq. 4.2). Combining this constitutive model with existing field-theoretic methodology for simulating incompressible diblock copolymer melts, as well as a variable-cell relaxation method for automatically optimizing unit cell shape and size, we constructed the full mean-field diblock copolymer phase diagram, with prescribed species-dependent dielectric constants (ϵ_A, ϵ_B) and fixed electric field magnitude, E_0 .

Our results show agreement with the qualitative predictions made by Schick,³⁶ as well as the results of other previous studies that employed the same linear constitutive model of inhomogeneous dielectric response. The free energy of an ordered phase structure in the presence of an electric field depends on its orientation relative to the electric field vector. This anisotropic dielectric response is present even for cubic phases (such as BCC and GYR phases) beyond the linear-response regime. The contrast in anisotropy between phases is subsequently responsible for the shift in phase transitions. One observation of particular interest is that the O^{70} network phase becomes relatively more thermodynamically stable than GYR as E_0 is increased, which shifts the GYR- O^{70} order-order transition to larger segregation strengths. As the O^{70} phase has been obtained experimentally⁴⁵ and predicted by simulation to exhibit marginal stability in the presence of sufficiently weak fluctuations,¹⁹ we expect a window of stability to widen when a field of sufficient intensity is introduced, granting access to the O^{70} phase over a broader range of temperatures, chemistries, and molecular weights, and thus enhancing the materials design process when O^{70} is the desired microstructure.

The present results provide a prediction of the phase behavior of monocrystalline (*i.e.* consisting of perfectly repeating unit cells) BCP melts. However, experimental and industrial setups are much larger than a single unit cell of a microphase, and imperfect long-range structures containing locally ordered grains of the appropriate microstructure (as in Ref. 102), or

other defective states, exist as metastable melt configurations. In particular, the presence of a defect would have an orientation-sensitive – and highly case-dependent – effect on both the apparent OOT temperature associated with some desirable, field-induced transition (*e.g.* from GYR to O⁷⁰) and on the kinetics of this transition. However, we can make the assertion that there will be two general cases: 1) the defective structure remains metastable to the perfect crystal of the initial morphology upon introduction of an applied field, and 2) the defective structure becomes stable relative to the initial perfect structure in the presence of an applied field. In the former case, we predict little change to the OOT temperature or its kinetics, as we would expect the melt to recover the perfect initial morphology as an intermediate step, before a subsequent transition to the target structure, with the former transition having a much smaller free energy barrier, as it is simply a defect removal pathway. In the latter case, the OOT can be expected to shift in favor of the initial structure, as we are considering a defect that has a stabilizing effect in the presence of an electric field, delaying the onset of the OOT. The pathway for the eventual transition to the target structure would be distinct from that of the transition between two perfect morphologies; their relative free energy barriers would therefore need to be determined by experiment or simulation. Subsequent work in identifying these defective structures, their prevalence when a melt is quenched from the disordered state in the presence of an electric field, and the kinetic barriers associated with realignment of grains into a perfect microstructure – as well as other healing mechanisms – will therefore be of use to the experimentalist interested in using an applied electric field to obtain novel, defect-free morphologies. Additionally, the combination of applied electric fields with other techniques for enhancing the annealing process, such as the use of non-selective solvent,¹¹⁴ requires further consideration; for example, one would expect to need a larger electric field to obtain a desired shift in phase behavior when a solvent is present, as the solvent’s contribution to the dielectric character of the solution reduces the dielectric contrast between domains.

As described in Results, the LAM and HEX microphases possess an axis of dielectric uniformity, such that they may align their interfaces parallel to the electric field vector, their thermodynamic stability – relative to each other and to the DIS phase – is unchanged, and the sphere and network phases become selectively disfavored. Indeed, for sufficiently large electric fields, one could expect the sphere and network phases to be disfavored at all values of f and

χN , such that the resulting diblock phase diagram consists of only DIS, HEX, and LAM regions of stability, with corresponding phase boundaries that are insensitive to further increases in electric field strength. As a consequence, our results predict no shift in the BCP critical point lying at $f = 0.5$. However, experiment confirms that the critical point for a BCP shifts to larger χN values (lower temperature) in response to an applied electric field.¹¹³ Evidently, the present non-fluctuating SCFT model, which assumes a linear mixing rule for the dielectric behavior of the melt, is insufficient to describe this qualitative behavior.

As we illuminated in the preceding chapter, electric field-induced shifts in the single-phase stability of a dielectric fluid (corresponding to the DIS phase for the present case of a diblock copolymer melt) arise from composition-dependent, field-induced fluctuations, and no shift is observed at the mean-field level, which neglects fluctuations. In the macrophase-separating systems that we considered, the phase stability of an incompressible fluid is determined by the composition dependence of its free energy; using this property, the electric field-dependence of a fluid’s phase stability could be inferred from the composition dependence of its dielectric constant, which enters the free energy according to Eq. 3.2. In microphase-separating block copolymer systems, the stability of the DIS phase is instead determined by a wavevector-dependent function, $S(k)$ – referred to as the structure factor – which specifies the dependence of the system’s free energy on spatially inhomogeneous *composition fluctuations* associated with the wavevector \mathbf{k} .^{57,69} Determining the electric field-dependence of $S(k)$ for a fluctuating, dielectric block copolymer melt will therefore be instrumental in elucidating the behavior observed in Ref. 113.

Beyond the simple isotropic polarizability prescribed in the present dielectric model, one may also introduce an anisotropic polarizability, which couples chain conformation to the local electric field, altering phase boundaries and domain spacing.^{115,116} This effect is primarily only significant for systems containing stiff polymers in a magnetic field,¹¹⁷ wherein an equation analogous to Gauss’ law (Eq. 4.2) governs the diamagnetic response of the melt. For block copolymer systems composed of chemistries that are more strongly polarizable parallel to the chain backbone, and for which there is diamagnetic contrast between A and B monomer species, magnetostatic free energy contributions due to alignment of chains and to alignment of microstructure domains, respectively, compete; these types of physical systems thus exhibit

a rich, orientation-sensitive phase behavior.¹¹⁸

Chapter 5

Concluding Remarks

In this thesis, I outlined the general structure of a field theory for polarizable and/or charged molecular species. Using several simple representative fluid models – combined with the usual analytical and numerical methods for solving a statistical field theory – I illuminated emergent electrostatic phenomena, generated by the collective behavior of fluctuating, electrostatically-interacting charged and polarizable fluid species.

In addition to these fluctuation-induced correlation behaviors, the model was also shown to illuminate macroscopic material properties of the fluid, in particular the dielectric constant, which was identified as a *thermodynamic observable* that can be determined from the dependence of the system’s free energy on an applied electric field, \mathbf{E}_0 . In Chapters 3 and 4, the dielectric response of binary polarizable fluids was considered in detail: in the former case, fluctuation corrections to the dielectric constant were found to determine the \mathbf{E}_0 -dependence of the phase stability of 3 classes of macrophase-separating fluid mixtures; in the latter case, the \mathbf{E}_0 orientation dependence of the free energy of different block copolymer microphase free energies implied a tensor-valued correction $\Delta\epsilon$ to the macroscopic dielectric constant of the melt, relative to the dielectric constant of the DIS/mixed phase.

In Chapter 2, I introduced the structure of the field theory, and discussed in detail the procedure for imposing dielectric properties at the scale of individual “bead” particles. The polarization response of beads arises from a pair of fluctuating partial charges, which are linked to their center of mass to form a Drude oscillator; the Drude oscillator link can be any desired bonded interaction, and in this Thesis I chose a harmonic spring, corresponding to induced-

dipole behavior, which can subsequently be approximated by a polarizability α that quantifies the magnitude of the bead’s average polarization response to a local electric field. I combined this bead model with the existing Model F field theoretic framework, which is derived from a particle model that assigns a Coulomb interaction between all charges within the system, as well as a non-specific contact excluded volume interaction, which prevents collapse of the fluid due to electrostatic attractions.

I further showed that one can construct molecules of arbitrary complexity, containing any number of these dielectric bead species, connected using an appropriate bonded interaction. Since these details are captured by an associated *single-molecule partition function*, the resulting field theory retains the Model F structure, which serves to enumerate the two aforementioned non-bonded interactions. Further identifying an effective chemical potential field for each bead type, which collects contributions from both Model F fields, I outlined the general workflow for constructing dielectric polymer molecules, which can invoke any model from the existing library of polymer linker statistics and chain architectures, with an arbitrary sequence of bead species identities.

I subsequently discussed the behavior of a binary dielectric electrolyte fluid, represented using the field theory. Using a Gaussian fluctuation approximation, I showed that this simple model correctly generates behavior predicted in Debye Hückel solution theory,⁵⁴ with a long-range average pair interaction between unpaired charges that admits both charge- and dielectric-screening effects. Additionally, the osmotic pressure of the fluid was found to include contributions from short-range ion-dipole and dipole-dipole average pair interactions between beads. The latter interaction was also found to favor phase separation of the two bead types when they had dissimilar polarizabilities; the magnitude of this fluctuation-induced immiscibility between the two bead species was related to a Flory parameter χ , which is an effective property of chemistry pairs known to originate from polarizability contrast,⁵⁵ but generally imposed phenomenologically as an average contact repulsion.

In Chapter 3, I derived the form of the field theory for a dielectric fluid in the presence of a uniform applied electric field, \mathbf{E}_0 . I showed that the average dielectric displacement, \mathbf{D} , could be obtained from an \mathbf{E}_0 -derivative of the system’s free energy, and is thus a thermodynamic property obtained from the average behavior of the fluctuating fluid. I further showed that

linear relation $\mathbf{D} = \epsilon \mathbf{E}_0$ becomes accurate in the limit of small electric field magnitudes, and subsequently inferred the dielectric constant, ϵ , as an additional thermodynamic property, with an associated field-theoretic operator that can be obtained as a function of single-molecule properties.

For a macrophase-separating binary mixture, I further noted that the composition-dependence of ϵ directly determines the direction and magnitude of the \mathbf{E}_0 -dependence of the fluid's phase stability, provided \mathbf{E}_0 is within the linear regime of the fluid. I defined a contribution χ_E to the effective Flory parameter between the two species, which quantifies this miscibility shift.

I computed an analytical expression for χ_E using a Gaussian approximation, and found that in the absence of contrast between the two molecular components, χ_E was strictly positive – indicating a shift in favor of demixing. For sufficiently strong contrast in the molecular structure of two species – which was imposed either by choosing contrasting smearing functions for the two bead types, or by assigning each species to have a different molecular architecture – I found regimes that gave $\chi_E < 0$ – favoring mixing.

Using both the Gaussian approximation and the CL numerical sampling method, I examined the character of χ_E in 3 classes of binary systems – a binary simple fluid, a binary homopolymer blend, and a homopolymer solution (polymer-solvent mixture) – and compared my observations to relevant experimental results. I attributed the qualitative disagreement between my model and 3 of these results^{23,31,33} to the soft, isotropic polarizability that was specified for each bead type in my model, which fails to adequately coarse-grain the average behavior of molecules that respond anisotropically to an inhomogeneous local electric field. I identified the highly-localized, highly-anisotropic hydrogen bonds that are present in the chemistries considered in Refs. 31 and 23 as an obvious feature not captured by the model. I concluded by proposing several modifications to the single-bead partition function that would include the desired anisotropic dependence on higher-order variations in the local electric potential.

In Chapter 4, I determined the phase behavior of a dielectric block copolymer (BCP) melt in the present of an applied electric field, \mathbf{E}_0 . I implemented a previously-derived^{39,42,64} *ad hoc* procedure for performing SCFT simulations of a BCP represented by the usual Model E³ field theory. I found that this procedure is equivalently obtained from the saddle-point (SCFT) condition for an extended Model E field theory that assigns each monomer segment an explicit

induced dipole, where the SCFT condition for the associated electrostatic auxiliary field is exactly Gauss' law.

When the two monomer types have contrasting dielectric constants, species interfaces that are not in-plane with the electric field vector carry a net free energy penalty, so that the melt's equilibrium microstructure rotates, distorts, or even changes to a new phase, giving rise to a field-induced order-order transition (OOT). For a specified electric field magnitude and contrasting monomer dielectric constants, I computed the diblock phase diagram, determining the phase that has the lowest free energy, once it has minimized its free energy with respect to rotation and distortion. Consequently, the phase diagram shifted in favor of microphases that admitted a stronger anisotropic dielectric response, due to their orientation-dependent distribution of species interfaces. In addition to favoring the LAM, HEX, and DIS phases, which all have at least one axis with no species interfaces, the presence of this \mathbf{E}_0 -generated penalty also stabilized the Fddd network with respect to double gyroid. The latter behavior was determined to be a consequence of Fddd's inherently anisotropic structure, which admits an orientation-dependent applied field response, even in the linear response regime.

In conclusion, I discussed in this Thesis the construction of a spherical bead model for the coarse-grained representation of dielectric molecular species; by explicitly enumerating two paired partial charges that account for each bead's net dipole moment, and subsequently specifying an unscreened Coulomb interaction between all charges, the bead model could be inserted into the familiar, pre-existing Model F field theory. The generality of this crude spherical bead model proved to be advantageous when performing the studies discussed in this Thesis, since I showed it to capture many of the relatively universal behaviors known to arise from the net dipole moment of molecular species in a fluctuating fluid – in addition to correctly recovering a consistent continuum prescription for electrostatic behavior, suitable for performing simulations at the mean-field level.

However, this molecular model quickly becomes inappropriate when one's desired results enter the realm of quantitative accuracy and/or qualitative behavior due to finer molecular detail; for example, several qualitative discrepancies were identified in Chapter 3 when comparing with experiments, evidently due to molecular details not captured by a polarizable, spherical bead. To address this deficiency, I have shown that one can straightforwardly modify the single-

molecule partition function to include arbitrarily fine details of a molecule's local net charges; in particular, the atomistically-derived partition function given in Eq. 3.93 provides the most flexible general structure, so long as the limitations I discussed in the passages following Eq. 3.93 can be addressed.

Bibliography

- [1] F. S. Bates, M. F. Schulz, A. K. Khandpur, S. Forster, J. H. Rosedale, K. Almdal, and K. Mortensen. Fluctuations, conformational asymmetry and block copolymer phase behaviour. *Faraday Discuss.*, 98:7–18, 1994.
- [2] M. W. Matsen and F. S. Bates. Unifying weak- and strong-segregation block copolymer theories. *Macromolecules*, 29:1091–1098, 1996.
- [3] G. H. Fredrickson. *The Equilibrium Theory of Inhomogeneous Polymers*. Oxford University Press, New York, 2006.
- [4] M. Winter and R. J. Brodd. What are batteries, fuel cells, and supercapacitors? *Chem. Rev.*, 104:4245–4270, 2004.
- [5] R. C. Agrawal and G. P. Pandey. Solid polymer electrolytes: materials designing and all-solid-state battery applications: an overview. *J. Phys. D: Appl. Phys.*, 41:223001, 2008.
- [6] S. Ghosh and O. Inganäs. Conducting polymer hydrogels as 3d electrodes: Applications for supercapacitors. *Adv. Mater.*, 11:1214–1218, 1999.
- [7] B. Smitha, S. Sridhar, and A. A. Khan. Solid polymer electrolyte membranes for fuel cell applications - a review. *J. Membrane Sci.*, 259:10–26, 2005.
- [8] Q. Wang and J. B. Schlenoff. The polyelectrolyte complex/coacervate continuum. *Macromolecules*, 47:3108–3116, 2014.

- [9] M. A. C. Stuart, B. Hofs, I. K. Voets, and A. de Keizer. Assembly of polyelectrolyte-containing block copolymers in aqueous media. *Curr. Opin. Colloid Interface Sci.*, 10:30–36, 2005.
- [10] G. Riess. Micellization of block copolymers. *Prog. Polym. Sci.*, 28:1107–1170, 2003.
- [11] Y. O. Popov, J. Lee, and G. H. Fredrickson. Field-theoretic simulations of polyelectrolyte complexation. *J. Polym. Sci. B: Polym. Phys.*, 45:3223–3230, 2007.
- [12] J. Lee, Y. O. Popov, and G. H. Fredrickson. Complex coacervation: A field theoretic simulation study of polyelectrolyte complexation. *J. Chem. Phys.*, 128:224908, 2008.
- [13] K. T. Delaney and G. H. Fredrickson. Theory of polyelectrolyte complexation – complex coacervates are self-coacervates. *J. Chem. Phys.*, 146:224902, 2017.
- [14] S. P. O. Danielsen, J. McCarty, J. Shea, K. T. Delaney, and G. H. Fredrickson. Molecular design of self-coacervation phenomena in block polyampholytes. *Proc. Natl. Acad. Sci.*, 116:8224–8232, 2019.
- [15] C. E. Sing. Development of the modern theory of polymeric complex coacervation. *Adv. Colloid Interface Sci.*, 239:2–16, 2017.
- [16] F. London. Zur theorie und systematik der molekularkräfte. *Zeitschrift für Physik*, 60:491–527, 1930.
- [17] J. M. Martin, W. Li, K. T. Delaney, and G. H. Fredrickson. Statistical field theory description of inhomogeneous polarizable soft matter. *J. Chem. Phys.*, 145:154104, 2016.
- [18] M. C. Villet and G. H. Fredrickson. Efficient field-theoretic simulation of polymer solutions. *J. Chem. Phys.*, 141:224115, 2014.
- [19] K.T. Delaney and G.H. Fredrickson. Recent developments in fully fluctuating field-theoretic simulations of polymer melts and solutions. *J. Phys. Chem. B*, 120:7615–7634, 2016.
- [20] Z. G. Wang. Fluctuation in electrolyte solutions: The self energy. *Phys. Rev. E*, 81:021501, 2010.

- [21] J. D. Jackson. *Classical Electrodynamics*. Wiley, 1998.
- [22] P. Debye and K. Kleboth. Electrical field effect on the critical opalescence. *J. Chem. Phys.*, 42:3155–3162, 1965.
- [23] D. Beaglehole. A critical binary liquid in an electric field. *J. Chem. Phys.*, 74:5251–5255, 1981.
- [24] J. Wyman. The dielectric constant of mixtures of ethyl alcohol and water from -5 to 40°. *J. Am. Chem. Soc.*, 53:3292–3301, 1931.
- [25] C. Moreau and Gérard Douhéret. Thermodynamic and physical behaviour of water + acetonitrile mixtures. dielectric properties. *J. Chem. Thermo.*, 8:403–410, 1976.
- [26] A. Luzar. Dielectric behaviour of DMSO-water mixtures. a hydrogen-bonding model. *J. Mol. Liq*, 46:221–238, 1990.
- [27] J. G. Kirkwood. On the theory of dielectric polarization. *J. Chem. Phys.*, 4:592–601, 1936.
- [28] F. Wooten. *Optical Properties of Solids*. Academic Press, 1972.
- [29] J. S. Lee, A. A. Prabu, K. J. Kim, and C. Park. Phase separation and crystallization behavior of poly(vinylidene fluoride)/ poly(1,4-butylene adipate) blends under an electric field. *Macromolecules*, 41:3598–3604, 2008.
- [30] J. S. Lee, A. A. Prabu, and K. J. Kim. UCST-type phase separation and crystallization behavior in poly(vinylidene fluoride)/poly(methyl methacrylate) blends under an external electric field. *Macromolecules*, 42:5660–5669, 2009.
- [31] A. Kriisa and C. B. Roth. Electric fields enhance miscibility of polystyrene/poly(vinyl methyl ether) blends. *J. Chem. Phys.*, 141:134908, 2014.
- [32] A. Kriisa and C. B. Roth. Jumping in and out of the phase diagram using electric fields: Time scale for remixing of polystyrene/poly(vinyl methyl ether) blends. *ACS Macro Lett.*, 8:188–192, 2019.

- [33] D. Wirtz and G. G. Fuller. Phase transitions induced by electric fields in near-critical polymer solutions. *Phys. Rev. Lett.*, 71:2236, 1993.
- [34] W. A. P. Luck. Spectroscopic studies concerning the structure and the thermodynamic behaviour of H₂O, CH₃OH and C₂H₅OH. *Discuss. Farad. Soc.*, 43:115–127, 1967.
- [35] M. W. Matsen and M. Schick. Stable and unstable phases of a diblock copolymer melt. *Phys. Rev. Lett.*, 72:2660–2663, 1994.
- [36] M. Schick. Thermodynamics and the phase diagrams of block copolymers in electric fields. In Y. Tsori and U. Steiner, editors, *Polymers, Liquids, and Colloids in Electric Fields: Interfacial Instabilities, Orientation, and Phase Transitions*, chapter 1, pages 197–214. World Scientific, 2009.
- [37] K. Amundson, E. Helfand, D. D. Davis, X. Quan, S. S. Patel, and S. D. Smith. Effect of an electric field on block copolymer microstructure. *Macromolecules*, 24:6546–6548, 1991.
- [38] K. Amundson, E. Helfand, X. Quan, and S. D. Smith. Alignment of lamellar block copolymer microstructure in an electric field. 1. alignment kinetics. *Macromolecules*, 26:2698–2703, 1993.
- [39] C. Lin, M. Schick, and D. Andelman. Structural changes of diblock copolymer melts due to an external electric field: A self-consistent-field theory study. *Macromolecules*, 38:5766–5773, 2005.
- [40] M. W. Matsen. Stability of a block-copolymer lamella in a strong electric field. *Phys. Rev. Lett.*, 95:258302, 2005.
- [41] Y. Tsori, D. Andelman, C. Lin, and M. Schick. Block copolymers in electric fields: A comparison of single-mode and self-consistent-field approximations. *Macromolecules*, 39:289–293, 2006.
- [42] M. W. Matsen. Converting the nanodomains of a diblock-copolymer thin film from spheres to cylinders with an external electric field. *J. Chem. Phys.*, 124:074906, 2006.

- [43] C. A. Tyler and D. C. Morse. Orthorhombic *fddd* network in triblock and diblock copolymer melts. *Physical Review Letters*, 94:208302, 2005.
- [44] K. Yamada, M. Nonomura, and T. Ohta. Fddd structure in ab-type diblock copolymers. *J. Phys. Condens. Matter*, 18:421–427, 2006.
- [45] M. I. Kim, T. Wakada, S. Akasaka, S. Nishitsuji, K. Saijo, H. Hasegawa, K. Ito, and M. Takenaka. Stability of the Fddd phase in diblock copolymer melts. *Macromolecules*, 41:7667–7670, 2008.
- [46] M. W. Matsen. Effect of architecture on the phase behavior of ab-type block copolymer melts. *Macromolecules*, 45:2161–2165, 2012.
- [47] W. Li, K. T. Delaney, and G. H. Fredrickson. Fddd network phase in ABA triblock copolymer melts. *J. Polym. Sci. B: Polym. Phys.*, 54:1112–1117, 2016.
- [48] X. Lu, W. P. Steckle, and R. A. Weiss. Ionic aggregation in a block copolymer ionomer. *Macromolecules*, 26:5876–5884, 1993.
- [49] Y. Schneider, M. A. Modestino, B. L. McCulloch, M. L. Hoarfrost, R. W. Hess, and R. A. Segalman. Ionic conduction in nanostructured membranes based on polymerized protic ionic liquids. *Macromolecules*, 46:1543–1548, 2013.
- [50] M. Born. Volumen und hydrationswärme der ionen. *Zeitschrift für Physik*, 1:45–48, 1920.
- [51] I. Nakamura, A. C. Shi, and Z. G. Wang. Ion solvation in liquid mixtures: Effects of solvent reorganization. *Phys. Rev. Lett.*, 109:257802, 2012.
- [52] I. Nakamura and Z. G. Wang. Salt-doped block copolymers: ion distribution, domain spacing and effective χ parameter. *Soft Matter*, 8:9356–9367, 2012.
- [53] L. M. Brown. Hideki yukawa and the meson theory. *Phys. Today*, 39:55–62, 1986.
- [54] P. Debye and E. Hückel. De la theorie des electrolytes. i. abaissement du point de congelation et phenomenes associes. *Physikalische Zeitschrift*, 24:185–206, 1923.

- [55] F. S. Bates. Polymer-polymer phase behavior. *Science*, 251:898–905, 1991.
- [56] S. F. Edwards. The theory of polymer solutions at intermediate concentration. *Proc. Phys. Soc.*, 88:265–280, 1966.
- [57] L. Leibler. Theory of microphase separation in block copolymers. *Macromolecules*, 13:1602–1617, 1980.
- [58] R.A. Riggleman, R. Kumar, and G.H. Fredrickson. Investigation of the interfacial tension of complex coacervates using field-theoretic simulations. *Journal of Chemical Physics*, 136:024903, 2012.
- [59] A. Z. Panagiotopoulos. Direct determination of phase coexistence properties of fluids by Monte Carlo simulation in a new ensemble. *Mol. Phys.*, 61:813–826, 1987.
- [60] R. A. Riggleman and G. H. Fredrickson. Field-theoretic simulations in the Gibbs ensemble. *J. Chem. Phys.*, 132:024104, 2010.
- [61] D. J. Audus. *Field-Based Simulations of Nanostructured Polyelectrolyte Gels*. PhD thesis, University of California Santa Barbara, 2013.
- [62] V. A. Parsegian. *Van der Waals Forces: A Handbook for Biologists, Chemists, Engineers, and Physicists*. Cambridge University Press, 2005.
- [63] M. Olvera de la Cruz, S. F. Edwards, and I. C. Sanchez. Concentration fluctuations in polymer blend thermodynamics. *J. Chem. Phys.*, 89:1704–1708, 1988.
- [64] Y. Tsori and D. Andelman. Thin film diblock copolymers in electric field: transition from perpendicular to parallel lamellae. *Macromolecules*, 35:5161–5170, 2002.
- [65] J. M. Martin, W. Li, K. T. Delaney, and G. H. Fredrickson. Scft study of diblock copolymer melts in electric fields: Selective stabilization of orthorhombic $Fddd$ network phase. *Macromolecules*, 51:3369–3378, 2018.
- [66] A. Onuki. Electric-field effects in fluids near the critical point. *Europhys. Lett.*, 29:611–616, 1995.

- [67] K. Orzechowski, M. Adamczyk, A. Wolny, and Y. Tsori. Shift of the critical mixing temperature in strong electric fields. theory and experiment. *J. Phys. Chem. B*, 118:7187–7194, 2014.
- [68] G. H. Fredrickson. Entropic corrections to the flory-huggins theory of polymer blends: Architectural and conformational effects. *Macromolecules*, 27:2503–2511, 1994.
- [69] J. Qin, P. Grzywacz, and D. C. Morse. Renormalized one-loop theory of correlations in disordered diblock copolymers. *J. Chem. Phys.*, 135:084902, 2011.
- [70] D. J. Grzetic, K. T. Delaney, and G. H. Fredrickson. The effective χ parameter in polarizable polymeric systems: One-loop perturbation theory and field-theoretic simulations. *Journal of Chemical Physics*, 148:204903, 2018.
- [71] D. J. Grzetic, K. T. Delaney, and G. H. Fredrickson. Contrasting dielectric properties of electrolyte solutions with polar and polarizable solvents. *Phys. Rev. Lett.*, 122:128007, 2019.
- [72] N. Fuson, M-L. J. Josien, R. L. Powell, and E. Utterback. The NH stretching vibration and NHN hydrogen bonding in several aromatic compounds. *J. Chem. Phys.*, 20:145–152, 1952.
- [73] J. A. Pathak, R. H. Colby, G. Floudas, and R. Jérôme. Dynamics in miscible blends of polystyrene and poly(vinyl methyl ether). *Macromolecules*, 32:2553–2561, 1999.
- [74] K. D. Dorfman. The statistical segment length of dna: Opportunities for biomechanical modeling in polymer physics and next-generation genomics. *J. Biomech. Eng.*, 140:020801, 2018.
- [75] J. P. Penning and R. St. John Manley. Miscible blends of two crystalline polymers. 1. phase behavior and miscibility in blends of poly(vinylidene fluoride) and poly(1,4-butylene adipate). *Macromolecules*, 29:77–83, 1996.
- [76] Dielectric constants of common materials. <https://www.kabusa.com/Dilectric-Constants.pdf>. Accessed: 2019-10-28.

- [77] F. S. Bates and G. H. Fredrickson. Block copolymer thermodynamics: Theory and experiment. *Ann. Rev. Phys. Chem.*, 41:525–557, 1990.
- [78] M. Trawick, D. Angelescu, P. Chaikin, and R. Register. Block copolymer nanolithography. In D. G. Bucknall, editor, *Nanolithography and Patterning Techniques in Microelectronics*, chapter 1, pages 1–38. Taylor & Francis, 2005.
- [79] I. W. Hamley. Nanostructure fabrication using block copolymers. *Nanotechnology*, 14:39–54, 2003.
- [80] D. J. C. Herr. Directed block copolymer self-assembly for nanoelectronics fabrication. *J. Mater. Res.*, 26:122–139, 2011.
- [81] M. A. Hillmeyer. Nanoporous materials from block copolymer precursors. In V. Abetz, editor, *Block Copolymers II*, chapter 3, pages 137–181. Springer Berlin Heidelberg, 2005.
- [82] E. A. Jackson and M. A. Hillmeyer. Nanoporous membranes derived from block copolymers: From drug delivery to water filtration. *ACS Nano*, 4:3548–3553, 2010.
- [83] J. K. Kim, S. Y. Yang, Y. Lee, and Y. Kim. Functional nanomaterials based on block copolymer self-assembly. *Prog. Polym. Sci.*, 35:1325–1349, 2010.
- [84] G. H. Fredrickson and E. Helfand. Fluctuation effects in the theory of microphase separation in block copolymers. *J. Chem. Phys.*, 87:697–795, 1987.
- [85] M. W. Matsen. The standard Gaussian model for block copolymer melts. *J. Phys. Condens. Matter*, 14:R21–R47, 2001.
- [86] S. B. Darling. Directing the self-assembly of block copolymers. *Prog. Polym. Sci.*, 32:1152–1204, 2007.
- [87] H. U. Jeon, H. M. Jin, J. Y. Kim, S. K. Cha, J. H. Mun, K. E. Lee, J. J. Oh, T. Yun, J. S. Kim, and S. O. Kim. Electric field directed self-assembly of block copolymers for rapid formation of large-area complex nanopatterns. *Mol. Syst. Des. Eng.*, 2:560–566, 2017.

- [88] Y. Rokhlenko, K. Zhang, M. Gopinadhan, S. R. Larson, P. W. Majewski, K. G. Yager, P. Gopalan, C. S. O'Hern, and C. O. Osuji. Magnetic alignment of block copolymer microdomains by intrinsic chain anisotropy. *Physical Review Letters*, 115:258302, 2015.
- [89] M. Gopinadhan, Y. Choo, K. Kawabata, G. Kaufman, X. Feng, Y. Rokhlenko X. Di, L. H. Mahajan, D. Ndaya, R. M. Kasi, and C. O. Osuji. Controlling orientational order in block copolymers using low intensity magnetic fields. *Proceedings of the National Academy of Sciences*, 104(45):E9437, 2017.
- [90] Y. Rokhlenko, P. W. Majewski, S. R. Larson, P. Gopalan, K. G. Yager, and C. O. Osuji. Implications of grain size variation in magnetic field alignment of block copolymer blends. *ACS Macro Letters*, 6:404–409, 2017.
- [91] H. M. Jin, D. Y. Park, S. Jeong, G. Y. Lee, J. Y. Kim, J. H. Mun, S. K. Cha, J. Lim, J. S. Kim, K. H. Kim, K. J. Lee, and S. O. Kim. Flash light millisecond selfassembly of high χ block copolymers for wafer-scale sub-10 nm nanopatterning. *Adv. Mater.*, 29:1700595, 2017.
- [92] D. Yong, H. M. Jin, S. O. Kim, and J. U. Kim. Laser-directed self-assembly of highly aligned lamellar and cylindrical block copolymer nanostructures: Experiment and simulation. *Macromolecules*, 51:1418–1426, 2018.
- [93] C. Liedel, C. W. Pester, M. Ruppel, V. S. Urban, and A. Böker. Beyond orientation: The impact of electric fields on block copolymers. *Macromol. Chem. Phys.*, 213:259–269, 2012.
- [94] A. Onuki and J. Fukuda. Electric field effects and form birefringence in diblock copolymers. *Macromolecules*, 28(26):8788–8795, 1995.
- [95] Y. Tsori, F. Tournilhac, D. Andelman, and L. Leibler. Structural changes in block copolymers: Coupling of electric field and mobile ions. *Phys. Rev. Lett.*, 90:145504, 2003.
- [96] A. Dehghan, M. Schick, and A. Shi. Effect of mobile ions on the electric field needed to orient charged diblock copolymer thin films. *J. Chem. Phys.*, 143:134902, 2015.

- [97] M. W. Matsen. Converting the nanodomains of a diblock-copolymer thin film from spheres to cylinders with an external electric field. *J. Chem. Phys.*, 124:074906, 2006.
- [98] Y. Tsori, D. Andelman, C. Lin, and M. Schick. Block copolymers in electric fields: a comparison of single-mode and self-consistent-field approximations. *Macromolecules*, 39:289–293, 2006.
- [99] D. Q. Ly, T. Honda, T. Kawakatsu, and A. V. Zvelindovsky. Kinetic pathway of gyroid-to-cylinder transition in diblock copolymer melt under an electric field. *Macromolecules*, 40:2928–2935, 2007.
- [100] D. Q. Ly, T. Honda, T. Kawakatsu, and A. V. Zvelindovsky. Hexagonally perforated lamella-to-cylinder transition in a diblock copolymer thin film under an electric field. *Macromolecules*, 41:4501–4505, 2008.
- [101] D. Q. Ly, T. Honda, T. Kawakatsu, and A. V. Zvelindovsky. Electric field-induced transitions in perforated lamella of aba triblock copolymer thin film. *Soft Matter*, 5:4814–4822, 2009.
- [102] M. Pinna, L. Schreier, and A. V. Zvelindovsky. Mechanisms of electric-field-induced alignment of block copolymer lamellae. *Soft Matter*, 5:970–973, 2009.
- [103] D. Q. Ly, M. Pinna, T. Honda, T. Kawakatsu, and A. V. Zvelindovsky. Kinetic pathways of sphere-to-cylinder transition in diblock copolymer melt under electric field. *J. Chem. Phys.*, 138:074904, 2013.
- [104] A. Böker, H. Elbs, H. Hänsel, A. Knoll, S. Ludwigs, H. Zettl, V. Urban, V. Abetz, A. H. E. Müller, and G. Krausch. Microscopic mechanisms of electric-field-induced alignment of block copolymer microdomains. *Phys. Rev. Lett.*, 89:135502, 2002.
- [105] G. J. A. Sevink, M. Pinna, K. M. Langer, and A. V. Zvelindovsky. Selective disordering of lamella-forming diblock copolymers under an electric field. *Soft Matter*, 7:5161–5170, 2011.

- [106] K. Amundson, E. Helfand, X. Quan, S. D. Hudson, and S. D. Smith. Alignment of lamellar block copolymer microstructure in an electric field. 2. mechanisms of alignment. *Macromolecules*, 27:6559–6570, 1994.
- [107] M. Ruppel, C. W. Pester, K. M. Langner, G. J. A Sevink, H. G. Schoberth, K. Schmidt, V. S. Urban, J. W. Mays, and A. Böker. Electric field induced selective disordering in lamellar block copolymers. *ACS Nano*, 7:3854–3867, 2013.
- [108] J-L. Barrat, G. H. Fredrickson, and S. W. Sides. Introducing variable cell shape methods in field theory simulation of polymers. *J. Phys. Chem. B*, 109:6694–6700, 2005.
- [109] J. Wu, X. Wang, Y. Ji, L. He, and S. Li. Phase diagrams of diblock copolymers in electric fields: A self-consistent field theory study. *Phys. Chem. Chem. Phys.*, 18:10309–10319, 2016.
- [110] D. Düchs, K. T. Delaney, and G. H. Fredrickson. A multi-species exchange model for fully fluctuating polymer field theory simulations. *J. Chem. Phys.*, 141:174103, 2014.
- [111] S. Li, Y. Jiang, Y. Ji, and X. Wang. Electric-field-induced sphere-cylinder phase transitions of diblock copolymers. *Polymer*, 54:6636–6643, 2013.
- [112] J. F. Nye. *Physical Properties of Crystals*. Clarendon Press, 1985.
- [113] H. G. Schoberth, C. W. Pester, M. Ruppel, V. S. Urban, and A. Böker. Orientation-dependent order-disorder transition of block copolymer lamellae in electric fields. *ACS Macro Letters*, 2:469–473, 2013.
- [114] A. Böker, H. Elbs, H. Hänsel, A. Knoll, S. Ludwigs, H. Zettl, A. V. Zvelindovsky, G. J. A Sevink, , V. Urban, V. Abetz, A. H. E. Müller, and G. Krausch. Electric field induced alignment of concentrated block copolymer solutions. *Macromolecules*, 36:8078–8087, 2003.
- [115] C. W. Pester, M. Ruppel, H. G. Schoberth, K. Schmidt, C. Leidel, P. van Rijn, K. A. Schindler, S. Hiltl, T. Czubak, J. Mays, V. S. Urban, and A. Böker. Block copolymers: Piezoelectric properties of nonpolar block copolymers. *Adv. Mater.*, 23:4047–4052, 2011.

- [116] E. Gurovich. On microphase separation of block copolymers in an electric field: Four universal classes. *Macromolecules*, 27:7339–7362, 1994.
- [117] C. W. Pester, C. Liedel, M. Ruppel, and A. Böker. Block copolymers in electric fields. *Progress in Polymer Science*, 64:182–214, 2017.
- [118] M. Gopinadhan, Y. Choo, and C. O. Osuji. Strong orientational coupling of block copolymer microdomains to smectic layering revealed by magnetic field alignment. *ACS Macro Letters*, 5:292–296, 2016.